ANTI-INFLAMMATORY ACTIVITIES OF FLUORINATED TRIARYLMETHANE DERIVATIVES IN LPS-ACTIVATED MACROPHAGE RAW 264.7

WIPADA SIRITANYONG

A THESIS SUBMITTED IN PARTIAL FULFILLMENT OF THE REQUIREMENTS FOR THE MASTER DEGREE OF SCIENCE IN BIOCHEMISTRY

FACULTY OF SCIENCE
BURAPHA UNIVERSITY

NOVEMBER 2019

The thesis of Wipada Siritanyong has been approved by the examining committee to be partial fulfillment of the requirements for the Master Degree of Science in Biochemistry of Burapha University

Advisory Committee

……Klaokwan S.……Principle advisor
(Associate Professor Dr. Klaokwan Srisook)

……Jaray Jaratjaroonphong……Co-advisor
(Associate Professor Dr. Jaray Jaratjaroonphong)

Examining Committee

……Wanlaya Tanechpongtamb……Principle examiner
(Assistant Professor Dr. Wanlaya Tanechpongtamb)

……Klaokwan S.……Member
(Associate Professor Dr. Klaokwan Srisook)

……Jaray Jaratjaroonphong……Member
(Associate Professor Dr. Jaray Jaratjaroonphong)

……Uthaiwan Sirion……Member
(Assistant Professor Dr. Uthaiwan Sirion)

This thesis has been approved by the Faculty of Science to be partial fulfillment of the requirements for the Master Degree of Science in Biochemistry of Burapha University

……E. Srisook…… Dean of the Faculty of Science
(Assistant Professor Dr. Ekaruth Srisook)
……November 29……, 2019

ACKNOWLEDGEMENT

I would like to express my sincere gratitude and deep appreciation to my major advisor, Associate Professor Dr. Klaokwan Srisook, for all her patience, motivation, enthusiasm, and immense knowledge. Her guidance helped me in all the time of research and writing of this thesis. Also, I would like to thanks my Co-Advisor, Associate Professor Dr. Jaray Jaratjaroonphong for his kindness synthesized compounds, guidance, support, attention and valuable advice throughout of my study. Great appreciation is also given to all committee members, Assistant Professor Dr. Wanlaya Tanechpongtamb and Assistant Professor Dr. Uthaiwan Sirion for their encouragement and insightful comments

Great appreciation is also given to all lecturer members in Department of Biochemistry for their support, attention, motivation.

I also would like to thank Burapha University, the Center for Innovation in Chemistry (PERCH-CIC), and Commission on Higher Education, Ministry of Education for the financially supported.

This work was partially supported by Science Innovation Facility, Faculty of Science, Burapha University (SIF-IN-600071)

Finally, I must express my very profound gratitude to my parents with unfailing support and continuous encouragement throughout my years of study and through the process of researching and writing this thesis. I also special thanks my friends for their support as well as other KS Lab members for your kindness, collaboration, suggestions and friendship. This accomplishment would not have been possible without them. **This means a lot to me**. Thank you.

Wipada Siritanyong

THE RELEVANCE OF THE RESEARCH WORK TO THAILAND

The main purpose of this study is to investigate the ability and mechanism underlying the anti-inflammatory effect of fluorinated triarylmethane derivatives. This research project provides the scientific evidence for the basic information of a new series anti-inflammatory agent and its possible useful compounds to support for development of anti-inflammatory agent.

58910083: MAJOR: BIOCHMISTRY; M.Sc. (BIOCHEMISTRY)
KEYWORDS: INFLAMMATION / NITRIC OXIDE / FLUORINATED / TRIARYLMETHANE / ANTI-INFLAMMATORY AGENTS

WIPADA SIRITANYONG: ANTI-INFLAMMATORY ACTIVITIES OF FLUORINATED TRIARYLMETHANE DERIVATIVES IN LPS-ACTIVATED MACROPHAGE RAW 264.7. ADVISORY COMMITTEE: KLAOKWAN SRISOOK, Ph.D., JARAY JARATJAROONPHONG, Ph.D. 129 P. 2019.

Macrophages play a crucial role in inflammatory response. Activated macrophages release various pro-inflammatory mediator such as nitric oxide (NO), prostaglandin E_2 (PGE_2) and pro-inflammatory cytokines such as tumor necrosis factor alpha (TNF-α) and interleukin-1β (IL-1β). Nevertheless, massive production NO, PGE_2, TNF-α and IL-1β are associated with many inflammatory diseases. In the present study, twenty-six fluorinated triarylmethane derivatives were newly synthesized and investigated their effect on NO production in lipopolysaccharide (LPS)-stimulated RAW264.7 macrophages. Among them, compounds JJBF9, JJBF10, JJBF11, JJBF12, JJBF14, JJBF15 and JJCF1 potently inhibited NO production than the other compounds with IC_{50} values ranging from 6.89 ± 0.47 to 14.20 ± 0.67 μM. Furthermore, JJBF14 being the most potent compound with the highest therapeutic index was selected to investigate underlying molecular mechanism of its anti-inflammatory activity.

JJBF14 inhibited LPS-induced production of NO and PGE_2 through decreasing protein expression of inducible nitric oxide synthase (iNOS) and cyclooxygenase-2 (COX-2). The compound significantly inhibited LPS-induced iNOS mRNA expression, but not COX-2. Moreover, JJBF14 attenuated the reduction of LPS-modulated COX-1 protein expression. JJBF14 also reduced the secretion pro-inflammatory cytokine TNF-α whereas it had no significant effect on reduction of IL-1β level. Additionally, JJBF14 inactivated nuclear factor-κB (NF-κB) by preventing phosphorylation of IκBα and nuclear translocation of NF-κB p65. Besides, JJBF14 markedly suppressed phosphorylated p38 mitogen-activated kinase (p38 MAPK) levels. However, it did not reduce the levels of phosphorylated c-Jun N-terminal kinase (JNKs) and extracellular signal-regulated kinase (ERK). Furthermore, JJBF14

caused declined phosphorylation of activating transcription factor-2 (ATF-2), a major transcription factor target of p38 MAPK.

Taken together, these results indicated that JJBF14 suppressed the production of NO, PGE_2 and TNF-α in LPS-induced RAW264.7 macrophage via blockade of NF-κB and p38MAPK/ATF-2 signaling pathways. In addition, the selected fluorinated triarylmethane derivative, JJBF14 might be useful as a promising lead compound for future development of anti-inflammatory agent.

CONTENTS

Page

ABSTRACT IV

CONTENTS VI

LIST OF TABLES X

LIST OF FIGURES XI

CHAPTER

1. INTRODUCTION 1

1.1 Statement and significance of the problem 1

1.2 Objectives 3

1.3 Contribution to knowledge 3

1.4 Scope of the study 3

2. LITERATURE REVIEWS 5

2.1 Inflammation 5

2.2 Inflammation and diseases 6

2.3 Chemical mediators of inflammation 6

2.4 Role of macrophage in inflammation 6

2.5 Nitric oxide 7

2.6 Nitric oxide synthase inhibitor 10

2.6.1 L-Arginine site 10

2.6.2 Biopterin site 12

2.6.3 Heme-binding inhibitors 12

2.6.4 Flavoprotein and CaM inhibitors 12

2.7 Prostaglandins 12

2.8 Cytokines 14

2.9 Lipopolysaccharide and receptors 15

2.10 Signaling pathway in inflammation 17

2.10.1 Nuclear factor (NF)-κB signaling pathway 18

2.10.2 Mitogen activated protein kinases (MAPKs) signaling pathways 19

2.11 Anti-inflammatory drugs 21

CONTENTS (CONTINUED)

Chapter Page

2.12 Reviews on biological activities of triarylmethane 26

2.13 Reviews on biological activities of fluorinated compounds 30

3. RESEARCH METHODOLOGY 34

Part I : Screening for inhibitory effect on NO and PGE_2 production of fluorinated triarylmethane derivatives in RAW 264.7 macrophage cells

3.1 Materials and equipment 35

3.1.1 Equipments 35

3.1.2 Chemicals 35

3.2 Methods 36

3.2.1 Fluorinated triarylmethane used in this study 36

3.2.2 Chemical preparation 36

3.2.3 Cell culture 36

3.2.4 Cell viability test by MTT assay 41

3.2.5 Determination of nitrite concentration 42

3.2.6 Determination of PGE_2 concentration 42

3.2.7 Statistical analysis 42

Part II : Investigation of mechanism underlying the anti-inflammatory effect of the most potent fluorinated triarylmethane derivative in LPS-activated RAW 264.7 macrophages

3.3 Materials 43

3.3.1 Equipments 43

3.3.2 Chemicals 43

3.4 Methods 45

3.4.1 Calculation IC50 value of the five most potent compounds 45

3.4.2 Determination of PGE_2 concentration 46

3.4.3 iNOS activity assay 47

3.4.4 COX-2 activity assay 47

3.4.5 Determination of cytokines 47

CONTENTS (CONTINUED)

Chapter Page

3.4.5.1 Determination of TNF-α 47
3.4.5.2 Determination of IL-1β 48
3.4.6 Protein extraction for western blot analysis 49
3.4.6.1 Whole cell extraction for iNOS and COX-2 expression 49
3.4.6.2 Cytoplasmic protein extraction for IκB phosphorylation and nuclear protein extraction for NF-κB p65 translocation 49
3.4.6.3 Whole cell extraction for MAPKs phosphorylation 50
3.4.7 Western blot analysis for protein expression 50
3.4.7.1 Western blot analysis for iNOS and COX-2 expression 50
3.4.7.2 Western blot analysis for NF-κB p65 level 51
3.4.7.3 Western blot analysis for IκB phosphorylation 52
3.4.7.4 Western blot analysis of phosphorylation of MAPKs 52
3.4.8 Stripping and reprobing of Western blots 54
3.4.9 RNA isolation 54
3.4.10 Real time reverse transcription-polymerase chain reaction (Real-rime PCR) 56
3.4.11 Statistical analysis 58
4. RESULTS 59
4.1 Effect of fluorinated triarylmethane derivatives on cell viability of RAW264.7 macrophages 59
4.2 Effect of fluorinated triarylmethane derivatives on NO production in LPS-stimulated RAW264.7 macrophages 61
4.3 The IC_{50} values of NO inhibition of selected fluorinated triarylmethanes 64
4.4 JJBF14 inhibited NO production in a concentration dependent manner 66
4.5 Effect of JJBF14 on LPS-induced iNOS expression in RAW 264.7 69

CONTENTS (CONTINUED)

Chapter Page

4.6 Effect of JJBF14 on LPS-induced iNOS enzymatic activity in RAW 264.7 macrophages 71

4.7 Effect of JJBF14 on LPS-induced PGE_2 production in RAW 264.7 macrophages 72

4.8 Effect of JJBF14 on LPS-induced COX-2 expression in RAW 264.7 macrophages 74

4.9 Effect of JJBF14 on LPS-induced COX enzymatic activity in RAW264.7 macrophages 77

4.10 Effect of JJBF14 on COX-1 protein expression in RAW264.7macrophages 78

4.11 Effect of JJBF14 on LPS-induced IL-1β and TNF-α production in RAW264.7 macrophages 82

4.12 Effect of JJBF14 on LPS-induced NF-κB p65 translocation in RAW 264.7 macrophage cells 84

4.13 Effect of JJBF14 on LPS-induced phosphorylation of MAPKs in RAW264.7 macrophages 87

4.14 Effect of JJBF14 on LPS-induced phosphorylation of ATF-2 in RAW264.7 macrophages 90

5. DISCUSSION AND CONCLUSION 91

REFERENCE 101

APPENDIX 113

APPENDIX A 114

APPENDIX B 118

APPENDIX C 123

BIOGRAPHY 128

LIST OF TABLES

Tables		Page
2-1	Classification of NSAIDs to their COX selectively	23
2-2	Classification of NSAIDs to their chemical structure	24
3-1	The chemical structure of fluorinated triarylmethane derivatives used in this study	37
3-2	The condition for specific primary antibody of MAPKs	53
3-3	The condition for specific secondary antibody of MAPKs	54
3-4	Sequences of primers used in Real time RT-PCR	57
3-5	The PCR cycling parameters	57
A-1	Molecular weight and volume of DMSO for dissolved Fluorinated triarylmethane derivatives	115

LIST OF FIGURES

Figures		Page
2-1	The pattern of leukocyte infiltration into wounds	5
2-2	The NOS catalyzed reaction	7
2-3	The structure and catalytic mechanisms of functional NOS	8
2-4	Schematic representation of the major conserved response elements in the murine iNOS promoter	9
2-5	The chemical structure of L-NMMA	10
2-6	The chemical structure of L-NNA	11
2-7	The chemical structure of L-NAME	11
2-8	The chemical structure of Aminoguanidine	11
2-9	Biosynthesis of PGE_2	13
2-10	Schematic representation of the major conserved response elements in the murine COX-1 promoter	14
2-11	Schematic representation of the major conserved response elements in the murine COX-2 promoter	14
2-12	The structure of LPS	15
2-13	LPS receptor on macrophage	16
2-14	The diagram illustrate pathways that triggered by TLR and cytokines receptor	17
2-15	The canonical of NF-κB signaling pathway	19
2-16	The activation of three main MAP kinases	21
2-17	The Chemical structures of inhaled glucocorticoids	22
2-18	The structure of 4,4-Dihydroxy-3,4-methylenedioxytriphenylmethane	26
2-19	The structure of thiophene containing triarylmethane derivatives	27
2-20	The structure of MPCV, DPCV and AEV	27
2-21	The structure of 1-[(2-chlorophenyl)-diphenylmethyl]-1*H*-pyrazole	28
2-22	The structure of bis[(5-methyl)2-furyl](4-nitrophenyl) Methane (JJSD9)	28
2-23	The structure of tris(5-ethyl-1H-pyrrol-2-yl) methane (JJST5)	29

LIST OF FIGURES (CONTINUED)

Figures		Page
2-24	The structure of studied tert-butyl2-((5-methylfuran-2-yl) (4-nitrophenyl) methyl)-1H-pyrrole-1-carboxylate (JJSRUN16)	30
2-25	The structure of anti-inflammatory drugs containing fluorine atom	31
2-26	The structure of fluorinated coumarins	32
2-27	The structure of 4-amino-5-fluorosalicylic acid	32
2-28	The structure of fluorinated quinolone incorporated benzimidazole derivatives	33
4-1	Effect of fluorinated triarylmethane derivatives on cell viability of RAW264.7 macrophages	59
4-2	Effect of fluorinated triarylmethane derivatives on NO production in RAW264.7 macrophages	62
4-3	The IC_{50} values of NO inhibition of selected fluorinated triarylmethane in LPS-stimulated RAW264.7 macrophages	64
4-4	Therapeutic index of selected fluorinated triarylmethane in LPS-activated macrophages	65
4-5	Effect of JJBF14 on NO production in RAW 264.7 macrophage cells	66
4-6	Effect of JJBF14 on cell viability in RAW 264.7 macrophages	68
4-7	Effect of JJBF14 on iNOS protein expression in LPS-stimulated RAW 264.7 macrophages	69
4-8	Effect of JJBF14 on LPS-induced iNOS mRNA expression in RAW264.7 macrophages	70
4-9	Effect of JJBF14 on LPS-induced iNOS enzymatic activity in RAW264.7 macrophages	71
4-10	Effect of JJBF14 on LPS-induced PGE_2 production in RAW 264.7 macrophages	72
4-11	Effect of JJBF14 on COX-2 expression in LPS-stimulated RAW 264.7 macrophages	74
4-12	Effect of JJBF14 on LPS-induced COX-2 mRNA expression in RAW264.7 macrophages	76

LIST OF FIGURES (CONTINUED)

Figures		Page
4-13	Effect of JJBF14 on COX-2 activity in RAW 264.7 macrophages	77
4-14	Effect of JJBF14 on COX-1 protein expression in RAW264.7 macrophages	79
4-15	Effect of JJBF14 on COX-1 protein in LPS-stimulated RAW264.7 macrophages	80
4-16	Effect of JJBF14 on COX-1 mRNA expression in LPS-stimulated RAW264.7 macrophages	81
4-17	Effect of JJBF14 on LPS-activated IL-1β production in RAW264.7 macrophages	82
4-18	Effect of fluorinated triarylmethane derivatives on TNF-α production in LPS-activated RAW 264.7 macrophages	83
4-19	Effect of JJBF14 on LPS-induced NF-κB p65 activation in RAW 264.7 macrophages	84
4-20	Effect of JJBF14 on LPS-induced phosphorylation of MAPKs in RAW264.7 macrophages	85
4-21	Effect of JJBF14 on LPS-induced phosphorylation of ATF-2 in RAW264.7 macrophages	90
5-1	Comparing the structure of JJAF1, JJAF2 and JJAF4 all have a 6-fluoroindole and benzene moiety	98
5-2	Comparing the structure of JJAF2 and JJAF3 all have a 6-fluoroindole and 2-methyl furan	98
5-3	Comparing the structure of JJAF5 and JJAF5 all have an indole with 4-fluorobanzaldehyde	99
5-4	Comparing the structure of 2,4,6-trimethoxybenzene, 2,4,5-trimethoxybenzene and 2,3,4-trimethoxybenzene one ring of variety of fluorine position on benzene ring	99
5-5	The simplified diagram action mechanism responsible for the suppressive effect of JJBF14 on LPS-stimulated inflammatory signaling partway	100

LIST OF FIGURES (CONTINUED)

Figures Page

C-1 Amplification curve (A) and melting curve (B) of iNOS 124

C-2 Amplification curve (A) and melting curve (B) of COX-2 125

C-3 Amplification curve (A) and melting curve (B) of COX-1 126

C-4 Amplification curve (A) and melting curve (B) of EF-2 127

CHAPTER 1
INTRODUCTION

1.1 Statements and significance of problem

Inflammation is complex immune response that induce by harmful stimulation such as infection from bacteria or virus, burns and chemicals (Ashley, Weil, & Nelson, 2012) leading to eliminating the invading pathogen, repairing any damage and returning tissue to a normal stage (Medzhitov, 2008) . In the inflammatory process, difference cell types are recruited to injured area, mast cells, neutrophils and monocytes that locally differentiate into macrophages (Koh & DiPietro, 2011). Macrophages play a key role in inflammatory response by generating pro-inflammatory mediators such as nitric oxide (NO) and prostaglandin E_2 (PGE_2) as well as inflammatory cytokines such as interleukin-1β (IL-1β), interleukin-6 (IL-6) and tumor necrosis factor-α (TNF-α) (Koh & DiPietro, 2011). However excessive of mediators leads to inflammation with occur in variety of inflammatory diseases including type 2 diabetes, cardiovascular, sclerosis, rheumatoid arthritis, atherosclerosis, gout and cancer (Medzhitov, 2008; Nathan, 2002).

NO is a free radical, generated from L-arginine and produced by nitric oxide synthases (NOSs). NO plays a role in mammalian physiology such as neurotransmission, vascular smooth muscle relaxing and killing of invading microbes (Pacher, Beckman,& Liaudet, 2007). Inducible NOS (iNOS) is expressed in many cell types including macrophages which produce large amount of NO in inflammatory response (Forstermann & Sessa, 2012). Prostaglandins (PGs), derived from arachidonic acid (AA) and produced by cyclooxygenase (COX), are pro-inflammatory mediators which have functions on maintaining homeostatic and inflammatory response (Ricciotti & FitzGerald, 2011).

The inhibition of inflammatory mediators that produce by macrophage be able to retaining inflammatory disease (Hwang et al., 2010). Nowadays, non-steroidal anti-inflammatory drugs (NSAIDs) are universally used in medications of numerous musculoskeletal and inflammatory disease (Atkinson et al., 2013). NSAIDs decreases pain and inflammation by inhibiting COX enzymes (Ricciotti & FitzGerald, 2011).

However, the non-selective inhibitory action on both COX-1 (important in tissue homeostasis) and COX-2 (plays a role in inflammatory response) causes some side effects such as gastrointestinal toxicity and ulcer (Lee et al., 2011). Moreover, a more selective COX-2, celecoxib has been reported to increase a risk of stroke and heart disease (Isanbor & O'Hagan, 2006). Consequently, the development of novel therapeutic agents is need for anti-inflammatory diseases.

Triarylmethanes (TRAMs) have been reported their multiple biological effects such as anti-oxidant, anti-tumor, anti-bacteria, anti-virus and anti-inflammation (Nair, Thomas, Mathew, & Abhilash, 2006). Previously, our group has reported several series of triarylmethane with anti-inflammatory activities (Duangked & Sawai, 2014; Jaratjaroonphong, Tuengpanya, Saeeng, Udompong, & Srisook, 2014; Siritanyong & Tongyen, 2015). Twenty analogs of bis(heteroaryl)alkane were synthesized and evaluated for the anti-inflammatory activity in LPS-stimulated RAW 264.7 macrophage. Among them, bis[(5-methyl)2-furyl] (4-fluorophenyl) methane which contain a fluorine atom at para-position of the benzene ring was shown the IC_{50} value of NO inhibitory effect at 44.8 ± 4.1 μM. It seems that the compound which containing a strong electron withdrawing group able to enhance the inhibitory effect. However, the IC_{50} is comparable with aminoguanidine as a positive control (IC_{50} = 43.3 ± 2.5 μM (Jaratjaroonphong et al., 2014).

At the present time, there were more than 138 drugs in the market with the occurrence of fluorine in their structure (El-Feky, Thabet, & Ubeid, 2014). The incorporation of fluorine into drugs increases lipophilicity resulting in enhancing absorption into the biological membranes whereby its small covalent radius can facilitate docking with their drug receptors (Ismail, 2002). It has been reported that coumarin derivatives containing fluorine showed significant anti-inflammatory activity compared to the other halogenated compounds (Kalkhambkar et al., 2008). Recently, some fluorinated quinoline derivatives exhibited superior anti-inflammatory activity than celecoxib (El-Feky, Thabet, & Ubeid, 2014). Thus, fluorinated triarylmethane, compound that consists of methane and substituted by aromatic or hetero aromatic which has fluorine atom, is interesting because it might be more potent on anti-inflammatory activity. In this study, as part of our continuing effort to develop optimal activities and reduce side effects of anti-inflammatory agent, twenty-

six analogs of fluorinated triarylmethane were synthesized and evaluated anti-inflammatory abilities on NO and PGE_2 production. The most potent compound was investigated the mode of the action on protein and mRNA expression of iNOS and COX-2. The upstream signaling cascade of anti-inflammation of the compound including NF-ĸB and MAPKs pathways were also studied.

1.2 Objectives

1. To evaluate anti-inflammatory ability of selected fluorinated triarylmethane derivatives in lipopolysaccharide (LPS)-activated RAW 264.7 macrophages.

2. To investigate the mechanism underlying anti-inflammatory behavior of the most potent fluorinated triarylmethane derivative in LPS-activated RAW 264.7 macrophages.

1.3 Contribution to knowledge

1. To understand the ability and mechanism of fluorinated triarylmethane derivatives in LPS-activated RAW 264.7 macrophages.

2. The basic information will be used to support for development of the anti-inflammatory agent.

1.4 Scope of the study

LPS-induced RAW 264.7 macrophage cells were used as a model of the inflammatory response. Twenty-six fluorinated triarylmethane compounds were treated into LPS-induced macrophage and evaluated the effect on cell viability by MTT assay, NO production by Griess assay. The most potent compound was examined the mechanism underlying anti-inflammatory activity. Besides, PGE_2, TNF-α and IL-1β production were performed by prostaglandin E_2 Enzyme Immunoassay Kit, mouse TNF-α and IL-1β Quantikine ELISA Kit, respectively. Moreover, the effect of selected compound on protein and mRNA expression of iNOS and COX-2 were studied by Western blot analysis and real time RT-PCR. The activation of

NF-κB was investigated by Western blot analysis. In addition, the levels of phosphorylation of MAPKs were investigated by Western blot analysis.

CHAPTER 2
LITERATURE REVIEWS

2.1 Inflammation

Inflammation is an immune response to infection and tissue injury and plays crucial role both in normal and pathological healing (Koh & DiPietro, 2011). This is a beneficial incidence to tissue injury and infection to repair any damage and return tissue to a normal stage (Ricciotti & FitzGerald, 2011). The inflammation can be classified as acute inflammation and chronic inflammation that depend on the duration time of the process and pathological features. Acute inflammation develops quickly and relatively short duration, lasts for minutes to a few days. At the site of infection, neutrophils are the most abundant infiltrated white blood cells. Mast cells that are adjacent in the tissue also increase in the wound. Then, monocytes enter to the wound and differentiate into mature tissue macrophages (Figure 2-1). The initial process, mast cells and macrophages produce a variety of inflammatory mediators, including vasoactive amines, cytokines, chemokines and eicosanoids (Nathan, 2002). However, if the acute inflammatory response cannot be removed the pathogen complete, by the inflammatory process continues and become chronic inflammation. The mononuclear cells including macrophage, lymphocytes and plasma cells are infiltrated to their tissue (Medzhitov, 2008).

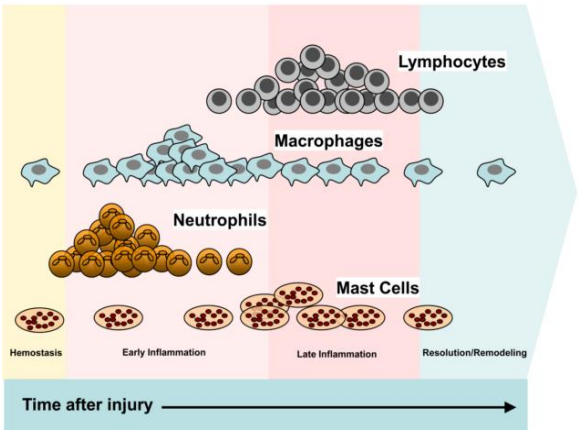

Figure 2-1 The pattern of leukocyte infiltration into wounds (Koh & DiPietro, 2011)

2.2 Inflammation and diseases

Inflammation triggers signaling cascades to activation of transcription factors, gene expression, increased of levels of inflammatory enzymes and release of various oxidants and pro-inflammatory molecules in inflammatory cells. The excessive of oxidants and inflammatory mediators have an unfavorable effect on normal tissue including toxicity, abnormal cell proliferation, loss of barrier function, inhibiting normal function and leading to systemic disorders (Barr & Belton, 1991). Chronic inflammation is characteristic feature in virtually all inflammatory diseases including chronic gastritis, rheumatoid arthritis, atherosclerosis, asthma, gout, aging, cancer and Alzheimer's diseases (Nathan, 2002).

2.3 Chemical mediators of inflammation

Mediators of inflammation have the effect in typical on the vascular and on the recruitment of leukocytes they can be classified according to their biochemical properties (Medzhitov, 2008). Vasoactive amines (histamine and serotonin) that produced during mast cells and platelets degranulation cause increased vascular permeability and vasodilation. Lipid mediators such as eicosanoid and platelet-activating factor are derived from phospholipid during the inflammatory responses that have a potent inducer of fever, vasodilation, vasoconstriction, increase vascular permeability and platelet activation. Inflammatory cytokines are produced by macrophage such as tumor necrosis factor-α (TNF-α), interleukin-1β (IL-1β) and interleukin-6 (IL-6) activate endothelium and leukocytes and induce the acute-phase response. Chemokines are produced by many cell types that response in inflammatory response and have a potent on chemotaxis towards the affected tissues and leukocyte extravasation and (Medzhitov, 2008).

2.4 Role of macrophage in inflammation

Macrophages are derived from blood monocytes and resides in all tissue. It has a specific function depending on the tissue in which they insides and plays many important roles in the innate and adaptive immune responses, as well as in tissue homeostasis. During the activation, macrophage are efficient phagocytes which

occurs to remove invading pathogens and unwanted material including apoptotic cells (Dunster, 2016). In the normal phase, macrophages produce only low levels of pro-inflammatory mediators. The activation of macrophage with pro-inflammatory cytokines, interferon, LPS and the other signaling molecules, macrophage produced a large number of mediators and cytokines such as NO, IL-1 β, IL-6 and TNF-α (Koh & DiPietro, 2011).

2.5 Nitric oxide

NO is a free radical and the smallest signaling molecule which has numerous molecular targets. NO plays role in mammalian physiology such as vasodilation, neurotransmission and killing of microbes. Moreover, NO can react with superoxide anion (O_2^-) to from peroxynitrite ($ONOO^-$) that much more powerful oxidant on oxidative damage, nitration, and S-nitrosylation of biomolecules including proteins, lipids, and DNA (Forstermann & Sessa, 2012).

NO is produced by NOS (EC 1.14.13.39). NOS enzymes synthesize NO via hydroxylation of L-arginine to N^{ω}-hydroxy-L-arginine intermediate and NOS oxidizes N^{ω}-hydroxy-L-arginine to L-citrulline and NO (Figure 2-2).

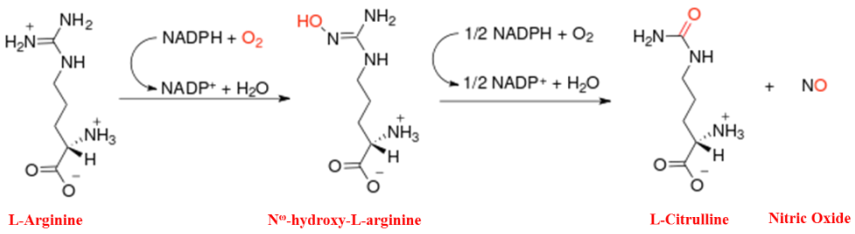

Figure 2-2 The NOS catalyzed reaction (Wegener & Volke, 2010)

NOS is a homo-dimeric enzyme consisting of two domains: a carboxy-terminal reductase domain and an amino-terminal oxidase domain (Figure 2-3). The reductase domain is composed of cofactor including flavin adenine dinucleotide (FAD) and flavin mononucleotide (FMN) and a binding site for co-substrate nicotinamide adenine dinucleotide phosphate (NADPH) and binding with calmodulin (CAM), which enhances electron transfer. The oxidase domain binds the substrate

arginine and contains the site for iron protoporphyrin IX (heme) and tetrahydrobioptrin (BH_4) (Smith, Fernhoff, & Marletta, 2012). A functional NOSs transfer an electron from NADPH through the FAD and FMN in the reductase domain of one monomer to the heme in oxygenase domain of the other monomer.

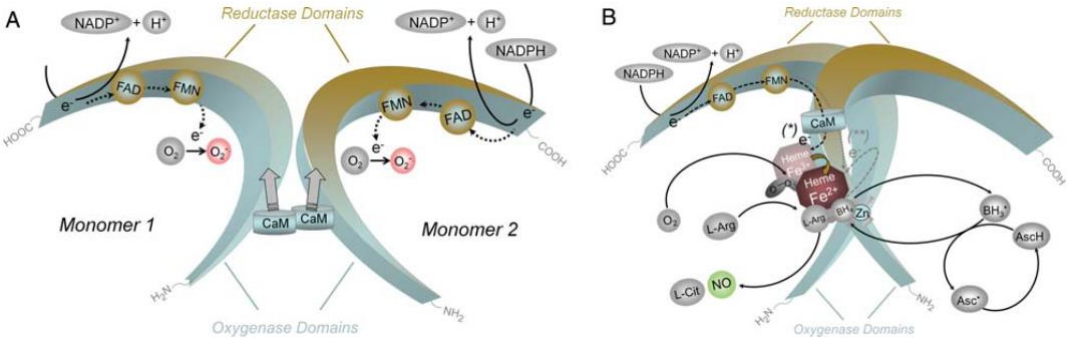

Figure 2-3 The structure and catalytic mechanisms of functional NOS (Forstermann & Sessa, 2012)

There are three isoforms of NOSs, neuronal NOS (nNOS or NOS I), endothelial NOS (eNOS or NOS III) and inducible NOS (iNOS or NOS II).

nNOS is a predominantly expressed in neuronal tissue and is constitutive-calcium and calmodulin dependent isoforms. nNOS has been involved in regulating physiological functions such as learning, memory, and neurogenesis (Forstermann & Sessa, 2012).

eNOS is a predominantly expressed in vascular endothelial cells and is constitutive calcium and calmodulin-dependent isoforms. NO that produced by eNOS play a crucial factor for the normal functional of the cardiovascular system including cardiac myocyte (Andrew & Mayer, 1999). In addition, NO amplifies all type of blood vessels by stimulating soluble guanylyl cyclase and rising cyclic GMP in smooth muscle cells (Forstermann & Sessa, 2012).

iNOS is expressed in many cell types that response to inflammation. The activated iNOS produces NO that has been described to have beneficial microbicidal, anti-viral, anti-parasital and anti-tumoral effects (Lee et al., 2012). Moreover, it seems to be involved in the pathophysiology of human diseases such as asthma, arthritis,

multiple sclerosis, neurodegenerative diseases, colitis, psoriasis, tumor development and septic shock (Kleinert, Pautz, Linker, & Schwarz, 2004).

The regulatory element that controls the transcription are in a 1.6 kb 5' flanking region of the mouse gene (Chu et al.,1998). The promoter of the mouse gene encoding iNOS (Figure 2-4) contains a TATA box and the potential binding site for numerous transcription factor involved in LPS-induced expression gene (Xie, Whisnant, & Nathan, 1993). Maximal induction of iNOS depends on two discrete regulatory regions upstream of the putative TATA box (Lowenstein et al., 1993). Region I (position -48 to -209) contains LPS-related responsive elements, including a binding site for octamer (Oct) (position -54 to -61), nuclear factor-κB (NF-κB) (position -76 to-85), tumor necrosis factor response element (TNF-RE) (position -102 to -109), nuclear factor for IL-6 (NF-IL6) (position -142 to -150) (Golding et al., 1996; Lowenstein et al., 1993; Xie et al., 1993). Region II (position -913 to -1029) contains IFN-responsive elements including gamma-activated sequences (GAS) (position -874 to -884 and -934 to -942), IFN-stimulated response elements (ISRE) (position -913 to -923 and -938 to -951) and NF-κB (position -974 to -960) (Gao et al., 1997; Golding et al., 1996; Kim et al., 1997; Lowenstein et al., 1993; Xie et al., 1993). Accordingly, both regions are contained binding site for NF-κB protein (Lowenstein et al., 1993). Furthermore, the transcription factor NF- κB seem to be a central target for mediating LPS induction of mouse iNOS gene (Lowenstein et al., 1993; Xie et al., 1993). In addition, it has been demonstrated that NF-κB downstream function as a core promoter, whereas the NF-κB upstream site does as an enhancer (Kim et al., 1997; Xie et al., 1993).

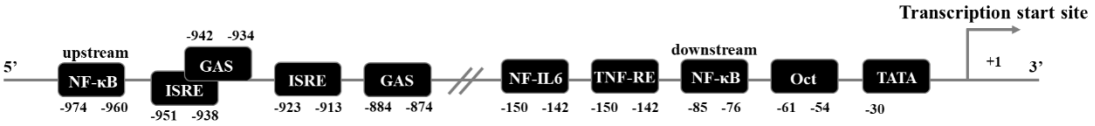

Figure 2-4 Schematic representation of the major conserved response elements in the murine iNOS promoter

2.6 Nitric oxide synthase inhibitor

Due to the consequence of NO in various pathological processes, NOSs are respected as an important pharmacological target. Inhibitors of NOSs can be classified according to the site of inhibitor binding to the NOS enzyme (arginine-binding site, mimic tetrahydrobiopterin cofactor, interacting directly with the heme and interacting with calmodulin or flavine cofactors) (Vitecek et al., 2012). There are four site of inhibitor binding to the NOS enzyme.

2.6.1 L-Arginine site

The arginine derivatives were first regarded as inhibitors for experimental use because they were expected to compete with arginine at the active site of NOS. Of these the most widely used have been N^G-monomethyl-L-arginine (L-NMMA), L-Nω-Nitroarginine (L-NNA) and its methyl ester prodrug (N^G-nitro-L-arginine methyl ester (L-NAME)) and aminoguanidine (Alderton, Cooper, & Knowles, 2001).

L-N^{ω}-Methylarginine (L-NMA or N^G-monomethyl-L-arginine (L-NMMA)) (Figure 2-5) is a product of the release of arginine-methylated proteins. L-NMA has been used widely in the laboratory to decrease NO bioavailability. The structure of L-NMA is very similar to arginine, it acts as a competitive inhibitor of all NOS. iNOS and nNOS slowly metabolize L-NMA in a NADPH- and BH_4- dependent manner to form N-hydroxyderivatives that is either processed to L-citrulline (Vitecek et al., 2012).

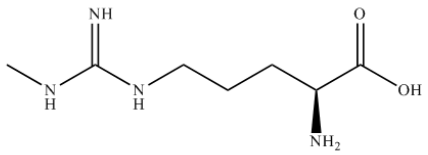

L-NMMA

Figure 2-5 The chemical structure of L-NMMA

L-Nω-Nitroarginine (L-NNA) (Figure 2-6) is one of NOS inhibitors. L-NNA is interacts with all NOSs noncovalently, its coupling with iNOS is instant and rapidly reversible with arginine. Nevertheless, the binding of L-NNA to eNOS and nNOS is dependent on time process with a relatively slow reversal.

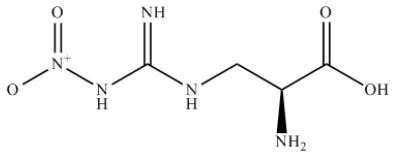

L-NNA

Figure 2-6 The chemical structure of L-NNA

L-N$^{\omega}$-nitroarginine methyl ester (L-NAME) (Figure 2-7) is an inhibitor of NOS. To become a fully functional inhibitor, L-NAME requires hydrolysis of the methyl ester by cellular esterase**.** There are report that L-NAME inhibits cGMP formation in endothelial cells (Wegener & Volke, 2010).

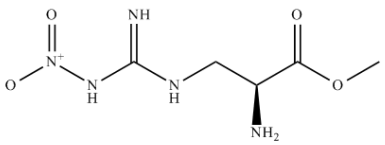

L-NAME

Figure 2-7 The chemical structure of L-NAME

Aminoguanidine (AG) (Figure 2-8) is a hydrazine derivative and the best characterized compound, which selectively decrease cGMP level product by iNOS. Moreover, AG is predominantly inhibitors of iNOS, with much less activity on the other isoforms (Wegener & Volke, 2010).

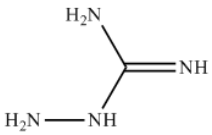

Aminoguanidine

Figure 2-8 The chemical structure of Aminoguanidine

2.6.2 Biopterin site

BH_4 binding site is located close to the arginine binding region and the heme cofactor. A range of compounds have been recognized which seem to interact with the pterin site with analogues, e.g. 4-amino-BH_4, BH_2, 7-NI, 2,4-diamino-5-(3-,4-dichlorophenyl) pyrimidine (Alderton, Cooper, & Knowles, 2001).

2.6.3 Heme-binding inhibitors

There are reports that numerous anti-fungal imidazoles exposed to inhibit NOS activity, not only interacting with the heme at the active site but also by acting in competition with CaM, this compound has also been shown to affect the assembly of iNOS monomers into active dimer, either promoting or inhibiting dimerization (Alderton, Cooper, & Knowles, 2001).

2.6.4 Flavoprotein and CaM inhibitors

A variety of inhibitors which have effects on difference of flavoproteins (e.g. diphenyleneiodonium) and CaM (e.g. trifluoperazine) have been shown to suppress NOS (Alderton, Cooper, & Knowles, 2001).

2.7 Prostaglandins

Prostaglandins (PGs) are derived from arachidonic acid and generated by COX (EC 1.14.99.1) (Figure 2-9). PGs are lipid autocoids that have a function on maintain homeostatic and inflammatory response. PGs play a crucial role in the generation of the inflammatory response. There are four bioactive prostaglandins, prostaglandin E_2 (PGE_2), prostaglandin D_2 (PGD_2), prostacyclin (PGI_2) and prostaglandin $F_{2\alpha}$ ($PGF_{2\alpha}$). COX exist in at least three isoforms. COX-1 is a constitutive enzyme that responsible for basal and expressed in many tissues and important in tissue homeostasis such as gastric epithelial cytoprotection (Lee et al., 2011). PGE_2 also has involved regulation of sodium reabsorption in the tubule and its acts as a counter-regulation factor under condition of increased sodium reabsorption (Hunter, Robison, & Gerbino, 2015). Under the physiological conditions, renal PGE_2 importantly to fluid metabolism and blood pressure regulation. COX-2 is rapidly

induced by inflammatory cells, hormones and growth factor and is the essential source of prostanoid formation in inflammation (Ricciotti & FitzGerald, 2011; Rouzer & Marnett, 2009). Lastly, COX-3 is a splice variant of COX-1 predominantly expressed in brain and heart (Legler, Bruckner, Uetz-von Allmen, & Krause, 2010). PGE_2 is one of PGs that is special interested because it is involved in all processes leading to the cardinal signs of inflammation include redness, pain and swelling (Legler et al., 2010).

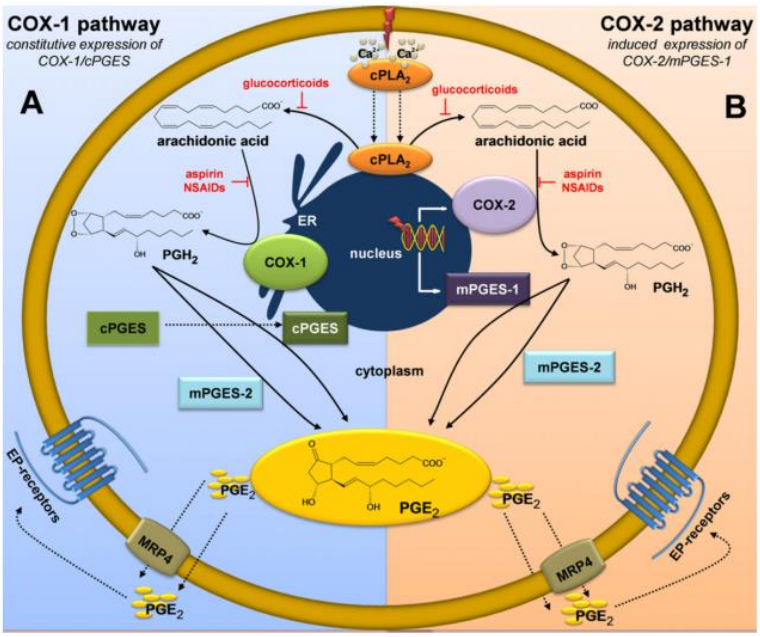

Figure 2-9 Biosynthesis of PGE_2 (Legler et al., 2010)

The regulation of COX-1 and COX-2 had been investigated. The data show that the promoter structure of COX-1 gene (Figure 2-10) consists of GC-rich, specificity protein 1 (SP-1), activating protein-1 (AP-1) and lacking of TATA are involving in transcription of the gene (Kraemer et al., 1992; Liu & Rose, 1996; Smith et al., 1996). The COX-2 promoter (Figure 2-11) contains a canonical TATA box and several inducible enhancer elements, such as NF-κB, cAMP response element (CRE), AP-1 and CCAAT enhancer binding protein (C/EBP) (Kang et al., 2006; Simmons, Botting, & Hla, 2004)

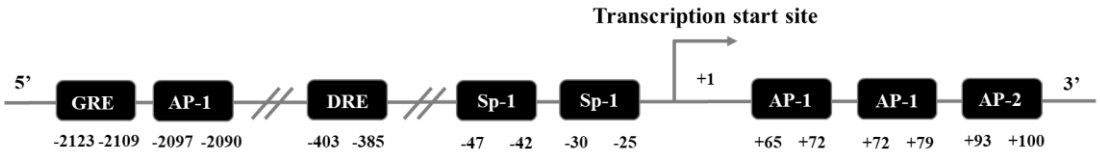

Figure 2-10 Schematic representation of the major conserved response elements in the murine COX-1 promoter

Figure 2-11 Schematic representation of the major conserved response elements in the murine COX-2 promoter

2.8 Cytokines

Cytokines are small proteins released by various different cell types including, monocytes, macrophages, dendritic cells, T-cells and B-cells (Turner, Nedjai, Hurst, & Pennington, 2014). Cytokines have been involved in balancing the innate and adaptive immune responses (Turner et al., 2014). It has been proposed that macrophages perhaps the main source of cytokines (Arango & Descoteaux, 2014). Pro-inflammatory cytokines are a group that produced for response to inflammatory stimuli. The essential pro-inflammatory cytokines include TNF-α, IL-1, IL-6, IL-8, IL-12, IL-18 and interferon-γ (IFN-γ) (Turner et al., 2014). Cytokines functions are communication to surrounding tissue to their receptor-mediated signaling pathways that present of infection or injury (Zhang & An, 2007). TNF-α and IL-1β are the important cytokines involved in the host physiology, such as fever and the acute phase reaction as well as contribution to inflammatory diseases. Moreover, anti-inflammatory cytokines are a group of cytokines that action to regulate of infection and inflammatory responses. The main anti-inflammatory cytokines include interleukin IL-1 receptor antagonist, IL-4, IL-10, IL-11, and IL-13 (Zhang & An, 2007).

2.9 Lipopolysaccharide and receptors

LPS is the major structure of the outer membrane present in almost all Gram -negative bacteria and one of the most effective inducers to initiate inflammation (Fujihara et al., 2003). In response to LPS, monocytes and macrophages produce biological response mediators, including pro-inflammatory cytokines, platelet activating factor, PGE_2 and NO (Fujihara et al., 2003). Moreover, macrophages are activated by LPS and trigger the cellular response that affects the transcription more than 1,000 different genes (Jerala, 2007).

The common structure of LPS can be classified into three regions (Figure 2-12). Lipid A is the highly hydrophobic domain and responsible for its endotoxic activities. It consists of two β(1-6)-linked D-glucosamine (GlcN or GlcN3N) residues carrying two phosphoryl groups (at positions 1 and 4′) which is recognized by Toll-like receptor 4 (TLR-4) and its co-receptor MD-2 on host cells (Erridge, Bennett-Guerrero, & Poxton, 2002; Maeshima & Fernandez, 2013). The core polysaccharide is divided into inner and outer core. The inner core is containing a high proportion of unusual sugar such as 3-deoxy-D-*manno*-oct-2-ulosonic acid (Kdo) and L-glycero-D-manno heptose (Hep). The outer core is consisting of the common sugars such as hexoses, hexosamines, glucose and galactose. A third region, O-polysaccharide or O-antigen is repeating subunits of one to eight monosaccharides. That response for an immune specificity of the bacterial cell (Erridge, Bennett-Guerrero, & Poxton, 2002).

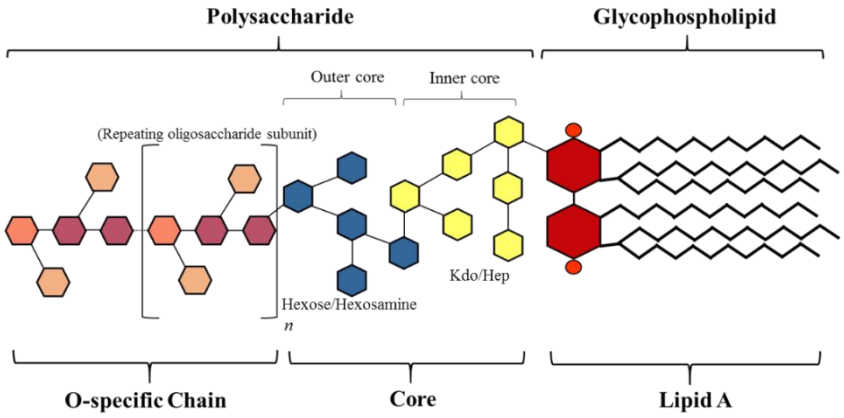

Figure 2-12 The structure of LPS (Modified from Erridge et al., 2002; Caroff et al., 2002)

There are various of inflammatory mediators that express in LPS-activated macrophages though transcription factor along with NF-κB and AP-1 (Fujihara et al., 2003). LPS activates macrophage via binding the LPS-receptor that is composed of CD14, Toll-like receptor 4 (TLR4), and myeloid differentiation protein-2 (MD-2) (Figure 2-13). LPS first binds to serum LPS binding protein (LBP), then transfer LPS to membrane-bound CD14 on monocytes and myeloid cells (Fujihara et al., 2003). CD14 is comprised of 10 copies leucine-rich repeats (LRR) motif, that is involved in ligand recognition and signal transduction (Fujihara et al., 2003). CD14 encourages LPS to the MD-2 and TLR4 receptor complex (Maeshima & Fernandez., 2013). MD-2 is a soluble protein from or associated with the extracellular domain of TLR4. MD-2 also plays a role in LPS recognition and regulates the cellular distribution of TLR-4 (Fujihara et al., 2003). TLR4 is a signaling transduction receptor that bind with the adaptor protein including myeloid differentiation factor 88 (MyD 88), IL-1 receptor-associated kinase (IRAK) and TNF receptor-activated factor 6 (TRAF6). TRAF6 was activated MAPKs that leading to activation AP-1 transcription factor and phosphorylation on inhibitor of κB (IκB) complex (Fujihara et al., 2003)

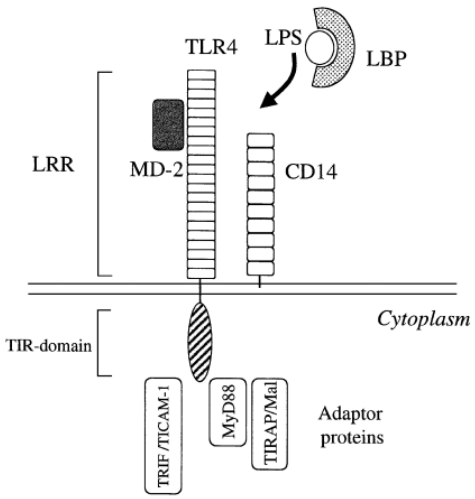

Figure 2-13 LPS receptor on macrophage (Fujihara et al., 2003)

2.10 Signaling pathway in inflammation

There are many of signaling pathways that involved in LPS-activated macrophages through TLR4 receptor complex such as NF-κB, mitogen activated protein kinases (MAPKs), phosphoinositide 3-kinase (PI3K)-Akt (Hawkins & Stephens, 2015; Kim & Choi, 2010; Lawrence, 2009). Moreover, Janus kinases (JAK)/ signal transducer of activation-1 (STAT1) is one of the pathways that responses to type I or type II interferons via IFNα/β receptor (Kaplan, 2013; Villarino, Kanno, Ferdinand, & O'Shea, 2015). All these pathways have significant role in host defense by regulating the major downstream signaling pathways in immune responses (Figure 2-14).

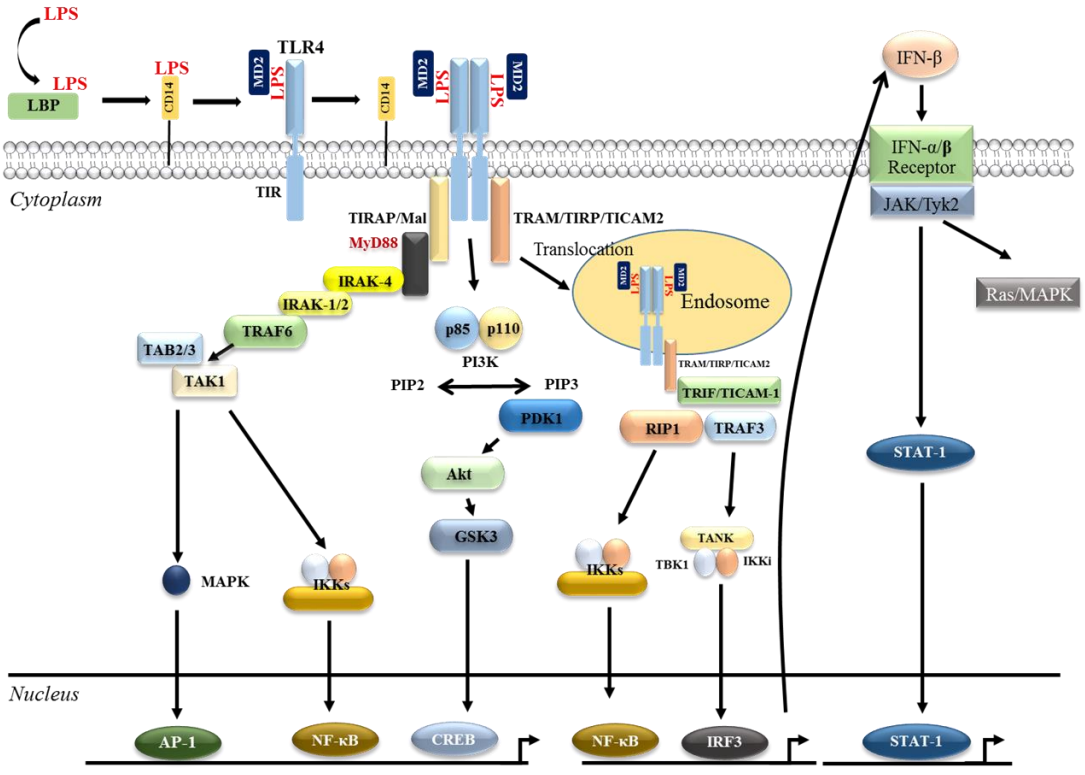

Figure 2-14 The diagram illustrate pathways that triggered by TLR and cytokines receptor

2.10.1 Nuclear factor (NF)-κB signaling pathway

TLR4 recognizes LPS and triggers downstream signaling cascades of inflammation. NF-κB is a crucial role not only inflammatory gene regulation and apoptosis but also in the development and processing of pathological pain (Hoesel & Schmid, 2013). NF-κB activation has been implicated in inflammatory diseases such as rheumatoid arthritis, atherosclerosis, asthma, multiple sclerosis and type I diabetes (Liu, Zhang, Joo, & Sun, 2017). The activation of NF-κB can be induced by various pathways. The classical, canonical pathway is important role for the activation of innate immunity and inflammation as well as inhibition of apoptosis (Figure 2-15) (Lawrence, 2009). This pathway involves stimulation of toll-like receptor (TLR), interleukin-1 receptor (IL-1R), tumor necrosis factor receptor (TNFR) and the signaling molecule are LPS, IL-1 and TNF-α. The activation is lead to phosphorylate of an IκB kinase (IKK) complex that the catalytically subunits IKK α and β (Niederberger & Geisslinger, 2008). Normally, NF-κB proteins in cytoplasm are associated with inhibitory protein as IκBs, whereas the main active form of NF-κB is a heterodimer composed of p65 and p50 subunits. NF-κB induction in response to pro-inflammatory stimuli involves the phosphorylation of IκBs by IKK complex. After IκB has been phosphorylated, it is ubiquitinated and degraded by 26S proteasome, and the resulting free NF-κB translocated to the nucleus, where it binds to κB binding sites in the promoter regions of target genes and induces the transcriptions of pro-inflammatory mediators and cytokines (Lawrence, 2009)

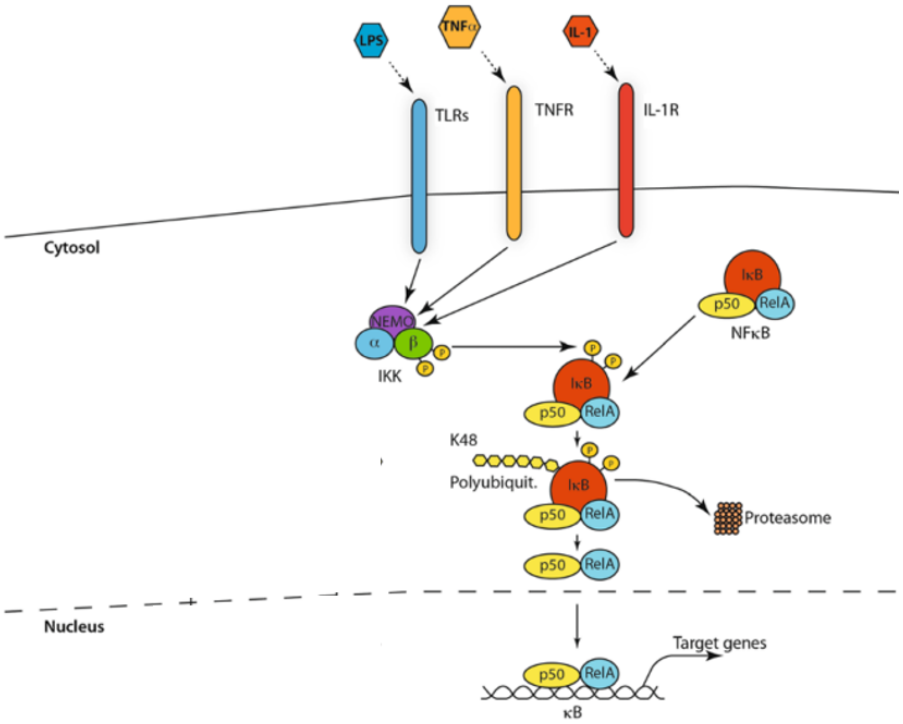

Figure 2-15 The canonical of NF-κB signaling pathway (Modified from Hoesel & Schmid, 2013)

2.10.2 Mitogen activated protein kinases (MAPKs) signaling pathways

MAPKs are a family of serine/threonine protein kinase that response to external stress signal with a range of cellular activities including cell proliferation, differentiation, survival, death and transformation (Kaminska, 2005). The mammalian MAPK consists of three main sub-families, JNKs, ERKs and p38-MAPK (Kim & Choi, 2010). Macrophage cells that induced by LPS causes stimulation of MAPK cascades via TLR4 and the pathway leading to activation of NF-κB. MAPKs are activated by signal to a cascade, MAP kinase kinase kinase (MKKK) are phosphorylated MAP kinase kinase (MKK) and MAPKs are phosphorylated by MKK (Figure 2-16) (Hommes, Peppelenbosch, & van Deventer, 2003).

There are two isoforms of ERK that are expressed to various extents in all tissues, with particularly high levels in the brain, skeletal muscle, thymus and heart. ERK1 and ERK2, these are often referred to as p42/p44 MAPK. It was found to be phosphorylated on tyrosine and threonine residues in response to growth factors.

ERK1/2 plays an important role in the regulator of cell proliferation (Cargnello & Roux, 2011). ERK signaling pathway activated through Elk1 and AP-1 transcription factor (Kim & Choi, 2010).

P38 MAPK is consisting of four isoforms including p38α, p38β, p38γ and p38δ. In most inflammatory cell, p38α plays a major role in the inflammation response. The activation of p38 MAPK is involve in iNOS expression in TNFα and IL-1β stimulated mouse astrocytes and in LPS-activated mouse macrophages. (Kaminska, 2005). P38 MAPK can regulate by phosphorylation several transcription factors including activating transcription factor-2 (ATF-2), GADD153 and myocyte enhancer factor 2C (MEF 2C) (Kaminska, 2005).

There are three JNK isoforms, JNK1, JNK2 and JNK3 (also known as SAPKγ, SAPKα, and SAPKβ). JNK1 and JNK2 have a broad tissue distribution, whereas JNK3 appears to be localized primarily to neuronal tissues, testis, and cardiac myocytes. The activation of JNK1 and JNK2 have been shown to play a crucial role to control proliferation of the cell, differentiation and apoptosis (Cargnello & Roux, 2011). JNK can regulated the pathway by signaling on transcription factor c-Jun and ATF-2 (Hommes et al., 2003)

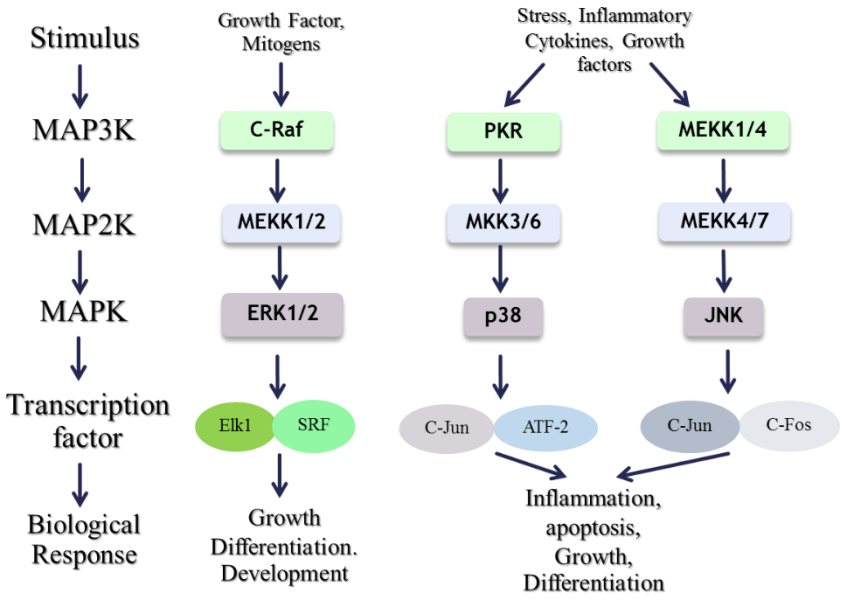

Figure 2-16 The activation of three main MAP kinases (Modification from Sweeney & Firestein, 2007)

2.11 Anti-inflammatory drugs

There are two anti-inflammatory medications that available on the market and are widely used in medicine including non-steroidal anti-inflammatory medications (NSAIDS) and steroids or corticosteroid. Both counteract the effects of PGE_2 which promote inflammation, fever and pain (Barnes, 2006).

In human, steroid use is based on a vertebrate's source and may constitute sex steroids, corticosteroids, and anabolic steroids. Corticosteroids are steroid hormones that acts on various systems such as inflammation, stress response, immune response, metabolism, and electrolyte levels. Corticosteroids are widely used to treat a variety of inflammatory, immune diseases, skin diseases tumors and joint pain (Barnes, 2006). Nowadays, the common use of corticosteroids (Figure 2-17) is in the treatment of asthma and other allergic diseases. Glucocorticoids act through glucocorticoid receptor to regulate transcription of various target genes. The anti-inflammatory effect of glucocorticoids is associated with the transcription factor NF-κB and AP-1, involved in activation of pro-inflammatory genes (Bosscher, 2000). Furthermore, glucocorticoids have been ascribed to their anti-inflammatory properties on the inhibition of phospholipase A_2 activity, an enzyme that hydrolyze phospholipids to arachidonic acid

(Ramamoorthy, 2016). However, use of corticosteroids has numerous side-effects. It also found the side effect particularly in children and when high inhaled doses are used. There are several case reports of side effects including dysphonia, oropharyngeal candidiasis, adrenal suppression, growth suppression, glaucoma and metabolic abnormalities (glucose, insulin, triglycerides) (Barnes, 2006). Moreover, long-term and higher dosage treatment of oral glucocorticoids is related to serious side effects including osteoporosis, Cushing syndrome and increased risk of cardiovascular disease (Coutinho & Neilson, 2011)

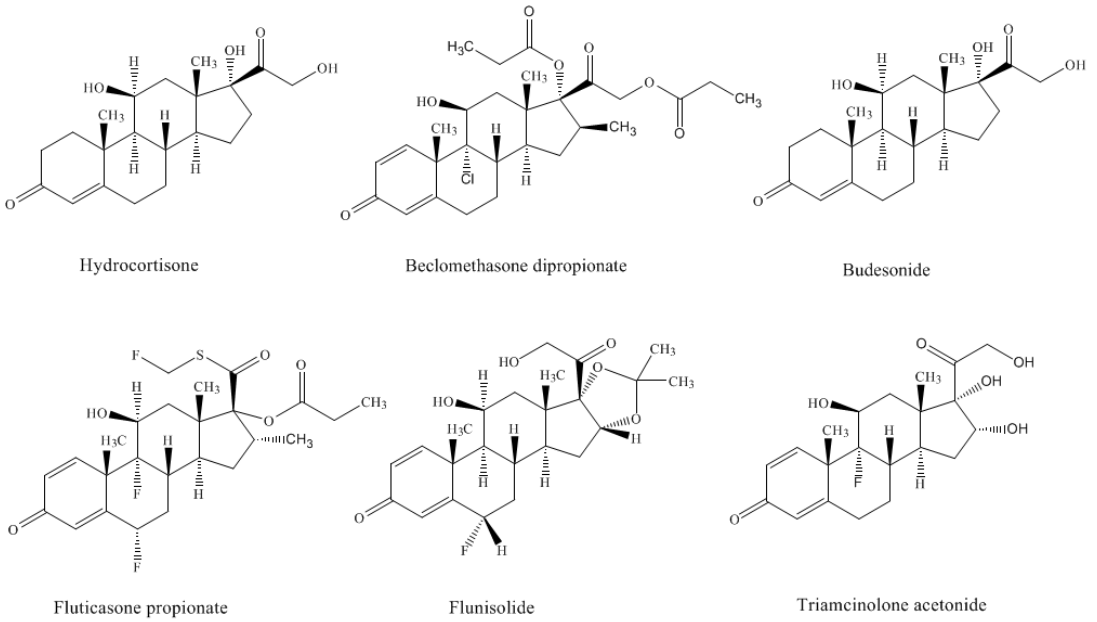

Figure 2-17 The Chemical structures of inhaled glucocorticoids

NSAIDs are used as therapeutics in the treatment of osteoarthritis (OA), rheumatoid arthritis (RA) and other inflammatory syndromes. The anti-inflammation of NSAIDs have been showed their ability to decreases pain and inflammation by inhibiting COXs (Ricciotti & FitzGerald, 2011). NSAIDs can be classified according to their affinity to COX selectively into 4 groups (Table 2-1) (Nowak, 2012) and their chemical structure into 9 groups (Table 2-2) (Calatayud, 2016). The COX inhibitor such as aspirin and indomethacin are the only clinical use NSAIDs that covalently modified the COX protein. The other NSAIDs act non covalently and most can be classified as either rapidly reversible, competitive inhibitors or slow and tight binding inhibitors (Rouzer &

Marnett, 2009). However, a range of side effect of which gastrointestinal toxicity including dyspepsia, peptic ulcers and ulcer perforations (De Groot et al., 2013). Apart from side effect on gastric intestinal tract, there are several reports on the renal effect of NSAIDs. PGE_2 have a function involved regulation of sodium reabsorption in the tubule and its acts as a counter-regulation factor under condition of increased sodium reabsorption. The most common renal effect of NSAIDs is the inhibition of PGE_2 synthesis by NSAIDs that can lead to increased sodium reabsorption, causing peripheral edema (Hunter, Robison, & Gerbino, 2015). Celecoxib is the selective COX-2 inhibitors, but it has been reported to increase a risk of stroke and heart diseases and also found the effect on renal function in patients who are considered to be at higher risk for NSAID-related adverse renal effects (Hunter et al., 2015). COXIBs is a drug that has the effect of inhibiting the COX-2 alone has side effects on the gastrointestinal tract less. However, it also found that there are serious side effects on the cardiovascular system. There is report that the use of NSAIDs such as naproxen and diclofenac increased risk of acute myocardial infarction in high-risk patients over the age of 50 years (Moodley, 2008).

Table 2-1 Classification of NSAIDs to their COX selectively

Class	Properties	Example
Group 1	NSAIDs that completely inhibit COX-1 and COX-2 with low selectively	Aspirin, diclofenac, ibuprofen, indomethacin, naproxen, piroxicam
Group 2	NSAIDs that inhibit COX-2 with a 5-50-fold selectively compared to COX-1	Celecoxib, meloxicam, nimesulide, etodolac
Group 3	NSAIDs that inhibit COX-2 with a selectively that is >50 times higher compared to COX-1	Refecoxib, NS-398
Group 4	NSAIDs that are weak inhibitors of both COX isoforms	5-aminosallicylic acid, sodium salicylate, sulfosalazine

Table 2-2 Classification of NSAIDs to their chemical structure

Derivatives	Examples
Salicylic acid	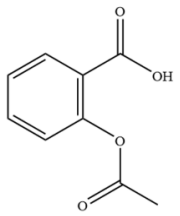 Aspirin **(Group 1)** 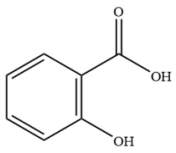 Salicylic acid **(Group 4)**
Propionic acid	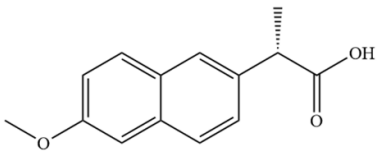 Ibuprofen **(Group 1)** 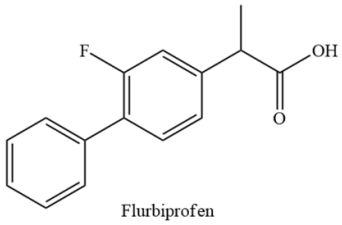 Flurbiprofen **(Group 1)** 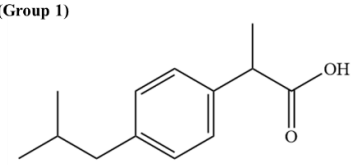 Naproxen **(Group 1)**
Acetic acid	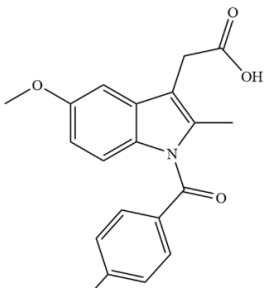 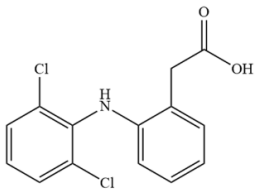 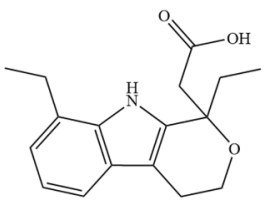 Etodolac **(Group 2)** 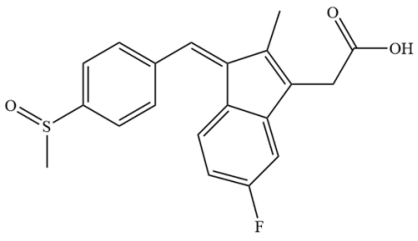 Sulindac

Table 2-2 (continued)

Derivatives	Examples
Enolic acid	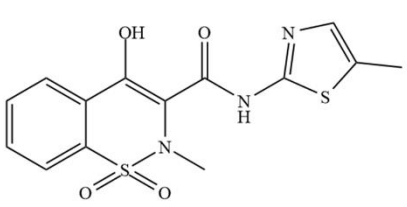 Meloxicam **(Group 2)** 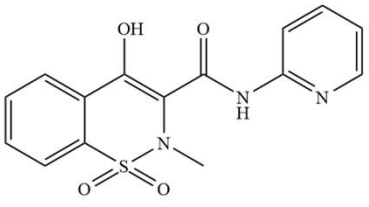 Piroxicam **(Group 1)**
Fenamic acid	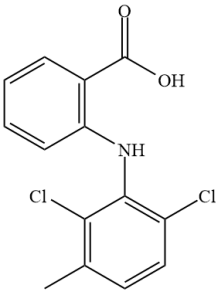 Meclofenamic acid 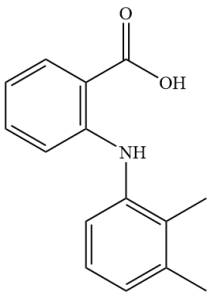 Mefenamic acid
Alkanones	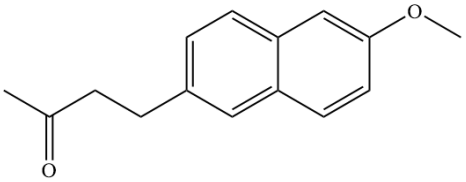 Nabumetone
Para-aminophenol	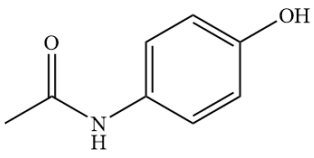 Paracetamol

Table 2-2 (continued)

Derivatives	Examples
Pyrazole	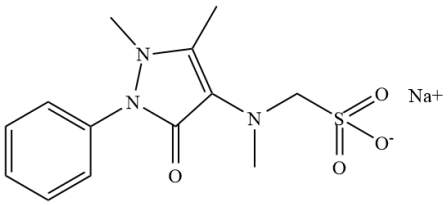 Metamizone
Diaryl heterocyclic	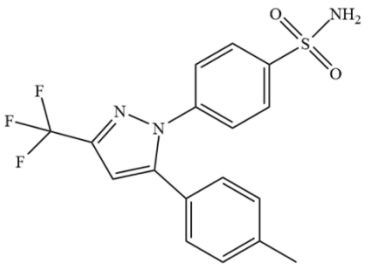 Celecoxib **(Group 2)** 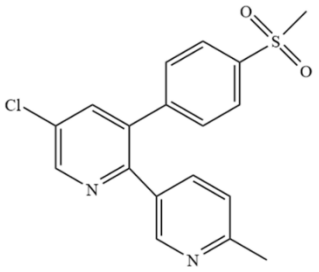 Parecoxib

2.12 Reviews on biological activities of triarylmethane

Triarylmethanes (TRAMs) have been reported to have multiple biological activities (Nair, Thomas, Mathew, & Abhilash, 2006). It has been showed that 4,4-dihydroxy-3,4-methylenedioxytriphenylmethane (Figure 2-18) had significant antiviral activity against herpes simplex virus type 1 (anti-HSV-1 activity) and less cytotoxicity in a plaque reduction assay (Mibu, Yokomizo, Uyeda, & Sumoto, 2005).

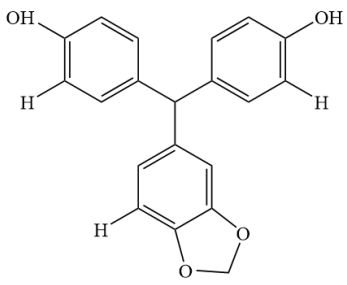

Figure 2-18 The structure of 4,4-Dihydroxy-3,4-methylenedioxytriphenylmethane

Parai, Panda, Chaturvedi, Manju, and Sinha (2008) reported a new series of anti-tubercular compounds that thiophene containing triarylmethane derivatives (Figure 2-19) have potent anti-microbial activity against *Mycobacterium tuberculosis* with the MIC of 3.12 µg/mL.

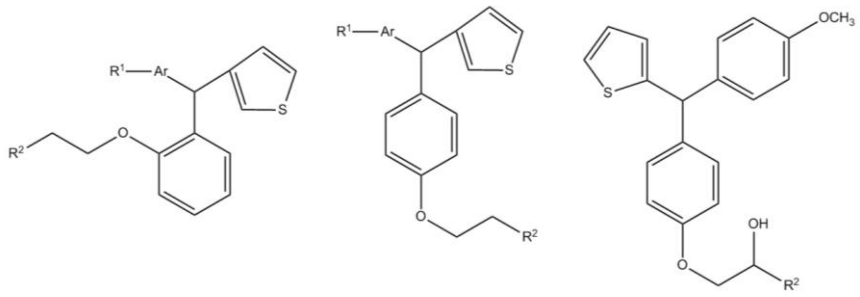

R^1 = m-OCH_3, o-OCH_3, p-SCH_3, p-Cl

R^2 = 1º, 2º and 3º amines

Figure 2-19 The structure of thiophene containing triarylmethane derivatives

Moreover, three newly triarlymethane synthesized compounds mono-piperazine modified CV (MPCV), di-piperazine modified CV (DPCV) and aliphatic amine-modified ethyl violet (AEV) (Figure 2-20) have the anti-bacterial effect against *Escherichia coli* (Li et al., 2014).

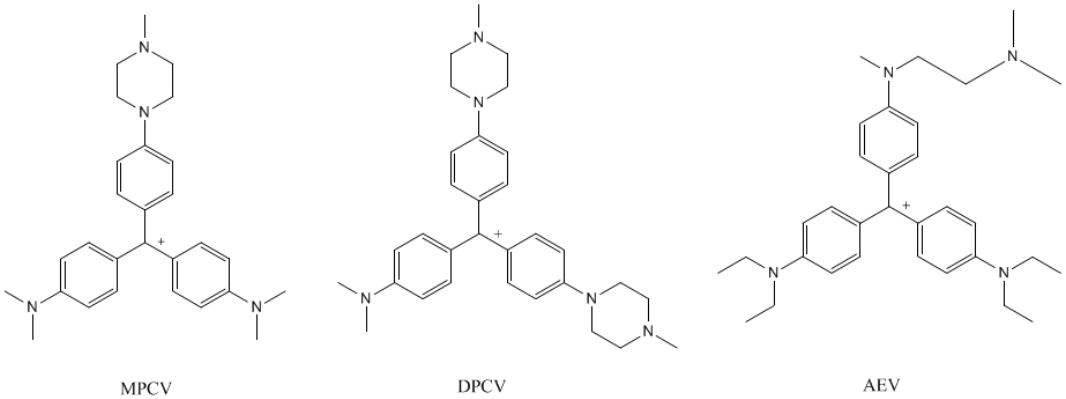

Figure 2-20 The structure of MPCV, DPCV and AEV

Al-Ghananeem et al. (2010) had synthesized 1-[(2-chlorophenyl)-diphenylmethyl]-1*H*-pyrazole (TRAM-34) (Figure 2-21) and investigated of microencapsulated on the potential immunosuppressant. The result showed encapsulation efficiency was 90 ± 1.9% and the percentage yield was found to be 91.5 ± 0.3%. Nevertheless, the oral bioavailability of TRAM-34 from the enteric microcapsules was still poor (1.7%) and the compound plasma concentration is below the therapeutic effective dose.

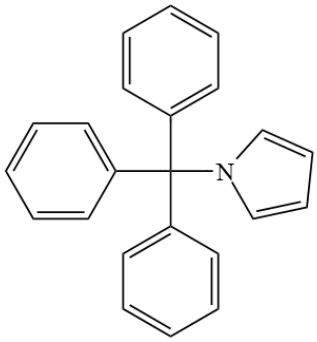

Figure 2-21 The structure of 1-[(2-chlorophenyl)-diphenylmethyl]-1*H*-pyrazole

There are several reports of anti-inflammatory activities of TRAMs. Jaratjaroonphong, Tuengpanya, Saeeng, Udompong, and Srisook (2014) studied the anti-inflammatory activity of the twenty-one newly synthesized of bis(heteroaryl)alkanes. Among them, bis[(5-methyl)2-furyl](4-nitrophenyl) methane (JJSD9) (Figure 2-22) exhibited the most potent inhibitory effect on NO production with IC_{50} values of 42.4 ± 1.3 μM. Moreover, JJSD9 inhibited of inducible nitric oxide synthase (iNOS) and cyclooxygenase-2 (COX-2) protein expression in LPS-stimulated cells in dose-dependent manner (Udompong, 2013).

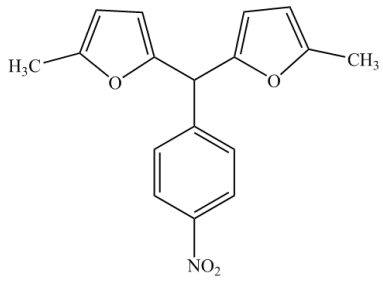

Figure 2-22 The structure of bis[(5-methyl)2-furyl](4-nitrophenyl) methane (JJSD9)

Duangked and Sawai (2014) investigated tris(5-ethyl-1H-pyrrol-2-yl) methane (JJST5) (Figure 2-23), a derivative of symmetrical triarylmethane suppressed LPS-induced NO production and PGE_2 with IC_{50} value 46.04 ± 3.41 μM and 23.06 ± 5.61 μM, respectively. However, the potent on NO production is similarly to aminoguanidine. Furthermore, JJST5 did not inhibit COX-1 mRNA expression. Moreover, JJST5 inhibited phosphorylation of JNKs, while did not effect nuclear translocation of NF-κB p65.

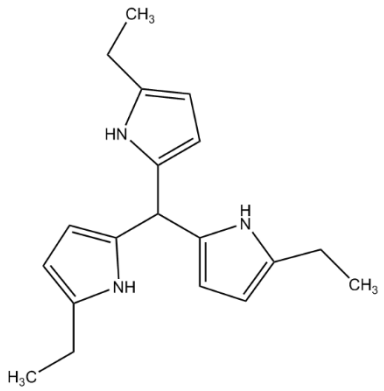

Figure 2-23 The structure of tris(5-ethyl-1H-pyrrol-2-yl) methane (JJST5)

Siritanyong and Tongyen (2015) studied tert-butyl-2-((5-methylfuran-2-yl) (4-nitrophenyl) methyl)-1H-pyrrole-1-carboxylate (JJSRUN16) (Figure 2-24), an unsymmetrical triarylmethane potently decreased NO production with IC_{50} value 6.77 ± 1.79 μM in LPS-stimulated macrophages. While JJSRUN16 did not affect the production of PGE_2 and COX-2. Also, the compound did not decrease the expression of COX-1 gene. Furthermore, the compound inhibited nuclear translocation of NF-κB p65 subunit into the nucleus, decreased phosphorylation of c-Jun N-terminal kinase (JNKs) and p38-mitogen activated protein kinase (p38-MAPK) but not extracellular signal-regulated kinases (ERKs).

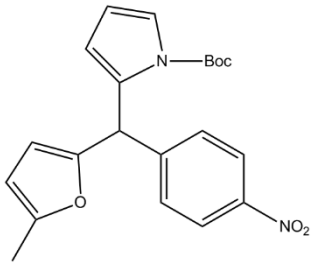

Figure 2-24 The structure of studied tert-butyl2-((5-methylfuran-2-yl) (4-nitrophenyl) methyl)-1H-pyrrole-1-carboxylate (JJSRUN16)

2.13 Reviews on biological activities of fluorinated compounds

Currently, there are more than 138 commercially available fluorine containing drugs (El-Feky, Thabet, & Ubeid, 2014). There have been extensively studied of pharmacological activities, such as phosphodiesterase inhibitors, anti-parasitic agents (especially anti-malaria's), anti-cancer (such as kinases) and anti-bacterial compounds (Ismail, 2002).

Isanbor and O'Hagan (2006) reviewed the anti-inflammatory drugs that have fluorine-containing such as dexamethasone and fluticasone propionate (Figure 2-25), which are widely used for inflammatory diseases and to alleviate pains associated with certain cancers. Furthermore, there are the fluorinated non-steroidal anti-inflammatory drugs (NSAID) e.g. flufenamic acid, niflumic acid, diflunisal, salindac sulfide, L-88,607 and fluoroindole-N-sulfonyl acids. However, the use of NSAIDs have some of side effects e.g. GI breeding.

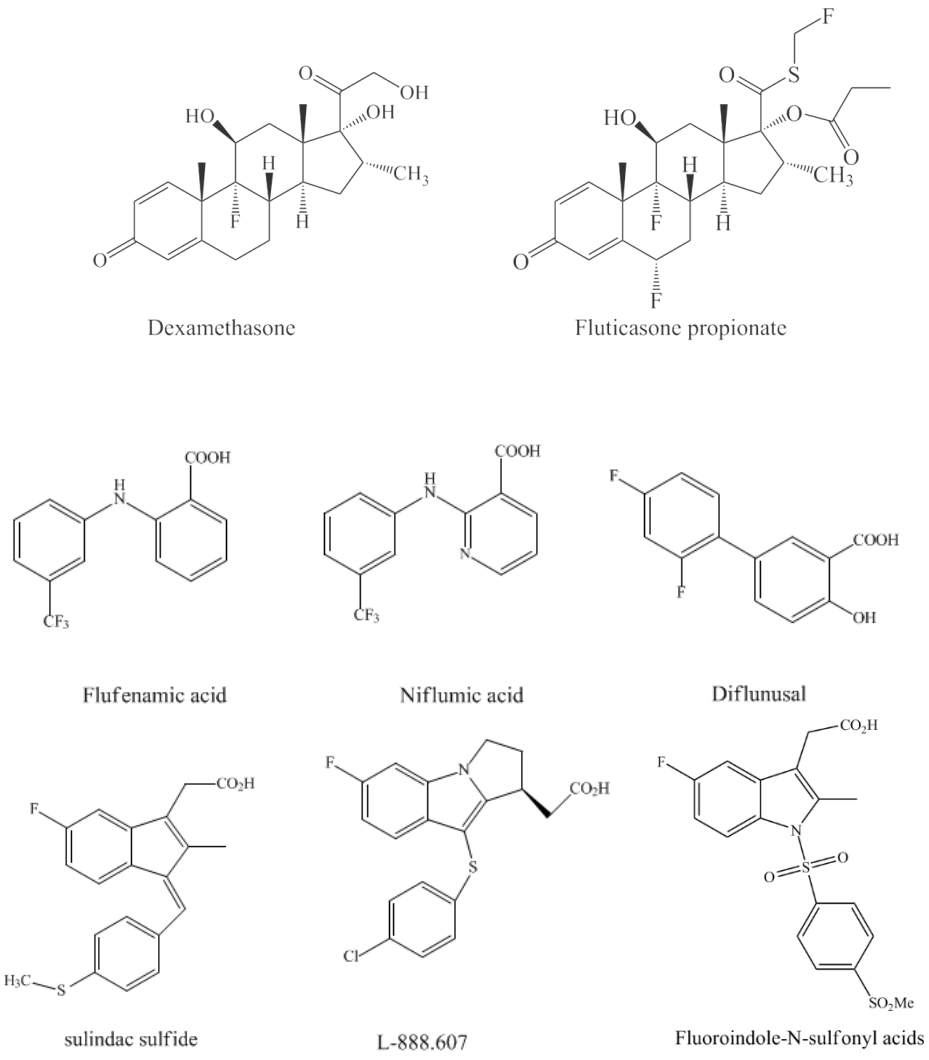

Figure 2-25 The structure of anti-inflammatory drugs containing fluorine atom

Kalkhambkar et al. (2008) synthesized a series of new fluorinated coumarins. The anti-inflammatory was determined by formalin-induced rat paw edema method. The result showed that most of the compounds had significant anti-inflammatory activity on NO inhibition of some coumarin derivatives (Figure 2-26). Moreover, 1-aza coumarins derivatives showed 85% and 80% inhibition. It is interesting that the present of fluorine at 4'-position induces better activity than the other halogenated compounds.

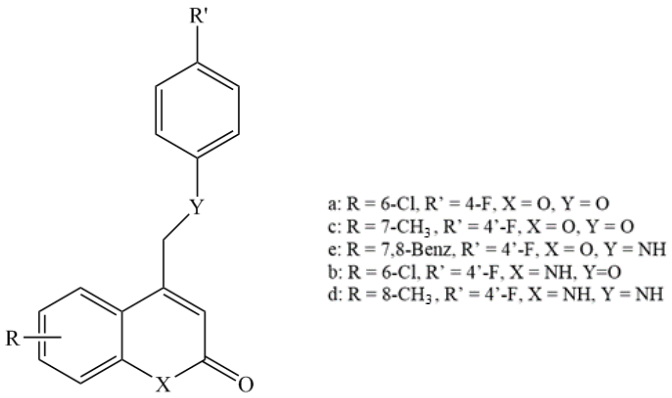

Figure 2-26 The structure of fluorinated coumarins

Esfahanizadeh et al. (2014) synthesized analogs of fluorinated p-aminosalicylic acid (PAS), thioacetazone and pyrazinamide compounds and evaluated theier activities against *M. tuberculosis.* The result showed that, the best compound is the thiacetazone substituent with fluoro on position 3 (Figure 2-27). Moreover, they suggested fluorine has the smallest size and the strongest electronegativity from the other hand of the halogen atoms. From its nature, it has many capabilities such as steric requirements at enzyme receptor site, increased lipid solubility effect to the enhancing rate of absorption and transport of drugs and increased oxidative and thermal stability.

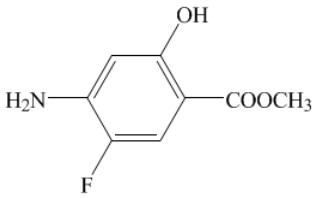

Figure 2-27 The structure of 4-amino-5-fluorosalicylic acid

El-Feky et al. (2015) synthesized the novel fluorinated quinoline incorporated benzimidazole and tested for their anti-inflammatory activities and ulcerogenic effect (Figure 2-28).

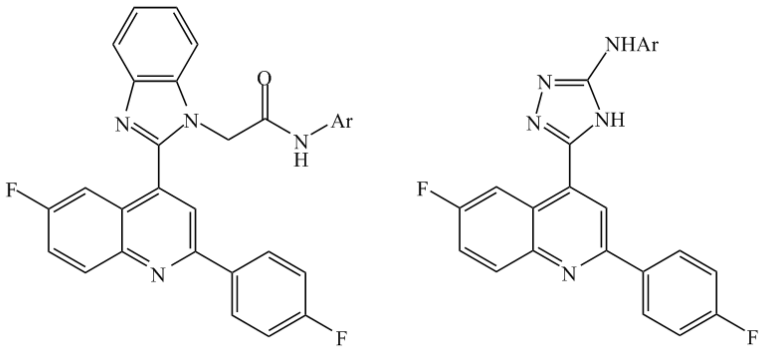

Ar = $C_6H_4OCH_3$-4
Ar = $C_6H_4OCH_3$-2
Ar = $C_6H_4CH_3$-2
Ar = $C_6H_4CH_3$-4
Ar = $C_6H_4COCH_3$-4
Ar = C_6H_5
Ar = C_6H_4Cl-4
Ar = C_6H_4Br-4
Ar = $C_6H_4CH_3$-4
Ar = $C_6H_4OCH_3$-4

Figure 2-28 The structure of fluorinated quinolone incorporated benzimidazole derivatives

CHAPTER 3

RESEARCH METODOLOGY

An overview of experiment

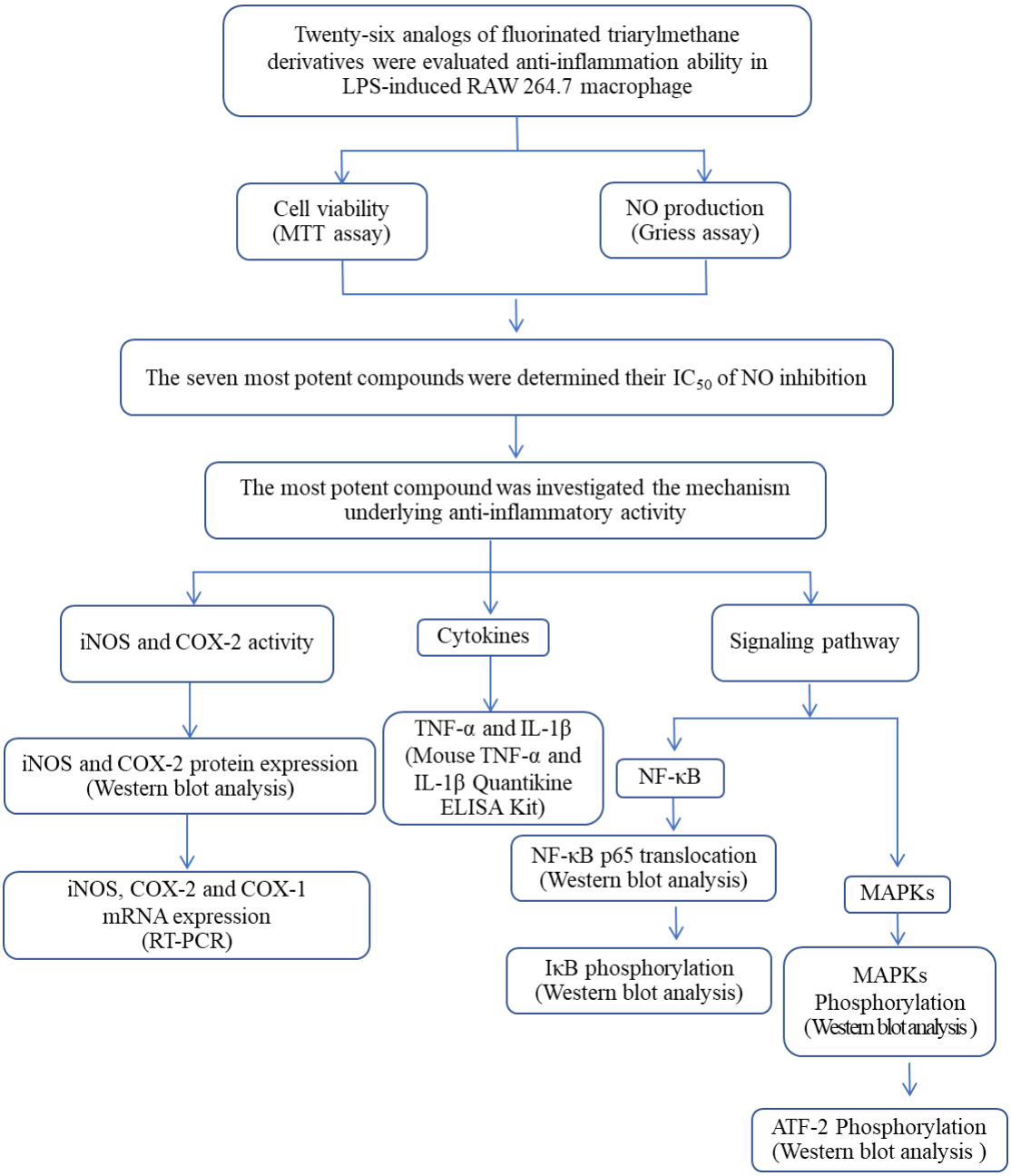

Part I: Screening for inhibitory effect on NO and PGE_2 production of fluorinated triarylmethane derivatives in RAW 264.7 macrophage cells

3.1 Materials and equipment

3.1.1 Equipments

1. Biological Safety Cabinet (BSL 2) (NU-440, Nuaire, USA)
2. 24 wells plate (Corning, USA)
3. 96 wells plate (Corning, USA)
4. 100 millimeters plate (Corning, USA)
5. Centrifuge (K240R, Centurion Scientific, UK)
6. CO_2 incubator (CB210, Binder, Germany)
7. Digital water bath (WB-22, Wise Bath, South Korea)
8. Hemocytometer (Blau Brand, Germany)
9. Inverted Microscope (Olympus IX70, Japan)
10. Microplate readers (Versa max, USA)

3.1.2 Chemicals

1. Aminoguanidine bicarbonate (Sigma, USA.)
2. D-glucose (Sigma, USA.)
3. Dimethoxy sulfoxide, DMSO (Fisher Chemical, UK)
4. Di-sodium hydrogenphosphate, NH_2PO_4 (Carlo Erba, Germany)
5. Dulbecco's modified eagle medium with phenol red (Gibco, USA.)
6. Dulbecco's modified eagle medium without phenol red (Sigma, USA.)
7. Fetal bovine serum, FBS (Gibco-Invitrigen, USA.)
8. Lipopolysaccharide, LPS from *Escherichia coli* 0111: B4 (Sigma, USA.)
9. N-(1-napthyl) ethylene diamine dihydrochloride (Sigma-Aldrich, USA.)
10. Penicillin/Streptomycin (Gibco, USA.)
11. Sodium nitrate (Sigma-Aldrich, USA.)
12. Sodium bicarbonate, $NHCO_3$ (Sigma, USA.)
13. Sterile distilled water (A.N.B. Laboratory, Thailand)
14. Sulfanilamide (Sigma-Aldrich, USA.)
15. Thiazoryl blue tetrazolium bromide, MTT (Sigma, USA.)

3.2 Methods

3.2.1 Fluorinated triarylmethane used in this study

Twenty-six analogs of fluorinated triarylmethane was synthesized by Assoc. Prof. Dr. Jaray Jaratjaroonphong and co-workers, Department of Chemistry, Faculty of Science, Burapha University. The chemical names and structures are displayed in table 3-1.

3.2.2 Chemical preparation

Fluorinated triarylmethane derivatives were dissolved in dimethyl sulfoxide (DMSO) as a stock solution at 50 mM and filtered by 0.22 µm nylon syringe filter and kept at -20ºC before used.

3.2.3 Cell culture

RAW 264.7 cells, a murine macrophages cell line were cultured in DMEM containing 25 mM D-glucose, 100 U/ml of penicillin, 100 µg/ml of streptomycin and 10% heat-inactivated FBS. Cells were incubated at 37 ºC in 5% CO_2 and sub cultured by scraping (Srisook et al., 2015).

Table 3-1 The chemical structure of fluorinated triarylmethane derivatives used in this study.

Compound	Structure
JJAF1 6-fluoro-3-(phenyl(2,4,5-trimethoxyphenyl)methyl)-1H-indole	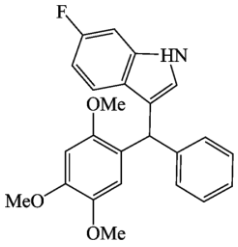
JJAF2 6-fluoro-3-((5-methylfuran-2-yl)(phenyl)methyl)-1H-indole	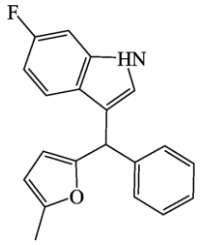
JJAF3 6-fluoro-3-((5-methylfuran-2-yl)(4-nitrophenyl)methyl)-1H-indole	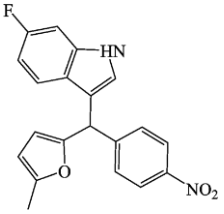
JJAF4 4-((6-fluoro-1H-indol-3-yl)(phenyl)methyl)-N,N-dimethylaniline	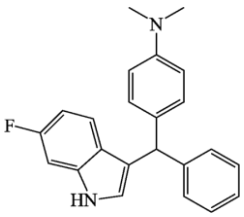
JJAF5 4-((4-fluorophenyl)(1H-indol-3-yl)methyl)-N,N-dimethylaniline	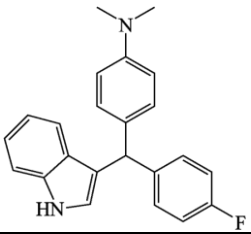
JJAF6 3,3'-((4-fluorophenyl)methylene)bis(1H-indole)	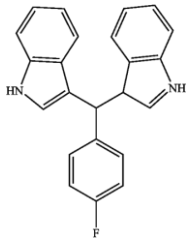

Table 3-1 (continued)

Compound	Structure
JJAF7 tris(6-fluoro-1H-indol-3-yl)methane	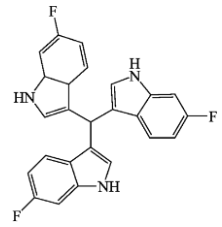
JJBF1 2,2'-((2-fluorophenyl)methylene)bis(1,3,5-trimethoxybenzene)	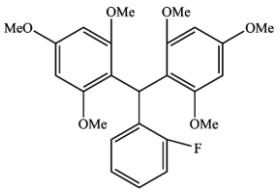
JJBF2 2,2'-((3-fluorophenyl)methylene)bis(1,3,5-trimethoxybenzene)	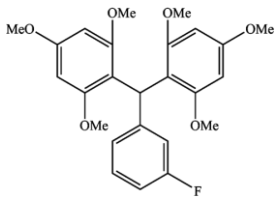
JJBF3 2,2’-((4-fluorophenyl)methylene)bis(1,3,5-trimethoxybenzene)	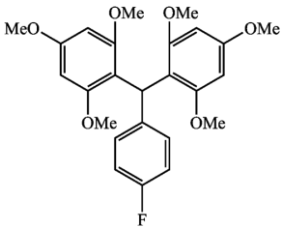
JJBF4 2,2'-((2,4-difluorophenyl)methylene)bis(1,3,5-trimethoxybenzene)	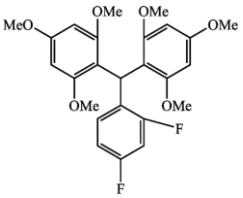
JJBF5 2,2'((3(trifluoromethyl)phenyl)methylene)bis(1,3,5-trimethoxybenzene)	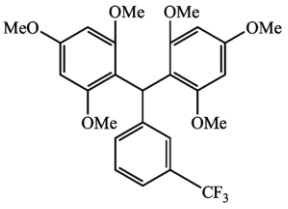

Table 3-1 (continued)

Compound	Structure
JJBF6 5,5'-((4-trifluoromethyl)phenyl)methylene) bis(1,3,5-trimethoxybenzene)	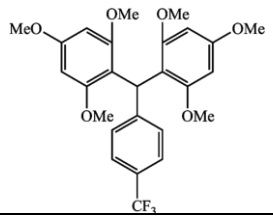
JJBF7 5,5'-((2-fluorophenyl)methylene)bis(1,2,4-trimethoxybenzene)	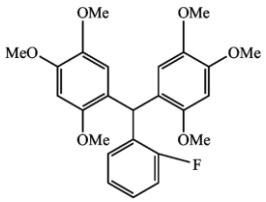
JJBF8 5,5'-((3-fluorophenyl)methylene)bis(1,2,4-trimethoxybenzene)	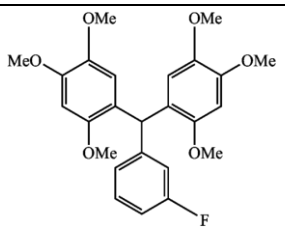
JJBF9 (5,5'-((4-fluorophenyl)methylene)bis(1,2,4-trimethoxybenzene))	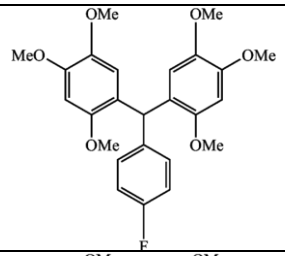
JJBF10 5,5'-((2,4-difluorophenyl)methylene)bis(1,2,4-trimethoxybenzene)	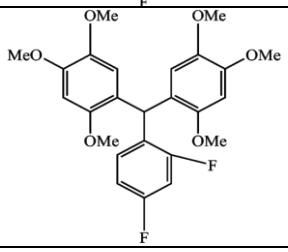
JJBF11 5,5'-((4-trifluoromethyl)phenyl)methylene) bis(1,2,4-trimethoxybenzene)	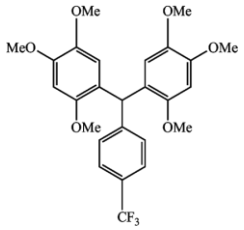

Table 3-1 (continued)

Compound	Structure
JJBF12 5,5'-((3-trifluoromethyl)phenyl)methylene) bis(1,2,4-trimethoxybenzene)	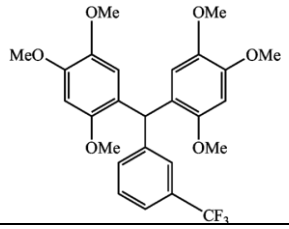
JJBF13 4,4'-((2-fluorophenyl)methylene)bis(1,2,3-trimethoxybenzene)	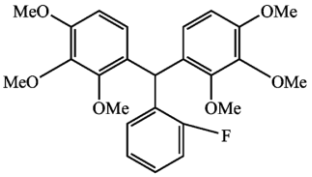
JJBF14 4,4'-((3-fluorophenyl)methylene)bis(1,2,3-trimethoxybenzene)	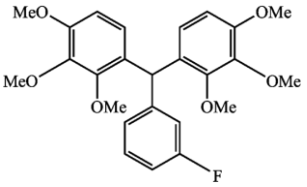
JJBF15 4,4'-((4-fluorophenyl)methylene)bis(1,2,3-trimethoxybenzene)	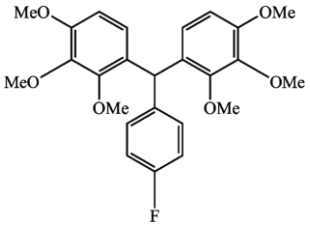
JJBF16 4,4'-((2,4-difluorophenyl)methylene)bis(1,2,3-trimethoxybenzene)	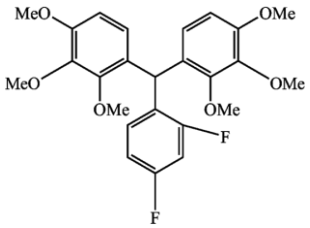
JJBF17 4,4'-((4-(trifluoromethyl)phenyl)methylene)bis (1,2,3-trimethoxybenzene)	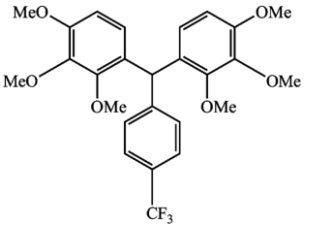

Table 3-1 (continued)

Compound	Structure
JJBF18 4,4'-((3-(trifluoromethyl)phenyl)methylene) bis(1,2,3-trimethoxybenzene)	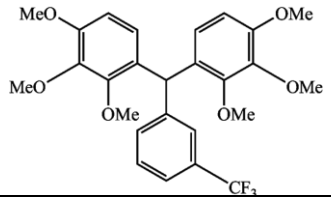
JJCF1 4,4'-((4-fluorophenyl)methylene)bis(N,N-dimethylaniline)	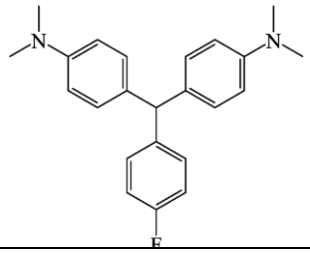

3.2.4 Cell viability test by MTT assay

The cell viability of the fluorinated triarylmethane on cultured cells was determined by MTT assay as described by Srisook et al., 2015. MTT salt was reduced to formazan by active dehydrogenase enzyme in viability cell. RAW 264.7 cells were seeded into a 24 well plate (1.5×10^5 cells/well). After an overnight growth, cells were treated with fresh DMEM containing fluorinated triarylmethane derivatives at 50 µM for 24 hours. At the end of the treatment period, culture media was discarded and 500 µl of DMEM containing 0.1 mg/mL MTT was added to each well. The cells were incubated in 37 ºC for 2 hours and the media was removed by aspiration. The formazan salt was dissolved by DMSO. At last, 200 µL formazan solution was transferred to a microplate and measured at 550 nm using a microplate reader. The formation of formazan is ratio to the number of living cells. Percentage of cell viability was expressed as: (absorbance of treated well/absorbance of control unstimulated cells well) × 100.

3.2.5 Determination of nitrite concentration

Nitrite is a stable product of NO oxidation, a major pro-inflammatory mediator. Cells were dispensed into a 24-well plate (1.5×10^5 cells/well) and incubated for 24 hours. The cells were treated with 50 µM of fluorinated triarylmethane derivatives or 50 µM of aminoguanidine (inhibitors of iNOS activity) in the presence or absence 1 µg/mL of LPS in phenol red-free DMEM for 24 hours. The culture media was collected and centrifuged at 9,500 g for 5 minutes at 4 ºC. 100 µl of culture media supernatant was collected and mixed with 100 µL of Griess reagent (0.1% N-(1-naphtyl)-ethylenediamine and 1% sulfanilamide in 5% orthophosphoric acid). They were incubated for 10 minutes at the room temperature. Next, the amount of azo compound was followed by absorbance reading at 546 nm. Nitrite concentration was determined from a standard curve of sodium nitrite that made up in phenol red-free DMEM (Srisook et al., 2015). Percentage of NO production was determined from: (nitrite concentration of treated cells/nitrite concentration of LPS-stimulated cells) × 100. Percentage of NO inhibition was calculated from: 100 - % of NO production.

3.2.6 Statistical analysis

All experiments were replicated at least three times independent experiments. The data was presented as the mean ± S.D. and analyzed statistical significance by analysis of variance (ANOVA), followed by Tukey's t test for multiple comparison. A value of $p < 0.05$ was considered to be significant.

Part II: Investigation of mechanism underlying the anti-inflammatory effect of the most potent fluorinated triarylmethane derivative in LPS-activated RAW 264.7 macrophages

3.3 Materials

3.3.1 Equipments

1. Western blot transfer chamber (Mini Trans-Blot Cell, Amercham bioscience, USA.)
2. Electrophoresis chamber (Mini Protein 3 cell, Bio-Rad, USA.)
3. Hyper cassette TM (Amersham Biosciences, USA.)
4. Immobilon-P Transfer Membrane (PVDF), 0.45 µm pore size (Millipore Corporation, USA.)
5. Medical X-Ray Cassette (Kodak, USA.)
6. PCR machine (Thermo hybaid, UK.)
7. Real-time PCR machine (CFX96TouchTM Real time PC R00, Bio-Rad, USA.)
8. Thermo Cycle (Thermo Hybrid, UK.)
9. UV Trans illuminator machine (model TVC-312A, Spectroline, USA.)
10. UV–VIS Spectrophotometer (UV-2501PC, SHIMADZU, Japan)

3.3.2 Chemicals

1. Anti-rabbit IgG (H+L) HRP conjugate antibody (Cell Signaling Technology, USA.)
2. 5X Bradford Dye Reagent (Bio-Rad, USA.)
3. 6X DNA Loading buffer (Promega, USA.)
4. Acrylamide (Sigma-Aldrich, USA.)
5. Agarose (Gene Pure LE, USA.)
6. Ammonuim persulfate (APS) (Plusone, Sweden)
7. Blot Stripping Buffer (Thermo Sciencefic, USA.)
8. Bovine serum albumin (BSA) (Thermo Sciencefic, USA.)
9. CL-X Posure Flim (Thermo Sciencetific, USA.)
10. Developer and replenisher solution (Kodak, USA.)
11. DL-1,4-Dithiothreitol (DTT) (Acros Organics, USA.)

12. Ethelenediaminetetra acetic acid disodium salt, EDTA (Carlo Erba, Germany)
13. Fixer and replenisher (Kodak, USA.)
14. Glycerol (Sigma-Aldrich, USA.)
15. Glycine (Research Organic, USA.)
16. Halt phosphatase inhibitor cocktail (Thermo scientific, USA.)
17. Halt protease inhibitot cocktail (Thermo scientific, USA.)
18. Illustra RNAspin Mini RNA Isolation Kit (GE Healthcare, UK)
19. Indomethacin (Sigma-Aldrich, USA.)
20. 5x iScript Reverse Transcription Supermix for RT-qPCR (Bio-Rad, USA.)
21. 2x iTaq™ Universal SYBR Green Supermix (Bio-Rad, USA.)
22. Methanol, ASC Grade (Honeywell, Korea)
23. Mouse anti COX-2 monoclonal IgG1 (BD Biosciences, USA.)
24. Mouse anti iNOS monoclonal IgG1 (BD Biosciences, USA)
25. Mouse anti phosphor-IκBα (Ser32/36) (5A5) monoclonal antibody (Cell Signaling Technology, USA.)
26. Mouse anti phospho-SAPK/JNK (Thr183/Tyr185) monoclonal antibody (Cell Signaling Technology, USA.)
27. Mouse TNF-α Quantikine ELISA Kit (R&D systems a biotechne brand, USA.)
28. Mouse IL-1β/IL-1F2 Quantikine ELISA Kit (R&D systems a biotechne brand, USA.)
29. Nonidet P-40 (Bio basic, Canada)
30. Potassium chloride (Carlo Erba, USA.)
31. Prostaglandin E_2 Enzyme Immunoassay Kit (Arbor Assay, USA.)
32. Rabbit anti ERK1(K-23) polyclonal antibody (Santa Cruz Biotechnology, USA.)
33. Rabbit anti GAPDH monoclonal IgG (Cell Signaling Technology, USA.)
34. Rabbit anti Lamin A polyclonal antibody (Santa Cruz Biotechnology, USA.)

35. Rabbit anti NF-κB p65 polyclonal antibody (Cell Signaling Technology, USA.)
36. Rabbit anti p38α (C-20) polyclonal antibody (Thermo Sciencefic, USA.**)**
37. Rabbit anti phospho-ATF-2 (Thr71) polyclonal antibody (Cell Signaling Technology, USA.)
38. Rabbit anti phospho-p38 MAP Kinase (Thr180/Tyr182) polyclonal antibody (Cell Signaling Technology, USA.)
39. Rabbit anti phospho-p44/42 MAPK (ERK1/2) (Thr202/Tyr204) polyclonal antibody (Cell Signaling Technology, USA.)
40. Rabbit anti SAPK/JNK polyclonal antibody (Cell Signaling Technology, USA.)
41. Skim Milk Powder (Fluka, Switzerland)
42. Sodium bicarbonate (Sigma-Aldrich, USA.)
43. Sodium chloride (Carlo Erb, Germany)
44. Sodium dodecyl sulfate (Ajax finechem, Australia)
45. SuperSignal® West Pico Chemiliminescent Substrate (Thermo Sciencetific, USA.)
46. TransAM™ NF-κB p65 Transcription kit assay (Active-Motif, USA.)
47. Tween-20 (ScharlauChemie S.A., Spain)
48. UltraPure™ DNase, RNase free Distilled Water (Gibco, USA.)
49. UltraPure™ TEMED (Invitrogen, USA.)
50. β-mercaptoethanol (Sigma-Aldrich, USA.)

3.4 Methods

3.4.1 Calculation IC_{50} value of nitric oxide inhibition of the seven most potent compounds

IC_{50} represents the concentration of compounds that is required for 50% inhibition. The cells were treated with various concentration of five selected fluorinated triarylmethane derivatives in the presence or absence 1 μg/mL of LPS in phenol red-free DMEM for 24 hours. Culture media was collected and determined the nitrite concentration by Griess reaction as described in method in 3.3.5, Part I**.** IC_{50}

value was determined from a linear equation of % inhibition of NO and concentration of selected compounds.

3.4.2 Determination of PGE_2 concentration

The concentration of PGE_2 in culture media from LPS-induced RAW 264.7 was determined using PGE_2 competitive enzyme immunoassay kit (Arbor assays, USA.) according to manufacturer's instructions. Briefly, RAW 264.7 macrophages were seeded into a 24 well plate (1.5×10^5 cells/well) and incubated for 24 hours. The cells were treated with 3.125 - 50 µM of fluorinated triarylmethane derivatives and 1 µM of indomethacin in the presence or absence 1 µg/mL of LPS in DMEM for 24 hours. The culture media was collected and centrifuged at 9,500 g for 5 minutes at 4 ºC. 100 µl of supernatant was transferred to a new microtube and diluted with 200 µL of assay buffer. The 100 µL of diluted culture media or PGE_2 standard was pipetted into a microplate that coated with an antibody to capture mouse IgG and then, incubated with 25 µL of the PGE_2-peroxidase conjugated to each well. The 25 µM of a monoclonal antibody to PGE_2 was added to each well and shake at room temperature for 2 hours to initiated the binding reaction. After that, the solution in microplate was aspirated and washed each well 4 times with 300 µL of wash buffer. Afterwards, 100 µL of TMB substrate was added to each well and incubated at room temperature for 30 minutes. Finally, 50 µL of stop solution was added to each well. The reaction was generated color that can measuring at 450 nm. The production of PGE_2 in the media culture was quantified using a PGE_2 standard curve. Percentage of PGE_2 production was expressed as: (PGE_2 concentration of treated cells/PGE_2 concentration of LPS-stimulated cells) × 100. Percentage of PGE_2 inhibition was calculated from: 100 – % of PGE_2 production.

3.4.3 iNOS activity assay

This method is modified from that of Tsao, Lee, Huang, Kuo, and Wang (2002). RAW 264.7 macrophage cells (1.5×10^5 cells/well) were plated in 24 well plate for 12-16 hours at 37ºC. Then, cells were treated with 1 µg/mL of LPS for 24 hours. After that, cells were washed 2 times with HBSS buffer and treated 500 µl of phenol red-free DMEM with the most active compound at various concentration, 0.1% v/v of DMSO and 50 µM of aminoguanidine (AG) for 6 hours at 37 ºC. At last, culture media was collected and measured the nitrite concentration by Griess reaction as describe in method in 3.2.5, Part I.

3.4.4 COX-2 activity assay

This method is modified from that of Wakabayashi and Yasui (2000). RAW 264.7 macrophage cells (1.5×10^5 cells/well) were plated in 24 well plate for 12-16 hours at 37ºC. Then, cells were treated with 1 µg/mL of LPS for 24 hours. After that, cells were washed 2 times with HBSS buffer and treated with the most compound at various concentration and 1 µM of indomethacin (IMC) for 6 hours at 37 ºC for 30 minutes. Next, 1 µM of arachidonic acid was added to each well and incubated at 37 ºC for 60 minutes. Lastly, culture media was collected and determined the PGE_2 concentration by PGE_2 competitive enzyme immunoassay kit describe in method 3.4.2, Part II.

3.4.5 Determination of cytokines

3.4.5.1 Determination of TNF-α

The concentration of TNF-α in culture media from LPS-induced RAW 264.7 were determined using Mouse TNF-α Quantikine ELISA Kit (R&D systems a biotechne brand, USA.) according to manufacturer's instructions. Briefly, RAW 264.7 macrophages were seeded into a 24 well plate (1.5×10^5 cells/well) and incubated for 24 hours. The cells were treated with 3.125 - 50 µM of fluorinated triarylmethane derivatives and 5 µM of BAY 11-7082 in the presence or absence 1 µg/mL of LPS in DMEM for 24 hours. The culture media was collected and centrifuged at 9,500 g for 5 minutes at 4 ºC. The 50 µL of assay diluent RD1-63 into a microplate that coated with a monoclonal antibody specific for mouse TNF-α and

then, incubated with 50 µL of standard, control or sample to each well, gently tapping the plate for 1 minute, and incubated at room temp for 2 hours to initiated the binding reaction. Next, the solution in microplate was aspirated and washed each well 4 times with 400 µL of wash buffer. After that, 100 µL of mouse TNF-α conjugated was added to each well and incubated for 2 hours at room temperature. Afterwards, washed each well 4 times with 400 µL of wash buffer. Then, 100 µL of substrate solution was added to each well and incubated for 30 minutes at room temperature and protected from light. Finally, 100 µL of stop solution was added to each well. The reaction was generated a blue product that turns yellow and can measure at 450 nm. The production of TNF-α in the media culture was quantified using a TNF-α standard curve. Percentage of TNF-α production was expressed as: (TNF-α concentration of treated cells/ TNF-α concentration of LPS-stimulated cells) × 100. Percentage of TNF-α inhibition was calculated from: 100 - % of TNF-α production.

3.4.5.1 Determination of IL-1β

The concentration of IL-1β in culture media from LPS-induced RAW 264.7 were determined using Mouse IL-1β/IL-1F2 Quantikine ELISA Kit (R&D systems a biotechne brand, USA.) according to manufacturer's instructions. Briefly, RAW 264.7 macrophages were seeded into a 24 well plate (1.5×10^5 cells/well) and incubated for 24 hours. The cells were treated with 3.125 - 50 µM of fluorinated triarylmethane derivatives and 5 µM of BAY 11-7082 in the presence or absence 1 µg/mL of LPS in DMEM for 24 hours. The culture media was collected and centrifuged at 9,500 g for 5 minutes at 4 ºC. The 50 µL of assay diluent RD1N into a microplate that coated with a monoclonal antibody specific for mouse IL-1β and then, incubated with 50 µL of standard, control or sample to each well, gently tapping the plate for 1 minute, and incubated at room temp for 2 hours to initiated the binding reaction. Next, the solution in microplate was aspirated and washed each well 4 times with 400 µL of wash buffer. After that, 100 µL of mouse IL-1β conjugated was added to each well and incubated for 2 hours at room temperature. Afterwards, washed each well 4 times with 400 µL of wash buffer. Then, 100 µL of substrate solution was added to each well and incubated for 30 minutes at room temperature and protected from light. Finally, 100 µL of stop solution was added to each well.

The reaction was generated a blue product that turns yellow and can measure at 450 nm. The production of IL-1β in the media culture was quantified using IL-1β standard curve. Percentage of IL-1β production was expressed as: (IL-1β concentration of treated cells/ IL-1β concentration of LPS-stimulated cells) × 100. Percentage of IL-1β inhibition was calculated from: 100 - % of IL-1β production.

3.4.6 Protein extraction for western blot analysis

3.4.6.1 Whole cell extraction for iNOS and COX-2 expression

iNOS and COX-2 protein were extracted by the method of Buapool et al. (2013). RAW 264.7 macrophage cells (1×10^6 cells/60-mm plate) were plated and incubated for 24 hours at 37 ºC. The cells were treated with the most potent compound at various concentration and 1µg/mL of LPS in the present or absence. After 24 hours, cells were washed with ice-cold 1X phosphate-buffered saline [PBS, 137 mM NaCl, 2.7 mM KCl, 1.8 mM KH_2PO_4 and 10 mM Na_2HPO_4] and scraped in the presence of cold RIPA lysis buffer [150mM Tris–HCl (pH 7.4),150 mM NaCl, 5 mM EGTA, 0.1% (w/v) SDS, 1% (w/v) sodium deoxycholate, and 1% (v/v) Nonidet P-40] containing 1 mM DL-1,4-dithiothreitol (DTT) and 1X protease inhibitor cocktail. Cell lysates were centrifuged at 12,000 g for 10 minutes at 4 ºC. Concentration of protein present in supernatant was measured with a Bradford reagent.

3.4.6.2 Cytoplasmic protein extraction for IκB phosphorylation and nuclear protein extraction for NF-κB p65 translocation

NF-κB p65 translocation was determined from nuclear protein which extracted by the method of Buapool et al. (2013). RAW 264.7 macrophage cells (5×10^6 cells/100-mm plate) were plated and incubated for 24 hours at 37 ºC Cells were treated with the most compound at various concentration for 30 minutes at 37 ºC and added 1µg/ml of LPS for 30 minutes at 37 ºC. Cells were lysed for analysis of nuclear translocation of NF-κB. After that, cells were washed with ice-cold PBS buffer and scraped in 500 µL of PBS and transfer to a new microtube as well as centrifuged at 9,500 g for 5 minutes at 4 ºC. Cell pellet was resuspended in 200 µL of lysis buffer 1 [25 mM HEPES (pH 7.9), 5 mM KCl, 0.5 mM MgCl2, 0.5 mM DTT,

0.5 mM PMSF, 1X protease inhibitor] and incubated on ice for 20 minutes and mixed by vortex every 5 minutes. After incubation, the cell suspensions were added with 200 µL lysis buffer 2 [5% (v/v) nonidet P-40 in lysis buffer 1] and rotated on ice for 20 minutes. The cell suspension was centrifuged at 13,700 g for 6 minutes at 4 ºC. The supernatant was collected into new microtubes as cytoplasmic protein extracts for IκB phosphorylation. The nuclei pellets were washed with 200 µL of lysis buffer 3 [1:1 mixture of buffer1 and buffer 2] and gently mixed for wash out the cytoplasmic protein. Supernatant was removed and resuspended the nuclei pellets with 70 µL buffer 4 [25 mM HEPES (pH7.9), 420 mM NaCl, 0.2 mM EDTA, 1.5 mM MgCl, 20% (v/v) glycerol, 0.5 mM DTT, 0.5 mM PMSF, 10X protease inhibitor]. Next, the suspension was incubated for 40 minutes on ice with vortex every 5 minutes to extract nuclear proteins. The suspension was centrifuged at 13,700 g for 20 minutes at 4 ºC. The supernatant was collected into new microtubes as nuclear protein extract. The protein concentration was determined by Bradford reagent.

3.4.6.3 Whole cell extraction for MAPKs phosphorylation

MAPKs phosphorylation were determined from whole cell protein which extracted by the method of Srisook et al. (2015). RAW 264.7 macrophage cells (5×10^6 cells/100-mm plate) were plated and incubated for 24 hours at 37 ºC. The cells were treated with the most potent compound at various concentration for 30 minutes before stimulation with 1µg/ml of LPS for 30 minutes. Cells were washed twice with ice-cold PBS and scraped in 100 µL ice-cold RIPA lysis buffer containing 1X phosphatase inhibitor cocktail, 1X protease inhibitor cocktail and 1 mM DTT. Lastly, the samples were centrifuged at 13,700 g for 10 minutes at 4 ºC. Supernatant was collected and determined the protein amount using Bradford reagent.

3.4.7 Western blot analysis for protein expression

3.4.7.1 Western blot analysis for iNOS and COX-2 expression

Equal amounts of soluble protein were mixed with 1X loading buffer [62.5 mM Trist-HCl (pH 6.8), 5% (v/v) β-mercaptoethanol, 10% (v/v) glycerol, 2% (w///v) SDS and 0.01 % (w/v) bromophenol blue]. The mixture was heated at 100 ºC using Digital Dry Bath for 5 minutes. After that, the mixture was spun down and

loaded onto 10% SDS-polyacrylamide gel electrophoresis (SDS-PAGE) in Tris-glycine buffer [0.025 mM Tris, 0.192 M glycine and 0.1 % (w/v) SDS] at constant voltage of 80 V for 2 hours. Separated protein was transferred to a polyvinylidene (PVDF) membrane in transfer buffer [192 mM glycine, 25 mM Tris and 10% (v/v) methanol] for overnight at 4 ºC under constant voltage of 25 V by using protein transfer tank. The non-specific binding was blocked with blocking solution [5% (w/v) skim milk powder in TBS-T buffer (10 mM Tris–HCl, pH 7.4, 100 mM NaCl and 1% (v/v) Tween 20)] for 1 hour at room temperature. The membrane was incubated with specific primary antibodies of GAPDH (1:1,000) dissolved in blocking solution for 1 hour or iNOS and COX-2 (1:500) dissolved in PBS containing 0.5 % (w/v) BSA and 0.5 % Tween 20 at room temperature for 2 hours. Then, membrane was washed with TBS-T buffer for 5 minutes 3 times and incubated with goat anti mouse IgG conjugated HRP secondary antibodies or goat anti rabbit IgG conjugated HRP secondary antibodies at dilution 1: 5,000 which diluted with blocking solution at room temperature for 1 hour. Next, membrane was washed with TBS-T buffer for 5 minutes 3 times. The specific protein band on PVDF membranes were detected on X-ray film activated with enhanced chemiluminescence using SuperSignal West Pico Chemiluminescent. The band on X-ray film was determined density using program Image Studio Lite version 5.2 (LI-COR Biosciences, USA.). Image densities of specific bands for iNOS and COX-2 were normalized with a density of GAPDH band.

3.4.7.2 Western blot analysis for NF-κB p65 level

Equal amount of soluble protein was separated onto 10% SDS-PAGE and transferred to a PVDF membrane. Next, the membrane was incubated in blocking solution for 1 hour. After that, membrane was incubated in 4 ºC for overnight with rabbit anti NF-κB p65 polyclonal antibody (1: 1,000) dissolved in TBS-T containing 5% (w/v) BSA or rabbit anti lamin A polyclonal antibody (1: 1,000) dissolved in 0.5% (w/v) BSA and 0.05% (v/v) Tween 20 in PBS. Membrane was washed 5 minutes 3 times with TBS-T and incubated with secondary antibody (goat anti-rabbit IgG, HRP-linked antibody) in blocking solution (1: 5,000) for 1 hour. Then, membrane was washed with TBS-T for 5 minutes 3 times. The specific protein band on PVDF membrane was detected on X-ray film activated with enhanced

chemiluminescence using SuperSignal West Pico Chemiluminescent. The band on X-lay film was determined density using program Image Studio Lite version 5.2 (LI-COR Biosciences, USA.). Image densities of specific bands for p65 NF-κB subunit were normalized with a density of lamin A band.

3.4.7.3 Western blot analysis for IκB phosphorylation

Equal amount of soluble protein was separated onto 10% SDS-PAGE and transferred to a PVDF membrane. Next, the membrane was incubated in blocking solution for 1 hour. After that, membrane was incubated in 4 ºC for overnight with mouse anti phosphor-IκBα monoclonal antibody (1: 1,000) dissolved in blocking solution or specific primary antibodies of GAPDH dissolved in blocking solution for 1 hour (1: 1,000). Membrane was washed 5 minutes 3 times with TBS-T and incubated with secondary antibody (goat anti mouse IgG conjugated HRP secondary antibodies or goat anti rabbit IgG conjugated HRP secondary) in blocking solution (1: 5,000) for 1 hour. Then, membrane was washed with TBS-T for 5 minutes 3 times. The specific protein band on PVDF membrane was detected on X-ray film activated with enhanced chemiluminescence using SuperSignal West Pico Chemiluminescent. The band on X-lay film was determined density using program Image Studio Lite version 5.2 (LI-COR Biosciences, USA.). Image densities of specific bands for phosphor-IκBα were normalized with a density of GAPDH band.

3.4.7.4 Western blot analysis of phosphorylation of MAPKs

Equal amounts of supernatant protein were separated onto 10% SDS-PAGE and transferred to a PVDF membrane. Next, the membrane was incubated in blocking solution for 1.5 hour and incubated with specific primary antibody for phosphorylation of p38, ERK1/2, JNK and ATF-2 and total protein of p38, ERK1/2, JNK and GAPDH as conditions shown in table 3-2. Then, membrane was washed for 5 minutes 3 times with TBS-T buffer and incubated with specific secondary antibody as conditions shown in table 3-3. The specific protein band on PVDF membranes was detected on X-ray film activated with enhanced chemiluminescence using SuperSignal West Pico Chemiluminescent. The band on X-lay film was determined density using program Image Studio Lite version 5.2 (LI-

COR Biosciences, USA.). The image densities of specific bands for p-ERK1/2, p-JNK, p-p38 and p-ATF-2 were normalized with the density of their total proteins band.

Table 3-2 The condition for specific primary antibody of MAPKs

Proteins	Primary antibody	Ratio of solution	solvent	Time and Temperature
p-p38	Rabbit anti p-p38 (pAb)	1:2,000	5% BSA in TBS-T	12 h., 4 ºC
p-ERK 1/2	Rabbit anti p-ERK1/2 (pAb)	1:1,000	5% BSA in TBS-T	12 h., 4 ºC
p-SAPK/JNK	Mouse anti p-JNK (moAb)	1:2,000	Blocking solution	12 h., 4 ºC
p-ATF-2	Mouse anti-ATF-2 (pAb)	1:1000	5% BSA in TBS-T	12h., 4 ºC
p38	Rabbit anti p38 (pAb)	1:2,500	0.5% in PBS and 0.05% Tween20	12 h., 4 ºC
ERK 1/2	Rabbit anti ERK1/2 (pAb)	1:2,500	0.5% in PBS and 0.05% Tween20	12 h., 4 ºC
JNK	Rabbit anti JNK (pAb)	1:500	5% BSA in TBS-T	12 h., 4 ºC

Table 3-3 The condition for specific secondary antibody of MAPKs

Proteins	Secondary antibody	Ratio of solution	solvent	Time and Temperature
p-p38	Goat anti-rabbit IgG	1:5,000	blocking solution	1h., room temp
p-ERK 1/2	Goat anti-rabbit IgG	1:5,000	blocking solution	1h., room temp
p-SAPK/JNK	Goat anti-mouse IgG	1:5,000	blocking solution	1h., room temp
p-ATF-2	Goat anti-rabbit IgG	1:5000	blocking solution	1h., room temp
p38	Goat anti-rabbit IgG	1:5,000	blocking solution	1h., room temp
ERK 1/2	Goat anti-rabbit IgG	1:5,000	0.5% in PBS and 0.05% Tween20	1h., room temp
JNK	Goat anti-rabbit IgG	1:5,000	5% BSA in TBS-T	1h., room temp

3.4.8 Stripping and reprobing of Western blots

Stripping a blot is used to remove the primary and secondary antibodies from a Western blot membrane. Membrane was washed with TBS-T for 5 minutes 3 times. After that, membrane was incubated in stripping buffer [10% SDS, 2 M Tris-HCl (pH 7.4), 98 mM β-mercaptoethanol] in the water bath at 55 ºC with shaking for 50 minutes. After that, membrane was washed with TBS-T for 5 minutes 3 times. Then, the membrane was used to probe again with another antibody.

3.4.9 RNA isolation

Briefly, the cells were lysed by incubation in a solution containing large amounts of chaotropic ions for immediately inactivation RNase and created appropriate binding conditions which favor adsorption of RNA to the silica

membrane. The contaminating of DNA was bound to the silica membrane and removed by a DNase solution. The salts, metabolite and macromolecule cellular components in the samples were removed by two different buffers. Pure RNA was eluted under the low ionic strength conditions with RNase free water. RAW 264.7 cells (1×10^6 cells/60-mm plate) were seeded and incubated for 24 hours at 37 ºC. After that, cells were treated with the most potent compound and LPS. After treated 9 hours, total cellular RNA was isolated with RNA isolation kit by illustra RNA spin Mini RNA Isolation Kit (GE Healthcare, UK) according to manufacturer's instructions. Cultured cells were collected for homogenization and lysis by centrifuge at 5,000 g for 1 minute. Next, supernatant was completely removed by aspiration. The pallet was washed with 500 µL of PBS and centrifuged at 5,000 g for 1 minute. Then, supernatant was completely removed by aspiration. The 350 µL of lysis solution and 3.5 µL of β-mercaptoethanol was added to pallet and pipetted up-and-down to re-suspend the cell pellet and lyse the cell directly. After that, lysate cell was reduced viscosity and clear the lysate by filtration through RNAspin Mini Filter. RNAspin Mini Filter was placed in a collection tube. Then, lysate was added to the RNAspin Mini Filter and centrifuged at 11,000g for 1 minute. RNAspin Mini Filter was discarded and transferred filtrate to a new 1.5 ml RNase-free microcentrifuge tube. After that, 350 µL of ethanol (70%) was added and mixed by voltexing, twice for 5 second each. After the addition of ethanol, a stringy precipitate may become visible. The lysate was pipetted up-and-down 3 times and loaded onto the RNAspin Mini Column. Then, the lysate was centrifuged at 8,000 g for 30 seconds and transferred the column to a new collection tube. Later, 350 µL of desalting buffer was added and centrifuged at 11,000g for 1 minute to dry the membrane. The flow through was discarded. RNAspin Mini Column was returned to the collection tube. DNase I reaction mixture was prepared in a sterile microcentrifuge tube for each isolation, added 10 µL reconstituted DNase I to 90 µL DNase Reaction Buffer. The 95 µL of DNase I reaction mixture was added directly onto the center of the silica membrane of the column and incubated at room temperature for 15 minutes. Next, 200 µL of wash buffer I was added to the RNAspin Mini Column and centrifuged at 11,000 g for 1 minute. The column was placed into a new collection tube. Wash Buffer I will inactivate DNase. For the second wash, 600 µL of Wash Buffer II was added to the

RNAspin Mini Column and centrifuged at 11,000 g for 1 minute. The flow through was discarded and placed the column back into the collection tube. For the third wash, 250 µL of Wash Buffer II was added to the RNAspin Mini Column and centrifuged at 11,000 g for 2 minutes to dry the membrane completely. Next, the column was placed into a nuclease-free 1.5 ml Microcentrifuge Tube. At the last step, RNA was eluted with 100 µL of RNase-free H_2O and centrifuged at 11,000 g for 1 minute. Total RNA concentration was determined by measuring at 260 nm to detect RNA and at 280 to detect protein concentration using a UV-VIS spectrometer. The ratio of A_{260}/A_{280} was used in range 1.8-2.2 indicates that the RNA is pure (according to manufacturer's instructions).

3.4.10 Real time reverse transcription-polymerase chain reaction (Real-rime PCR)

Complementary DNA (cDNA) was made by 1 µg of RNA template using mixture containing 4 µL of 5X iScript™ Reverse Transcription Supermix for RT-qPCR [iScript MMLV-RT ($RNaseH^+$), RNase inhibitor, dNTPs, oligo (dT), random primers, buffer, $MgCl_2$ and stabilizer], RNase and DNase-free water to make up volume 20 µL. The cDNA was synthesized under condition at 25 ºC for 5 minutes, at 42 ºC for 30 minutes and at 85 ºC for 5 minutes using Thermo Cycle (Thermo Hybrid, UK). Quantitative of the cDNA was analyzed by real-time PCR on CFX96 Touch™Real-Time PCR (Bio-rad, USA). The PCR reaction contains 2 µL of cDNA, 10 µl of 2x iTaq™ Universal SYBR Green Supermix [antibody mediated hot-start 2x iTaq DNA polymerase, dNTPs, $MgCl_2$, SYRB® Green dye], 0.5 µL of each forward and reward primers (10 µM) and 7 µL of DNase-free water. The sequences of specific primer for the COX-1, COX-2, iNOS and elongation factor-2 (EF-2) are shown in the table 3-4. The PCR cycle program was performed as conditions shown in the table 3-5.

Table 3-4 Sequences of primers used in Real time RT-PCR

Target	Primer sequences	Product size (bp)	Accession No.
COX-1	5'TGGGGTGCCCTCACCAGTCAA3'	170	NM_008969.3
	5'-GCCGCAGAGAATTCCGAAGCCA3'		
COX-2	5'-TGATCGAAGACTACGTGCAACACC3'	164	NM_011198.3
	5'-TTCAATGTTGAAGGTGTCGGGCAG3'		
iNOS	5'GCACAGCACAGGAAATGTTTCAGCAC3'	156	NM_010927.3
	5'AGCCAGCGTACCGGATGAGC3'		
EF-2	5'CTGAAGCGGCTGGCTAAGTCTGA3'	155	NM_007907.2
	5'GGGTCAGATTTCTTGATGGGGATG3'		

Table 3-5 The PCR cycling parameters

Gene	Cycle	Temperature	Time
COX-1, COX-2, iNOS and EF-2	Cycle 1: (1X) Step 1:	95.0	3.00
	Cycle 2: (40X)Step 1:	95.0	0.10
	(40X)Step 2:	63.0	0.20
	Cycle 4: (1X) Step 1:	95.0	0.10

Relative gene expression was calculated according to the comparative cycle of threshold (Ct) method (Giulietti et al., 2001) as equation shown below.

$$2^{-\Delta\Delta Ct} = \text{quantity of target DNA}$$

$$\Delta\Delta Ct = \Delta Ct \text{ (Sample)} - \Delta Ct \text{ (Calibrator)}$$

$$\Delta Ct = Ct \text{ of target gene} - Ct \text{ of Housekeeping gene}$$

Ct of COX-1, COX-2 and iNOS were compared with Ct of elongation factor 2 (EF-2) as a housekeeping gene. The data were expressed on the relative

quantification of target mRNA that compared with calibrator (control unstimulated cells) from formula $2^{-\Delta\Delta CT}$ as described.

3.4.11 Statistical analysis

All experiments were replicated at least three times independent experiments. The data were present as the mean ± S.D. and analyzed statistical significance by analysis of variance (ANOVA), followed by Tukey's test for multiple comparison. A value of $p < 0.05$ was considered to be significant.

CHAPTER 4
RESULTS

4.1 Effect of fluorinated triarylmethane derivatives on cell viability of RAW264.7 macrophages

The cytotoxicity of 26 fluorinated triarylmethane derivatives was determined using MTT assays. The cells were treated with 50 µM of each compound for 24 hours. Cell viabilities of cells treated with almost all fluorinated triarylmethane derivatives including JJBF1-JJBF2, JJBF4-JJBF18 and JJCF1 were more than 80% (Figure 4-1A). On the other hand, cytotoxicity of some compounds including JJAF1-JJAF7 were more than 70%, while, 0.1% DMSO, a vehicle, had no significant cytotoxic activity (Figure 4-1A). We also evaluated the effect of all fluorinated triarylmethane derivatives on cells viability in LPS-induced macrophage cells. As shown in Figure 4-1B, the cell viability of cells treated with LPS was not significantly different from control cells. JJBF6 and JJBF8 had no significant cytotoxic effect, whereas the other compounds exhibited significant cytotoxicity compared to control unstimulated cells (Figure 4-1B).

(A)

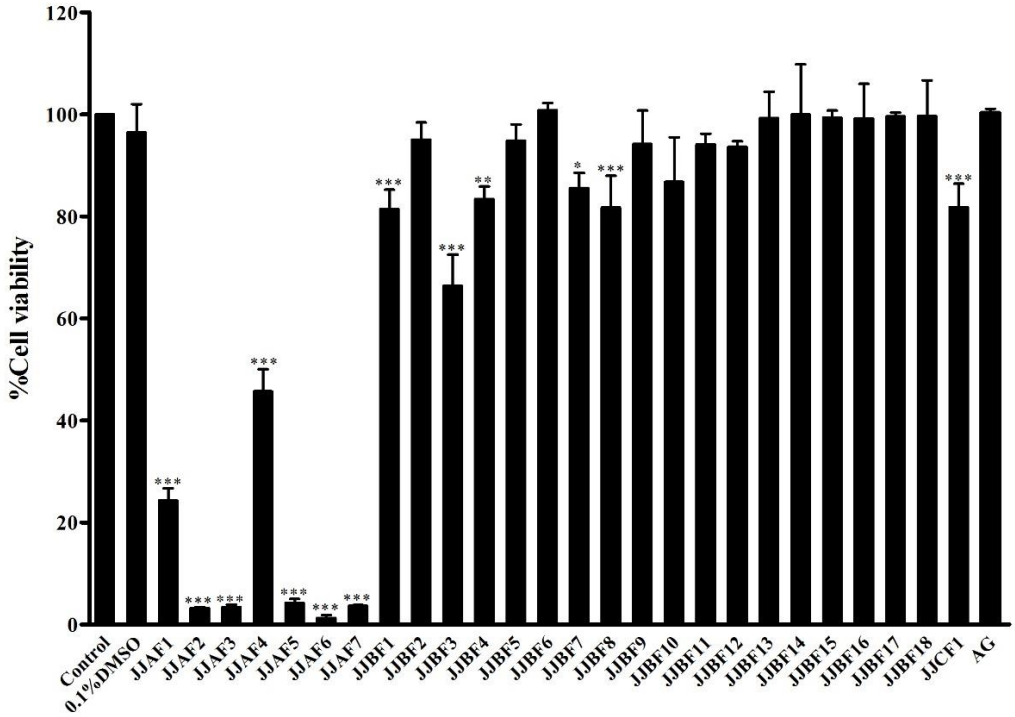

(B)

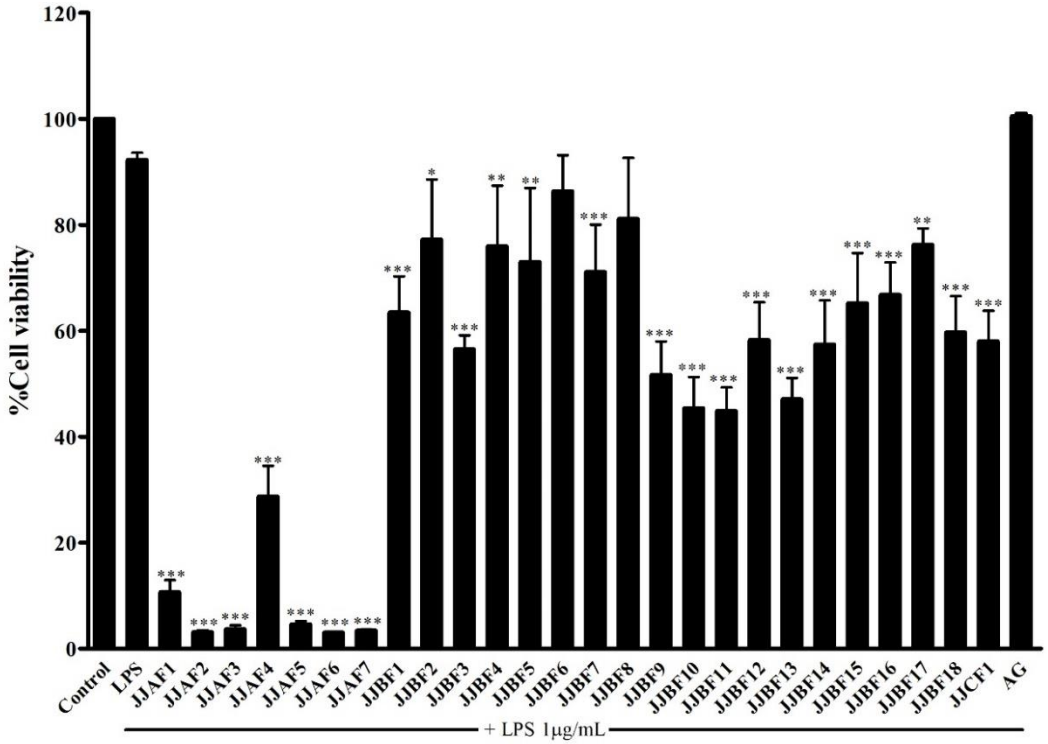

Figure 4-1 Effect of fluorinated triarylmethane derivatives on cell viability of RAW264.7 macrophages. (A) Cells were treated with 50 μM of each compound for 24 hours. (B) Cells were treated with 50 μM of each compound in the present of LPS (1 μg/mL) for 24 hours. Data are shown as mean ± SD of three independent experiments with triplicate samples. $^{*}P<0.05$, $^{**}P<0.01$, $^{***}P<0.001$ compared to the control unstimulated cells.

4.2 Effect of fluorinated triarylmethane derivatives on NO production in LPS-stimulated RAW264.7 macrophages

To estimate the anti-inflammatory activity of fluorinated triarylmethane derivatives, we first screened the effect of compounds on the NO production in LPS-stimulated RAW264.7 cells. Nitrite concentration of unstimulated cells was 1.26 ± 0.45 μM, while the levels in LPS-stimulated cells were increase to 27.31 ± 0.45 μM (Figure 4-2A). The nitrite concentrations of cells treated with most all fluorinated triarylmethane derivatives except JJBF1, JJBF2, JJBF4-6 were significantly less than LPS treatment (Figure 4-2A). Percentage inhibition of NO production of all compounds except JJBF1 and JJBF2 were higher than 25% (Figure 4-2B). Besides, 0.1% DMSO and the fluorinated triarylmethane derivatives itself did not affect on NO production in unstimulated RAW264.7 macrophages as compared to control unstimulated cells (Figure 4-2C). Since, 7 compounds, including JJBF9, JJBF10, JJBF11, JJBF12, JJBF14, JJBF15 and JJCF1 suppressed NO production more than 75%, they were selected to evaluate their IC_{50} values (Figure 4-2). Also, aminoguanidine, a specific inhibitor of iNOS activity, moderated LPS-induced NO production by 51% inhibition.

(A)

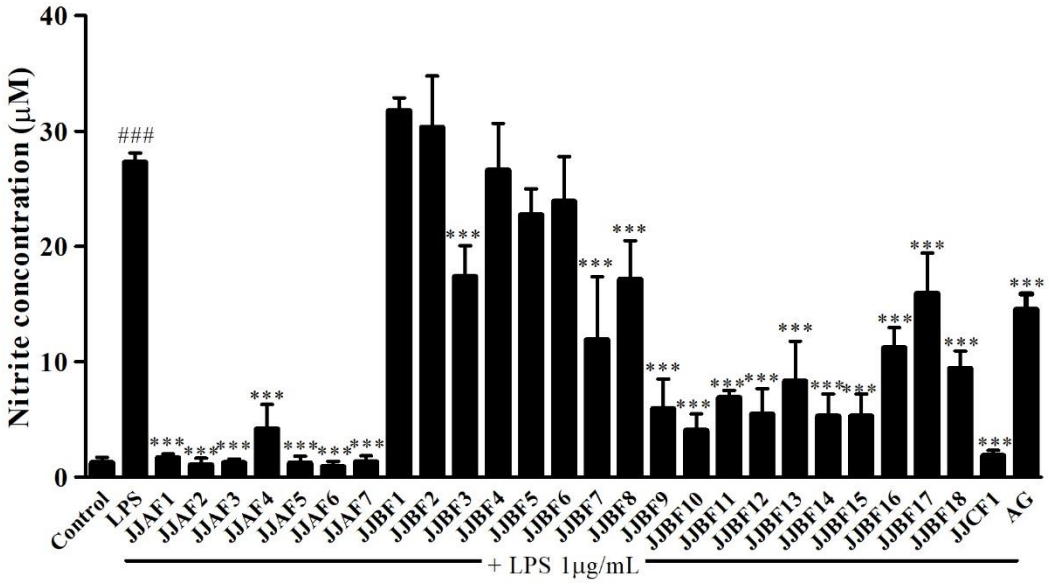
Nitrite concentration (μM)
40
30
20
10
0
###
***
Control
LPS
JJAF1
JJAF2
JJAF3
JJAF4
JJAF5
JJAF6
JJAF7
JJBF1
JJBF2
JJBF3
JJBF4
JJBF5
JJBF6
JJBF7
JJBF8
JJBF9
JJBF10
JJBF11
JJBF12
JJBF13
JJBF14
JJBF15
JJBF16
JJBF17
JJBF18
JJCF1
AG
+ LPS 1μg/mL

(B)

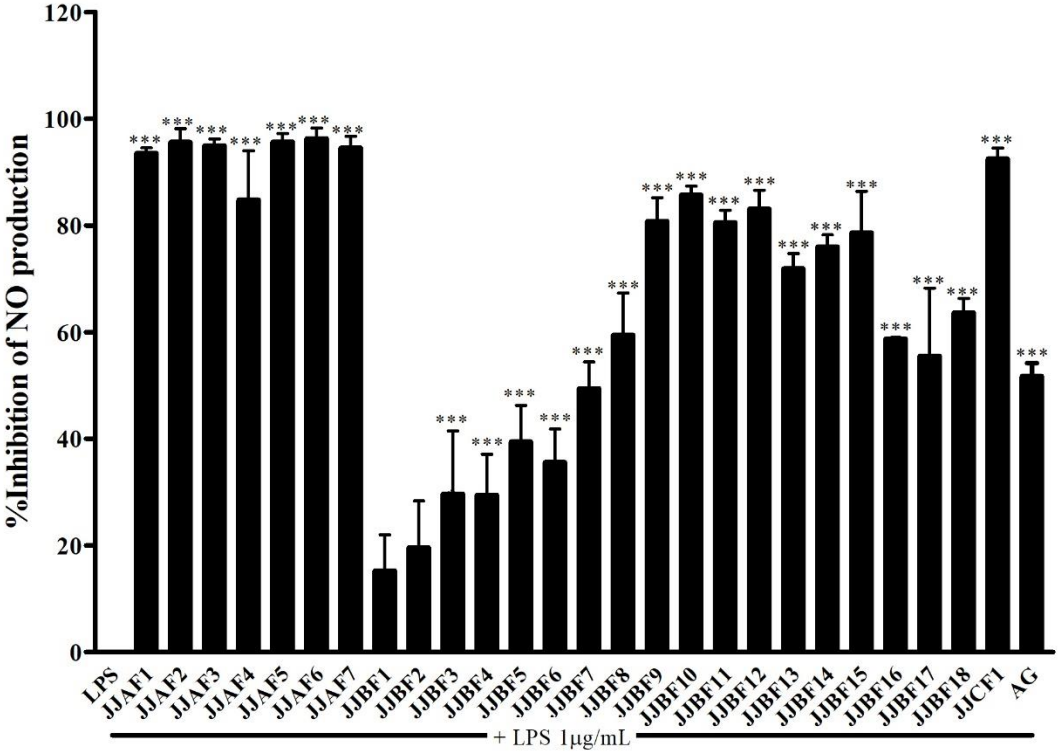
%Inhibition of NO production
120
100
80
60
40
20
0
***
LPS
JJAF1
JJAF2
JJAF3
JJAF4
JJAF5
JJAF6
JJAF7
JJBF1
JJBF2
JJBF3
JJBF4
JJBF5
JJBF6
JJBF7
JJBF8
JJBF9
JJBF10
JJBF11
JJBF12
JJBF13
JJBF14
JJBF15
JJBF16
JJBF17
JJBF18
JJCF1
AG
+ LPS 1μg/mL

(C)

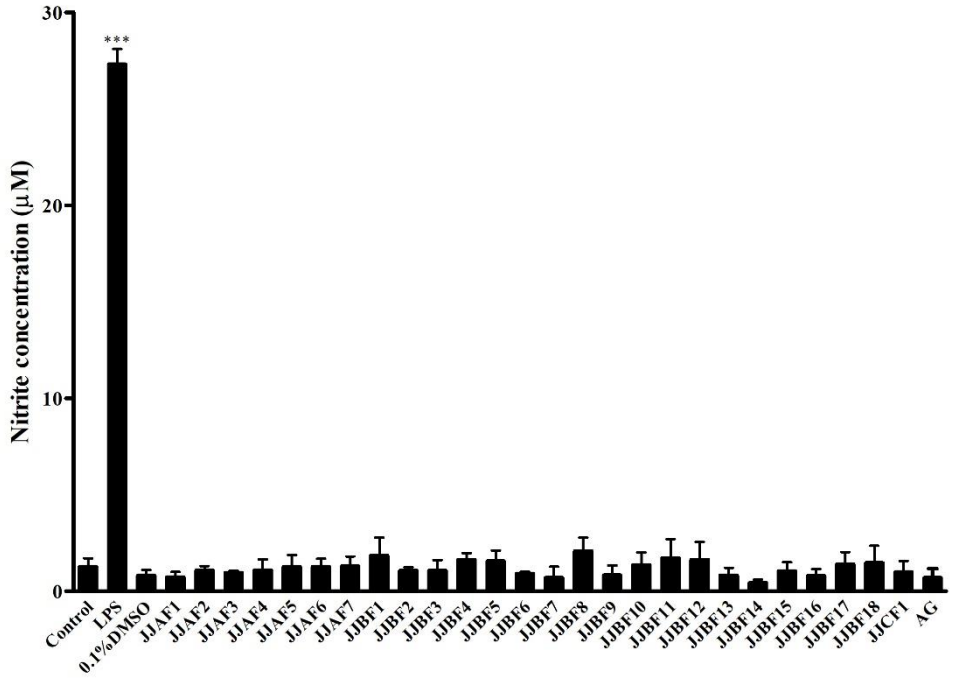

Figure 4-2 Effect of fluorinated triarylmethane derivatives on NO production in RAW264.7 macrophages. (A) Concentration of nitrite and (B) percent inhibition of NO production of cells treated with 50 μM of each compound in the present of LPS (1 μg/mL) for 24 hours. (C) Concentration of nitrite of cells treated with 50 μM of each compound for 24 hours. Data are shown as mean ± SD of three independent experiments with triplicate samples. $^{###}$ P<0.001 compared to control unstimulated cells. $^{***}P$<0.001 compared to the LPS-stimulated cells.

4.3 The IC_{50} values of NO inhibition of selected fluorinated triarylmethanes

The selected fluorinated triarylmethanes including, JJBF9, JJBF10, JJBF11, JJBF12, JJBF14, JJBF15 and JJCF1were evaluated their IC_{50} values in LPS-stimulated RAW264.7 macrophages. As indicated in Figure 4-3, IC_{50} values of JJBF11, JJBF12, JJBF14 and JJBF15 were ranging from 6.98 ± 0.47 to 10.58 ± 0.86 µM and did not show significant differ from each compound. An IC_{50} value of aminoguanidine was 56.91 ± 1.47 µM. Therapeutic index of selected fluorinated triarylmethane were shown in Figure 4-4. JJBF14 and JJCF1 showed the highest therapeutic index. However, JJBF14 was selected to further investigate the mechanism underlying its anti-inflammatory effect.

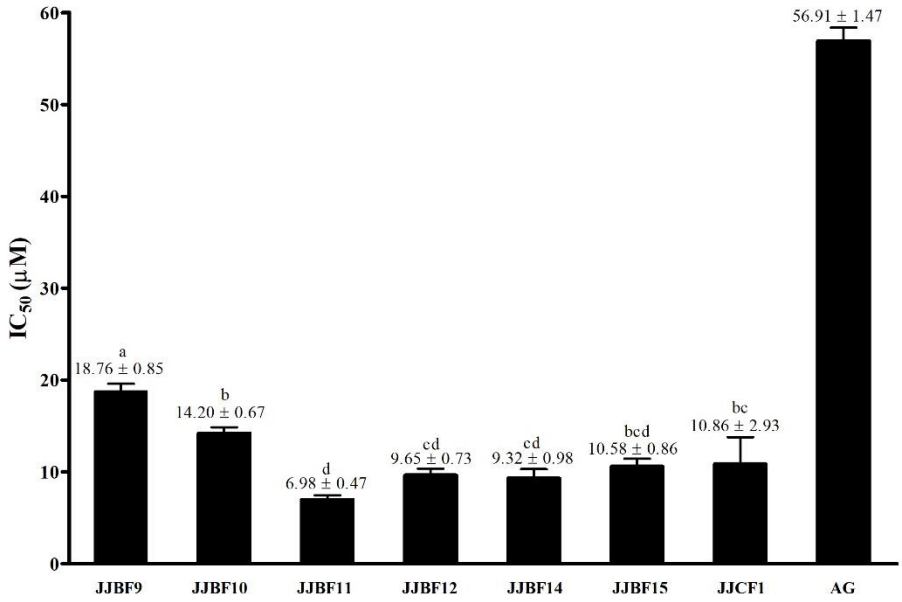

Figure 4-3 The IC_{50} values of NO inhibition of selected fluorinated triarylmethane in LPS-stimulated RAW264.7 macrophages. Cells were treated with various concentrations (3.125-50 µM) of each compound and aminoguanidine in the present of LPS (1µg/mL) for 24 hours. Data are shown as mean ± SD of concentration of compound was inhibited the production of nitrite with 50%. Letters a-d represents the significance statistical was considered by ANOVA followed Tukey's test (*P*-value<0.05).

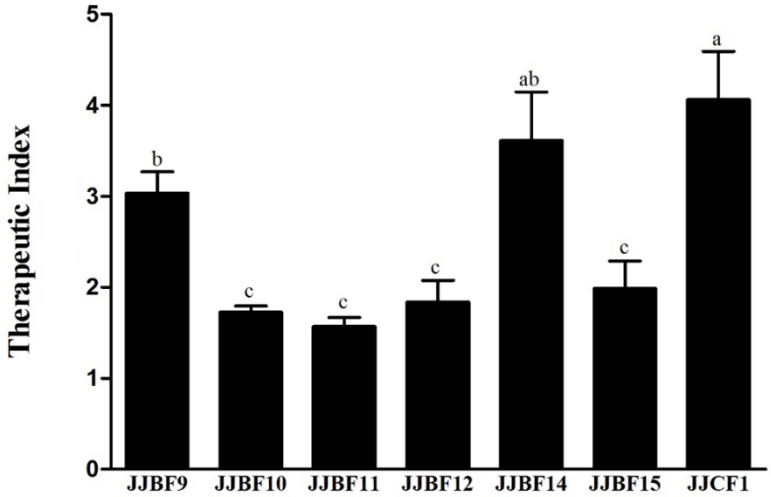

Figure 4-4 Therapeutic index of selected fluorinated triarylmethane in LPS-activated macrophages. Cells were treated with various concentrations (3.125-50 µM) of each compound in the present of LPS (1µg/mL) for 24 hours. Therapeutic index was determined from: (concentration of the compound inhibiting the production of NO at 50%)/ (concentration of the compound showing 50% cell viability). Letters a-c represents the significance statistical was considered by ANOVA followed Tukey's test (*P*-value<0.05).

4.4 JJBF14 inhibited NO production in a concentration dependent manner

In order to determine effect of JJBF14 on NO production, RAW264.7 cells were treated with JJBF14 at various concentration (3.125-50 μM) for 24 hours. JJBF14 (12.5-50 μM) significantly inhibited LPS-induced NO production more than 79% inhibition (Figure 4-5). While, BAY11-7082, an inhibitor of NF-κB, inhibited the production of NO by 70% inhibition. While, JJBF14 alone at 12.5 and 25 μM cause significant decreases in cell viabilities (Figure 4-6B). Additionally, JJBF14 at 12.5-50 μM exhibited significant cytotoxicity in LPS-stimulated RAW264.7 macrophages (Figure 4-6A). Unlike, IMC (1 μM) and BAY11-7082 (5 μM), inhibitor for COX activity and NF-κB, respectively, had no significant cytotoxic activity in RAW264.7 macrophages (Figure 4-6).

(A)

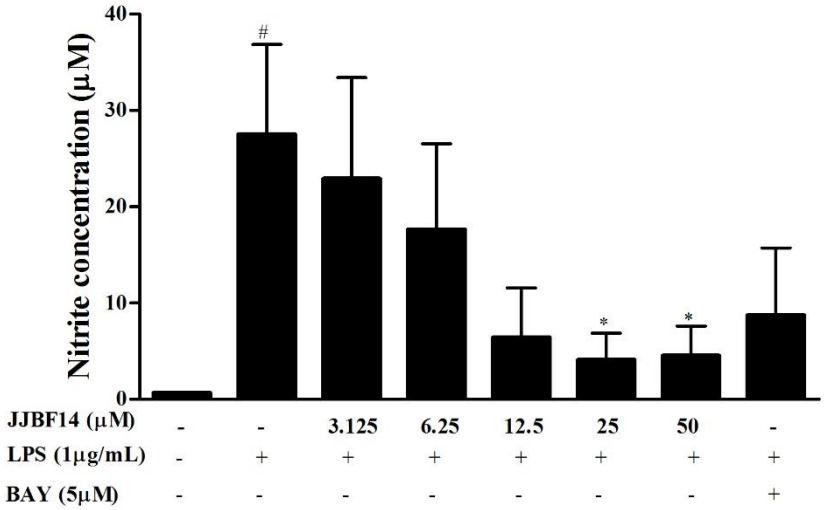

(B)

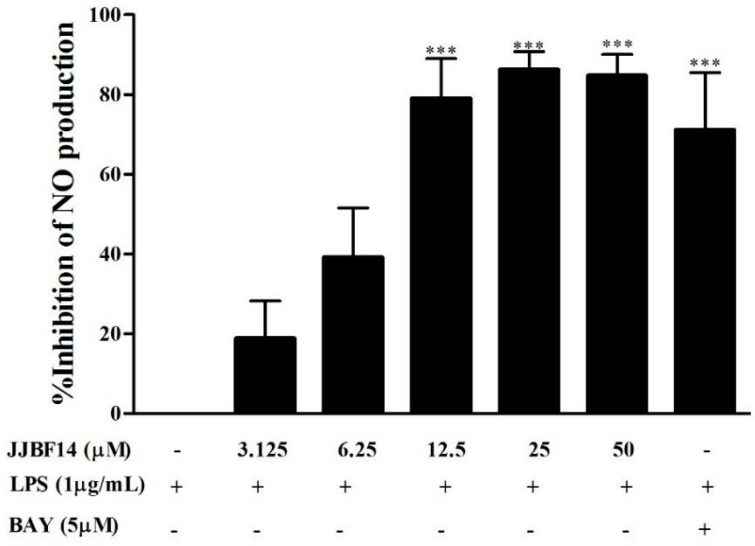

Figure 4-5 Effect of JJBF14 on NO production in RAW 264.7 macrophage cells. (A) Nitrite concentration of culture medium of cells treated with JJBF14 at various concentrations for 24 hours. (B) Percentage inhibition of NO production of cells treated with JJBF14 at various concentrations in the presence of LPS (1μg/mL) for 24 hours. Data are shown as mean ± SD of three independent experiments with triplicate samples. $^{\#}P<0.05$ compared to control unstimulated cells. $^{*}P<0.05$ and $^{***}P<0.001$ compared to the LPS-stimulated cells

(A)

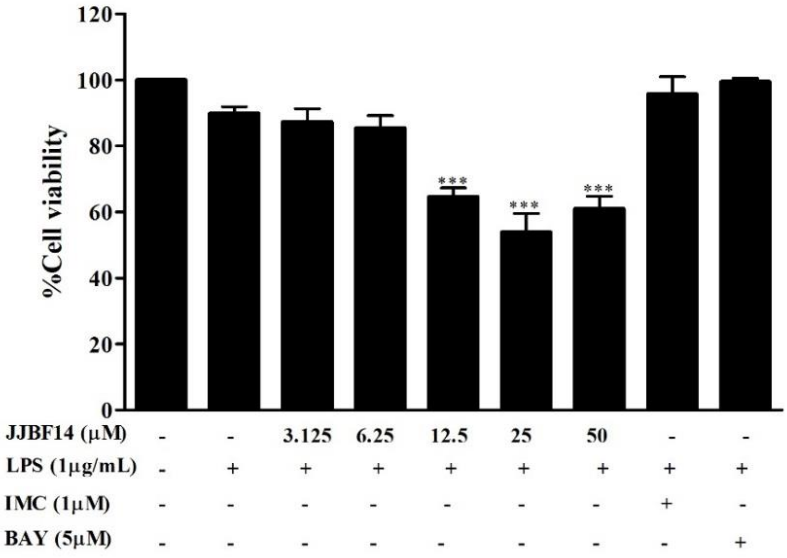

(B)

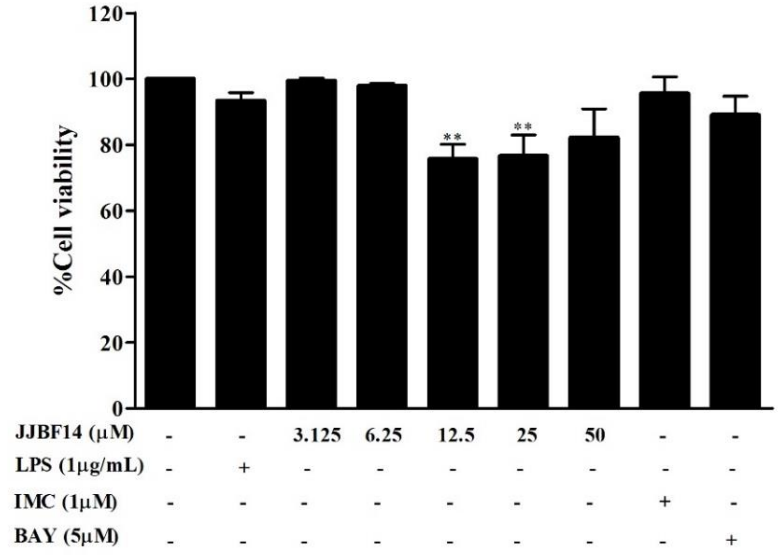

Figure 4-6 Effect of JJBF14 on cell viability in RAW 264.7 macrophages. (A) Cells were treated with JJBF14 of various concentrations for 24 hours. (B) Cells were treated with JJBF14 of various concentrations in the presence of LPS (1 μg/mL) for 24 hours. Data are shown as mean ± SD of three independent experiments with triplicate samples. IMC = indomethacin-treated cells and BAY = BAY11-7082-treated cells. $^{**}P<0.01$ and $^{***}P<0.001$ compared to the LPS-stimulated cells.

4.5 Effect of JJBF14 on LPS-induced iNOS expression in RAW264.7 macrophages

iNOS protein and mRNA are associated with NO production. To investigate whether the inhibition of NO production by JJBF14 was due to the modulation of iNOS expression, iNOS protein and mRNA levels were determined by Western blot and qRT-PCR analysis, respectively. As shown in Figure 4-7 and 4-8, expression of iNOS protein and mRNA was significantly increased by stimulation with LPS. Moreover, treatment with JJBF14 at 12.5-50 μM significantly attenuated iNOS protein and mRNA levels in the LPS-induced RAW 264.7 cells.

(A)

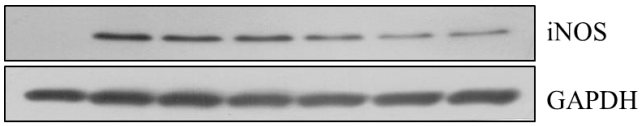

(B)

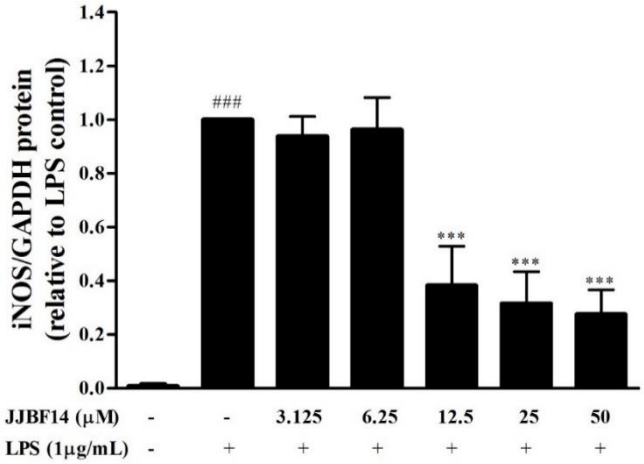

Figure 4-7 Effect of JJBF14 on iNOS protein expression in LPS-stimulated RAW 264.7 macrophages. Cells were treated with in the presence of LPS (1 μg/mL) for 24 hours. (A) The levels of iNOS protein expression were determined by Western blot analysis. (B) Each column shows the mean ± SD of densitometric analyses of iNOS protein and normalized with GAPDH. Data are presented as relative to LPS treated cells. $^{###}$ $P<0.001$ compared to control unstimulated cells. $^{***}P<0.001$ compared to the LPS-stimulated cells.

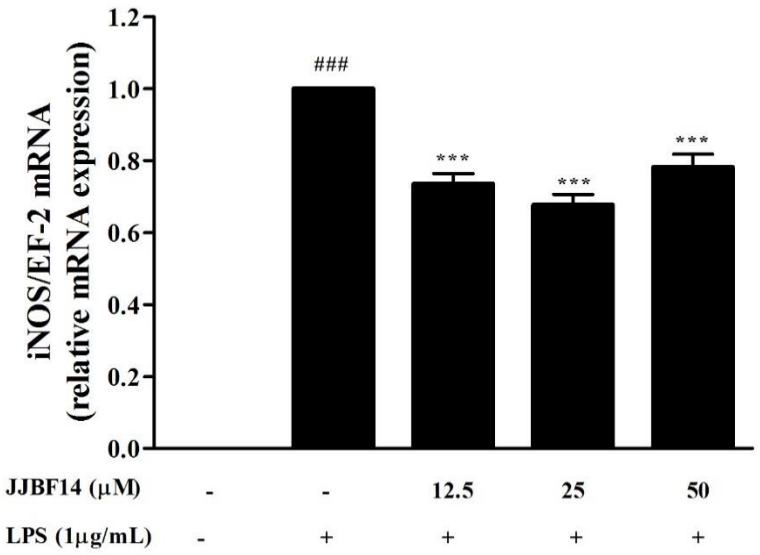

Figure 4-8 Effect of JJBF14 on LPS-induced iNOS mRNA expression in RAW264.7 macrophages. Cells were treated with JJBF14 in the presence of LPS (1 μg/mL) for 9 hours. The amount of iNOS mRNA was determined by real time RT-PCR which normalized with amount of EF-2 mRNA. Data are shown as mean ± SD of three independent experiments with triplicate samples. $^{###}P<0.001$ compared to control unstimulated cells. $^{***}P<0.001$ compared to the LPS-stimulated cells.

4.6 Effect of JJBF14 on LPS-induced iNOS enzymatic activity in RAW264.7 macrophages

We also determined on iNOS enzymatic activity by indirect method. The result showed that JJBF14 at all tested concentration did not show an inhibitory effect on iNOS activity (Figure 4-9). Aminoguanidine at 50 µM, a specific inhibitor of iNOS activity inhibited with value of 43.5 ± 3.0 %inhibition.

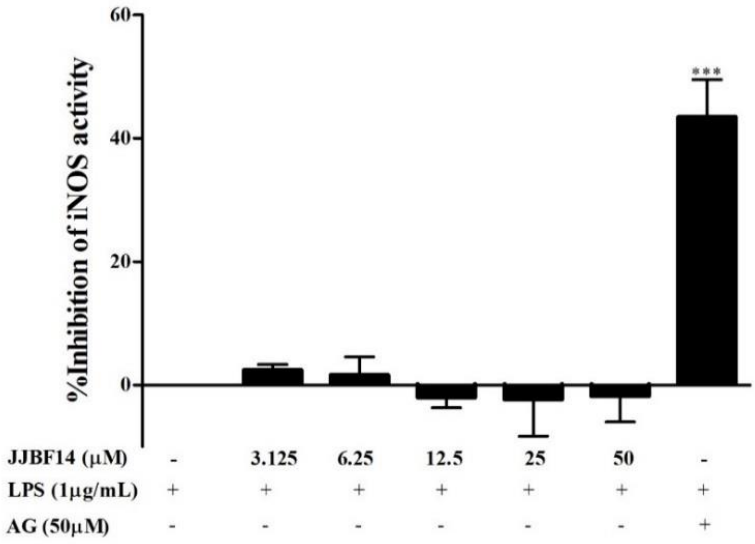

Figure 4-9 Effect of JJBF14 on LPS-induced iNOS enzymatic activity in RAW264.7 macrophages. Cells were activated with LPS (1 µg/mL) for 24 hours before treating with JJBF14 for 6 hours. Data are presented as mean ± SD of three independent experiments with triplicate samples. $^{***}P<0.001$ compared to the LPS-stimulated cells.

4.7 Effect of JJBF14 on LPS-induced PGE_2 production in RAW264.7 macrophages

To determine the effect of JJBF14 on the LPS-induced PGE_2 production in RAW264.7 cells, we assessed the PGE_2 production using PGE_2 competitive enzyme immunoassay kit. The results showed that JJBF14 (50μM) significantly decreased the level of PGE_2 in LPS-treated macrophages by 16% (Figure 4-10). Furthermore, IMC (1 μM), COX inhibitor, clearly suppressed PGE_2 production in LPS-stimulated macrophages. Its inhibition was almost 90%.

(A)

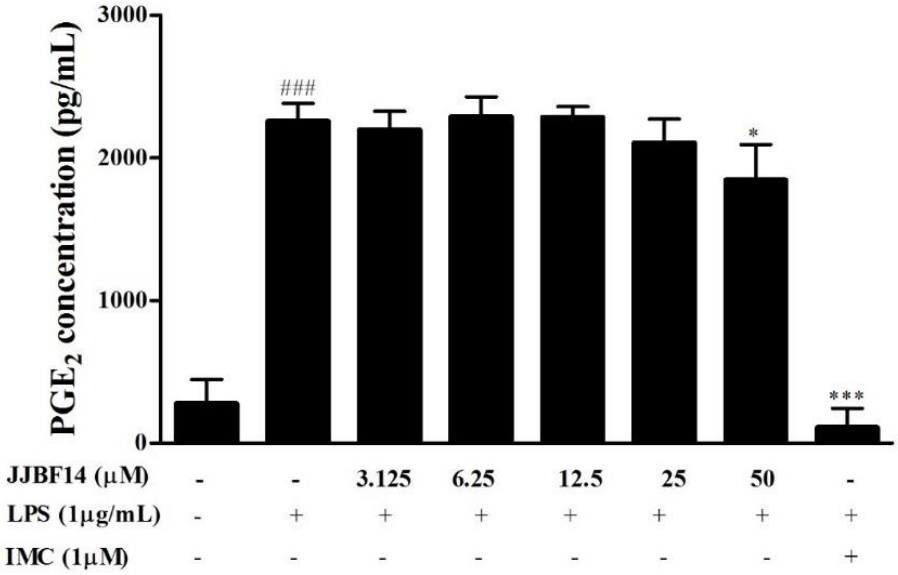

(B)

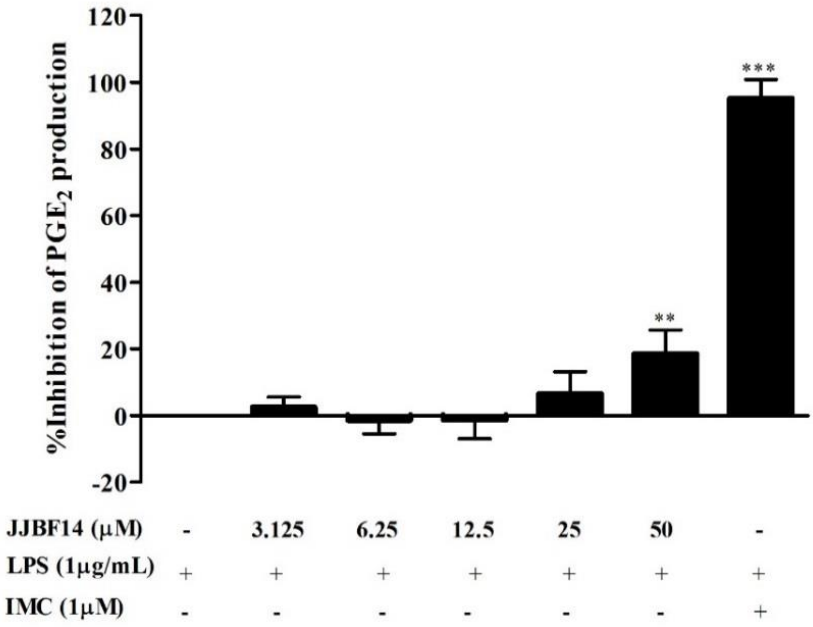

Figure 4-10 Effect of JJBF14 on LPS-induced PGE_2 production in RAW 264.7 macrophage cells. (A) PGE_2 concentration in culture medium of cells treated with JJBF14 at various concentrations for 24 hours. (B) Percentage inhibition of PGE_2 production of cells treated with JJBF14 at various concentrations in the presence of LPS (1μg/mL) for 24 hours. IMC = indomethacin-treated cells. Data are presented as mean ± SD of three independent experiments with triplicate samples. $^{###}P<0.001$ compared to control unstimulated cells. $^{*}P<0.05$, $^{**}P<0.01$ and $^{***}P<0.001$ compared to the LPS-stimulated cells.

4.8 Effect of JJBF14 on LPS-induced COX-2 expression in RAW264.7 macrophages

We further investigated whether the inhibitory effect of JJBF14 on PGE_2 production results from modulation of COX-2 expression in LPS-stimulated macrophage. Therefore, we examined the expression of COX-2 using Western blot and qRT-PCR. Our results showed that expression of COX-2 protein and mRNA markedly increased upon LPS-activation in RAW 264.7 cells (Figure 4-11 and 4-12). As shown in Figure 4-11, treatment of cells at 12.5-50 μM of JJBF14 caused a significant decrease in COX-2 protein expression. In contrast, COX-2 mRNA expression remained unchanged at all tested concentration of JJBF14 (Figure 4-12).

(A)

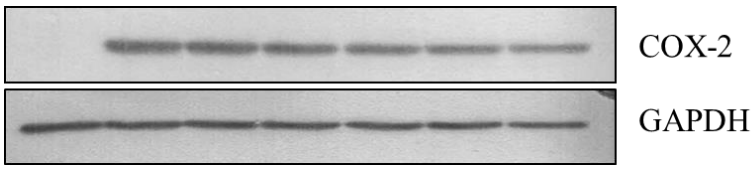

(B)

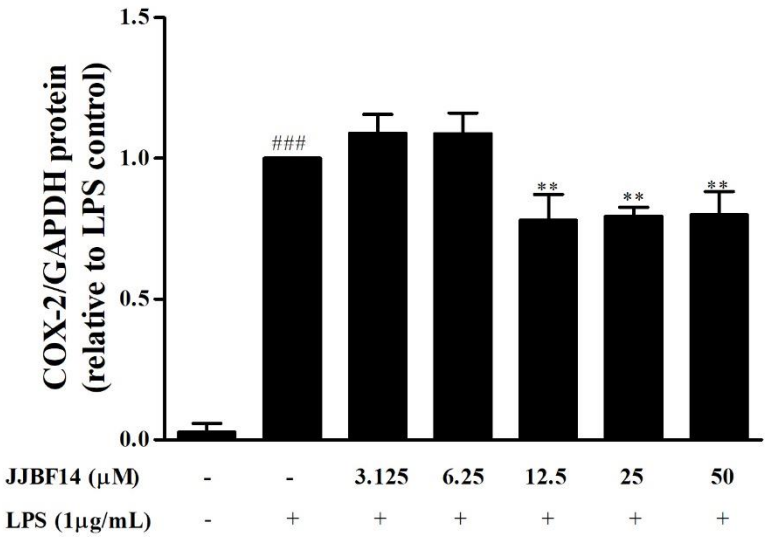

Figure 4-11 Effect of JJBF14 on COX-2 expression in LPS-stimulated RAW 264.7 macrophages. Cells were treated with JJBF14 in the presence of LPS (1 μg/mL) for 24 hours. (A) The levels of COX-2 protein expression were determined by Western blot analysis. (B) Each column shows the mean ± SD of densitometric analyses of COX-2 protein and normalized with GAPDH. Data are presented as relative to LPS control cells. $^{###}$ $P<0.001$ compared to control unstimulated cells. $^{**}P<0.01$ compared to the LPS-stimulated cells.

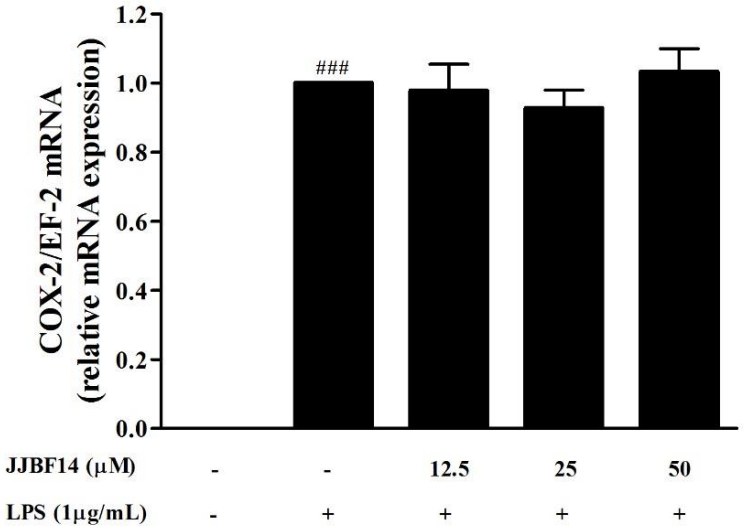

Figure 4-12 Effect of JJBF14 on LPS-induced COX-2 mRNA expression in RAW264.7 macrophages. Cells were treated with JJBF14 in the presence of LPS (1 μg/mL) for 9 hours. The amount of COX-2 mRNA was determined by real time RT-PCR which normalized with amount of EF-2 mRNA. Data are shown as mean ± SD of three independent experiments with triplicate samples. $^{###}$ $P<0.001$ compared to control unstimulated cells.

4.9 Effect of JJBF14 on LPS-induced COX enzymatic activity in RAW264.7 macrophages

We also investigated whether the inhibitory effect of JJBF14 on PGE_2 production was mediated by the inhibition of cyclooxygenase enzyme activity. COX-2 protein expression was induced by LPS and exogenous arachidonic acid was added as substrate. As a result, JJBF14 exposure did not inhibit COX-2 activity in LPS-stimulated macrophages (Figure 4-13). Furthermore, 1μM of indomethacin, the COX inhibitor, significantly inhibited LPS-induced cyclooxygenase enzyme activity (Figure 4-13).

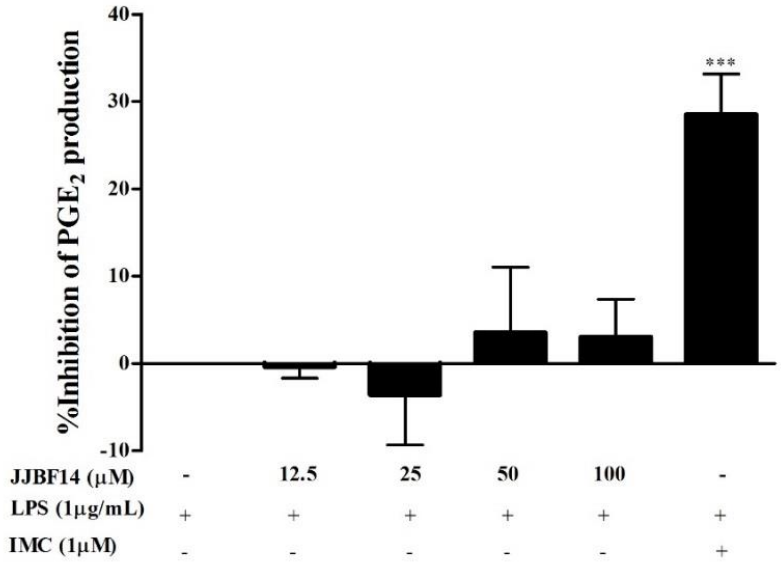

Figure 4-13 Effect of JJBF14 on COX-2 activity in RAW 264.7 macrophages. Cells were activated with LPS (1μg/mL) for 24 hours before treated with various concentrations of JJBF14 and IMC (1μM) for 30 minutes. 1 μM arachidonic acid was added and incubated further PGE_2. PGE_2 concentration in medium were determined. Data are presented as mean ± SD of three independent experiments with triplicate samples. ***P<0.001 compared to the LPS-stimulated cells.

4.10 Effect of JJBF14 on COX-1 protein expression in RAW264.7 macrophages

Next, the effect of JJBF14 on COX-1 expression was determined. As shown in Figure 4-14 to 4-16, COX-1 protein and mRNA expression were constitutively expression in control unstimulated cells, whereas treatment cells with LPS cause reduction of COX-1 expression. In unstimulated cells, COX-1 protein expression in cells treated with JJBF14 was not different from control cells (Figure 4-14). Furthermore, JJBF14 attenuated the reduction of LPS-modulated COX-1 protein expression (Figure 4-15), whereas it did not affect such a reduction of COX-1 mRNA by LPS (Figure 4-16).

(A)

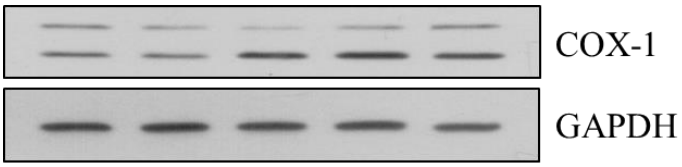

(B)

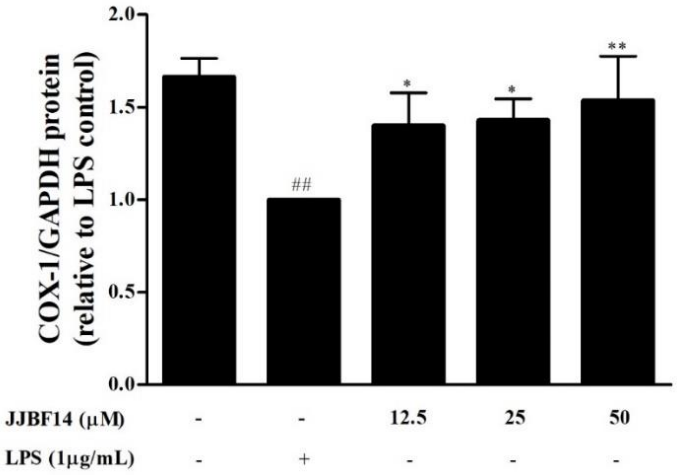

Figure 4-14 Effect of JJBF14 on COX-1 protein expression in RAW264.7 macrophages. Cells were treated with JJBF14 for 24 hours. (A) The levels of COX-1 protein expression were determined by Western blot analysis. (B) Each column shows the mean ± SD of densitometric analyses of COX-1 protein levels and normalized with GAPDH. Data are presented as relative to LPS control cells. $^{\#\#}$ $P<0.01$ compared to control unstimulated cells. $^{*}P<0.05$ and $^{**}P<0.01$ compared to the LPS-stimulated cells.

(A)

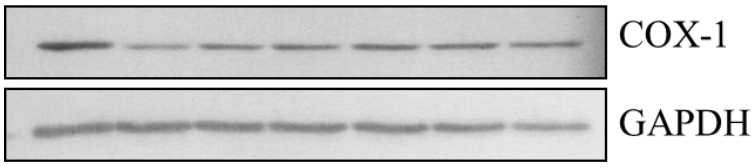

(B)

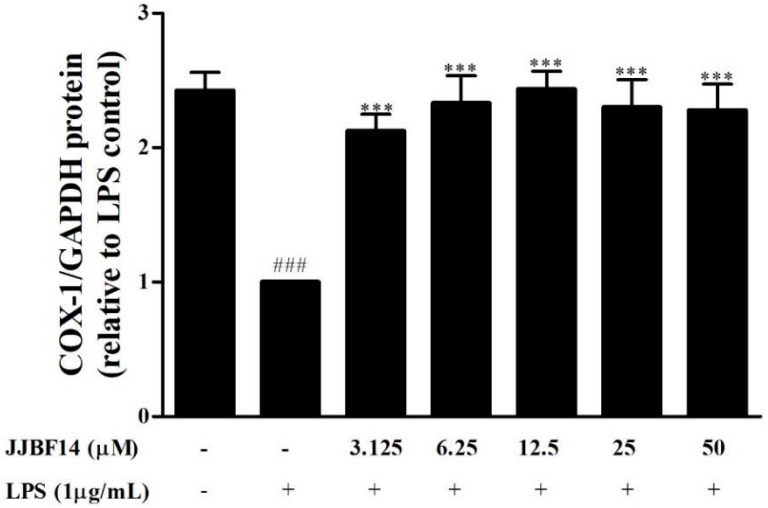

Figure 4-15 Effect of JJBF14 on COX-1 protein in LPS-stimulated RAW264.7 macrophages. Cells were treated with JJBF14 in the presence of LPS (1μg/mL) for 24 hours. (A) The levels of COX-1 protein were determined by Western blot analysis. (B) Each column shows mean ± SD of densitometric analyses of COX-1 protein levels and normalized with GAPDH. Data are presented as relative to LPS control cells. $^{###}$ P<0.001 compared to control unstimulated cells. $^{***}P$<0.001 compared to the LPS-stimulated cells.

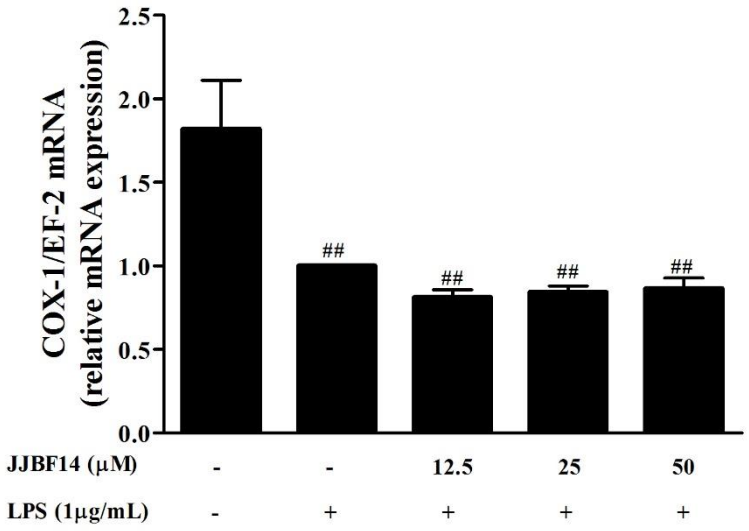

Figure 4-16 Effect of JJBF14 on COX-1 mRNA expression in LPS-stimulated RAW264.7 macrophages. Cells were treated with JJBF14 in the presence of LPS (1 μg/mL) for 9 hours. The amount of COX-1 mRNA was determined by real time RT-PCR which normalized with amount of EF-2 mRNA. Data are shown as mean ± SD of three independent experiments with triplicate samples. $^{\#\#}$ $P<0.01$ compared to control unstimulated cells.

4.11 Effect of JJBF14 on LPS-induced IL-1β and TNF-α production in RAW264.7 macrophages

To examine the effects of JJBF14 on LPS-induced release of IL-1β and TNF-α, the level of IL-1β and TNF-α production in medium were measured by ELISA kit. IL-1β and TNF-α production was induced in response to LPS stimulation compared to control unstimulated cells (Figure 4-17 and Figure 4-18). JJBF14 did not affect on IL-1β in LPS-stimulated cells (Figure 4-17). While, JJBF14 at 6.25-50 μM inhibited the TNF-α production in LPS-stimulated cells (Figure 4-18). Moreover, BAY 11-7082 (5μM), a NF-κB inhibitor, significantly suppressed the production of IL-1β and TNF-α in LPS-treated cells.

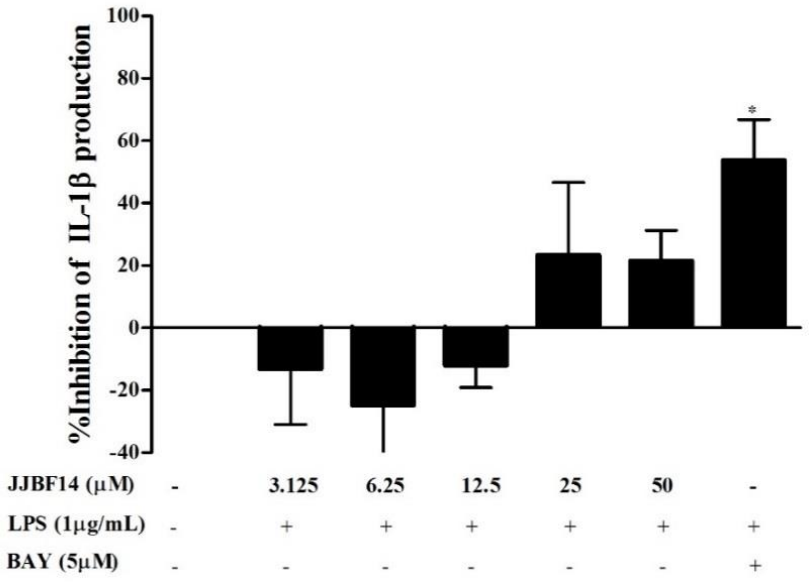

Figure 4-17 Effect of JJBF14 on LPS-activated IL-1β production in RAW264.7 macrophages. Percentage inhibition of IL-1β production of cells treated with JJBF14 at various concentrations in the presence of LPS (1 μg/mL) for 24 hours. BAY = BAY 11-7082-treated cells. Data are presented as mean ± SD of three independent experiments with triplicate samples. $^{*}P<0.05$ compared to the LPS-stimulated cells

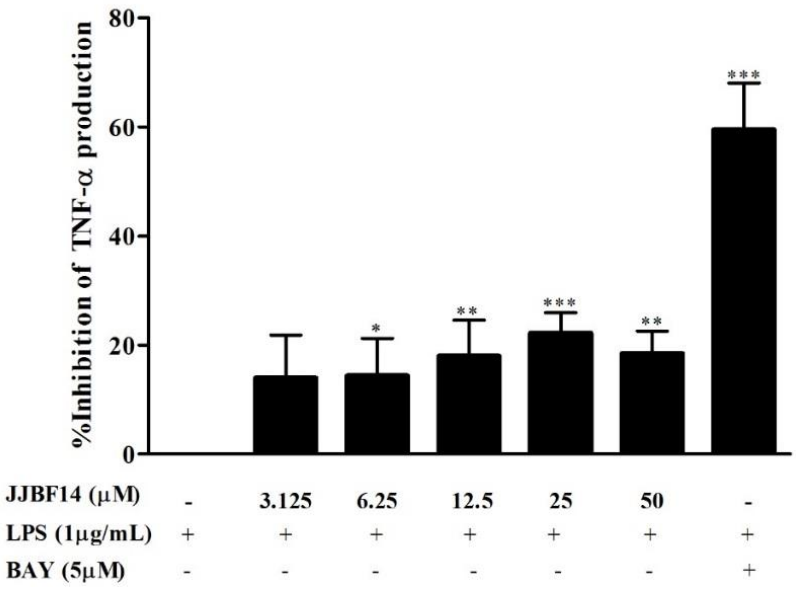

Figure 4-18 Effect of fluorinated triarylmethane derivatives on TNF-α production in LPS-activated RAW 264.7 macrophages. Percentage inhibition of TNF-α production of cells treated with JJBF14 at various concentrations in the presence of LPS (1 μg/mL) for 24 hours. BAY = BAY 11-7082-treated cells. Data are present as mean ± SD of three independent experiments with triplicate samples. $^{*}P<0.05$, $^{**}P<0.01$ and $^{***}P<0.001$ compared to the LPS-stimulated cells.

4.12 Effect of JJBF14 on LPS-induced NF-κB p65 translocation in RAW 264.7 macrophage cells

To further elucidate the signaling pathway underlying anti-inflammatory activity of JJBF14, we examined the effects on the regulation of NF-κB activation. We, thus, examined the effects of JJBF14 on the nuclear translocation of p65 NF-κB and phosphorylation of IκBα in LPS-stimulated macrophage cells using Western blot analysis. LPS stimulation for 15 and 30 minutes, markedly increased the level of the p65 NF-κB nuclear translocation and phosphorylation of IκB (Figure 4-19). Moreover, JJBF14 (50μM) inhibited the translocation of p65 NF-κB to nucleus at 30 minutes (Figure 4-19C). The compound at 25 and 50 μM also suppressed the phosphorylation of IκB in LPS-stimulation for 30 minutes (Figure 4-19D). However, JJBF14 failed to repress the p65 NF-κB nuclear translocation and phosphorylation of IκB at 15 minutes of LPS activation (Figure 4-19A and 4-19B). Besides, BAY 11-7082 attenuated both p65 NF-κB translocation and phosphorylation of IκB in LPS-induced activation at each time point (Figure 4-19).

(A)

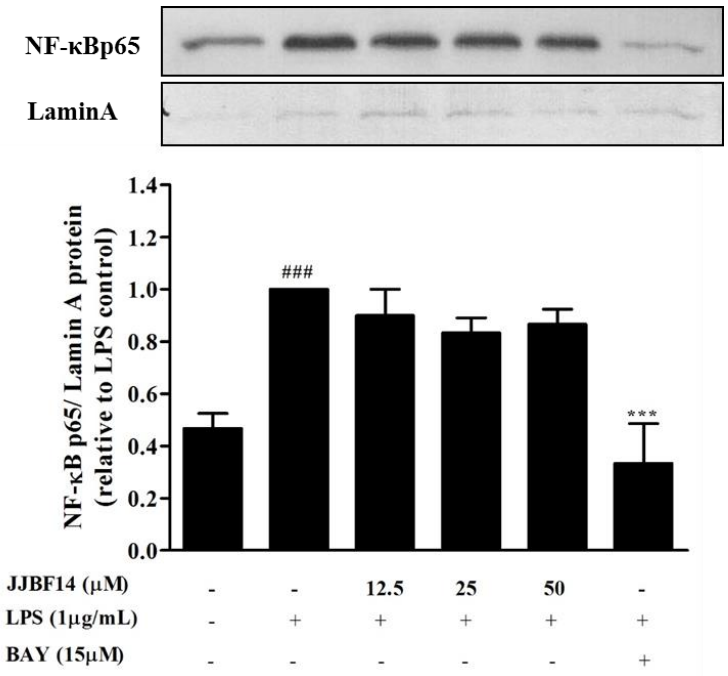

(B)

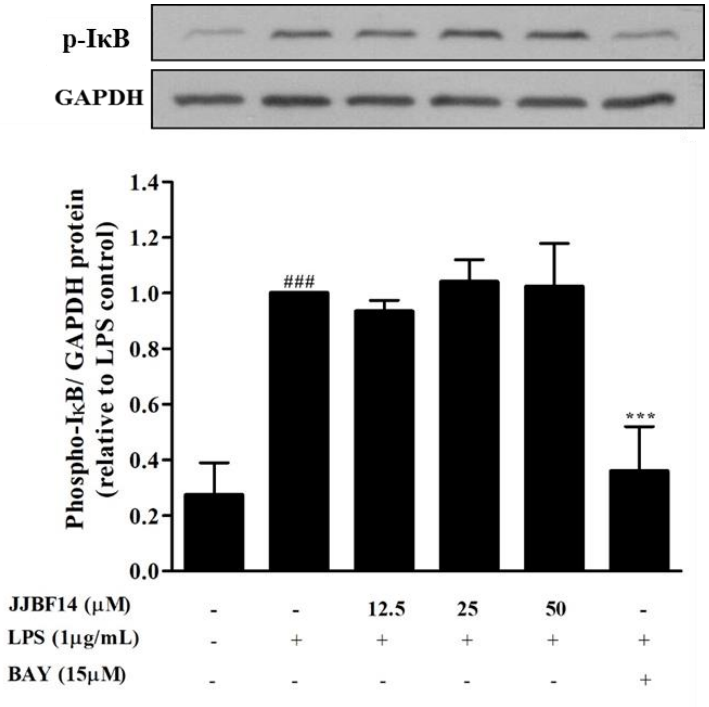
p-IκB
GAPDH
Phospho-IκB/ GAPDH protein (relative to LPS control)
1.4
1.2
1.0
0.8
0.6
0.4
0.2
0.0
###
***
JJBF14 (μM) - - 12.5 25 50 -
LPS (1μg/mL) - + + + + +
BAY (15μM) - - - - - +

(C)

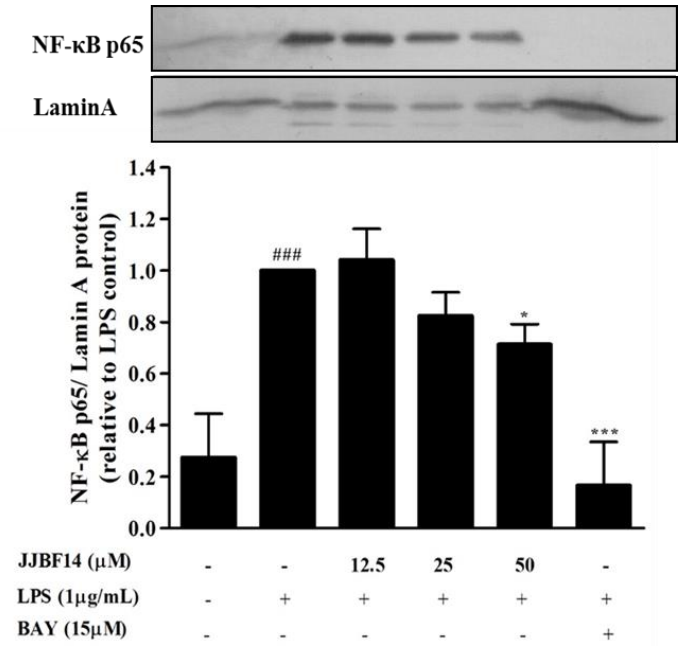
NF-κB p65
LaminA
NF-κB p65/ Lamin A protein (relative to LPS control)
1.4
1.2
1.0
0.8
0.6
0.4
0.2
0.0
###
*
***
JJBF14 (μM) - - 12.5 25 50 -
LPS (1μg/mL) - + + + + +
BAY (15μM) - - - - - +

(D)

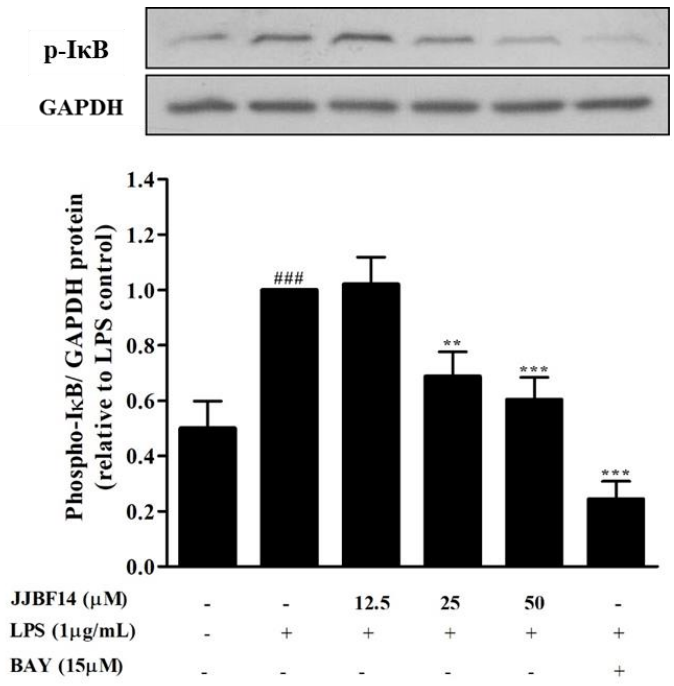

Figure 4-19 Effect of JJBF14 on LPS-induced NF-κB p65 activation in RAW 264.7 macrophages. Cells were pretreated with JJBF14 (12.5-50μM) for 1 hour and then stimulated with LPS (1μg/mL) for 15 (A, B) and 30 minutes (C, D). The levels of NF-κB p65 in nuclear protein (A, C) and p-IκB in whole cell extracts (B, D) were determined by Western blot analysis. Graph are shown as the mean ± SD (n=3) of densitometric analyses NF-κB p65 and p-IκB which normalized by LaminA and GAPDH densitometric values, respectively. Data are presented as relative to LPS control cells. $^{###}$ P<0.001 compared to control unstimulated cells. $^{*}P$<0.05, $^{**}P$<0.01 and $^{***}P$<0.001 compared to the LPS-stimulated cells.

4.13 Effect of JJBF14 on LPS-induced phosphorylation of MAPKs in RAW264.7 macrophages

To investigate the molecular mechanism underlying the inhibitory effect of JJBF14 on the LPS-induced production of pro-inflammatory mediators and cytokines, we examined the effect of JJBF14 on the phosphorylation of MAPKs by Western blot analysis. The LPS treatment significantly increased the phosphorylation levels of ERK1/2, JNK and p38, compared to the control unstimulated cells (Figure 4-21). Treatment with the JJBF14 (12.5-50μM) markedly repressed the phosphorylation of p38 MAPKs compared to the LPS-stimulated cells. However, JJBF14 did not affect on the LPS-induced phosphorylation of ERK1/2 and JNK. Moreover, JJBF14 alone did not induce the phosphorylated on MAPKs levels in unstimulated cells.

(A)

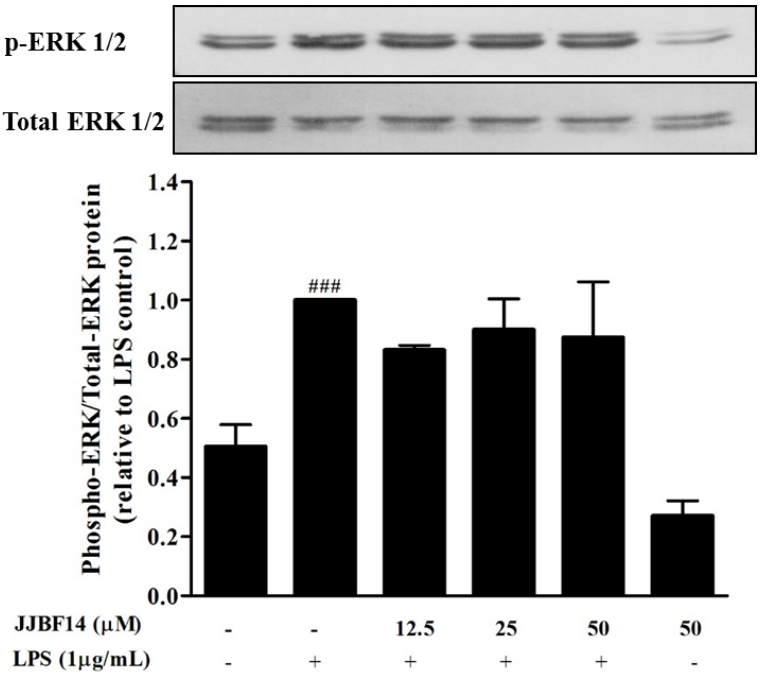
p-ERK 1/2
Total ERK 1/2
Phospho-ERK/Total-ERK protein (relative to LPS control)
1.4
1.2
1.0
0.8
0.6
0.4
0.2
0.0
###
JJBF14 (μM) - - 12.5 25 50 50
LPS (1μg/mL) - + + + + -

(B)

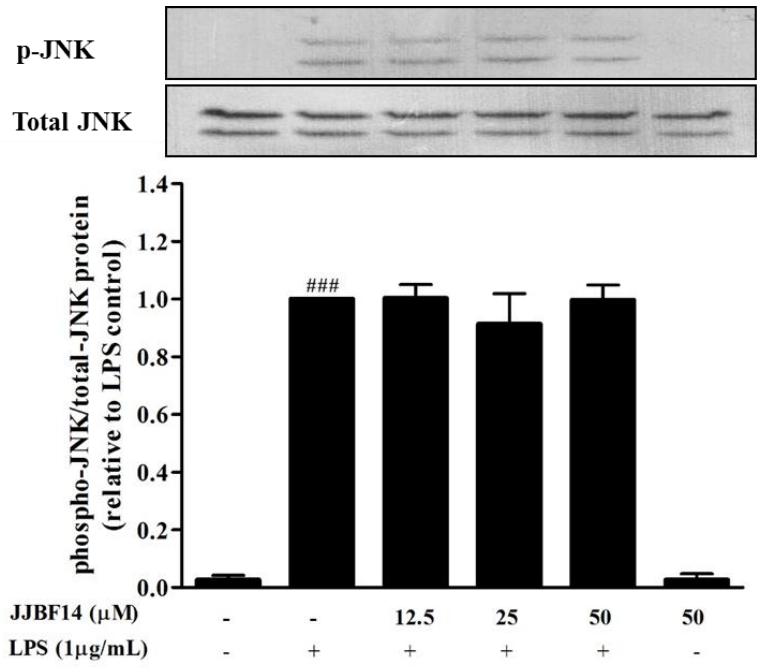
p-JNK
Total JNK
phospho-JNK/total-JNK protein (relative to LPS control)
1.4
1.2
1.0
0.8
0.6
0.4
0.2
0.0
###
JJBF14 (μM) - - 12.5 25 50 50
LPS (1μg/mL) - + + + + -

(C)

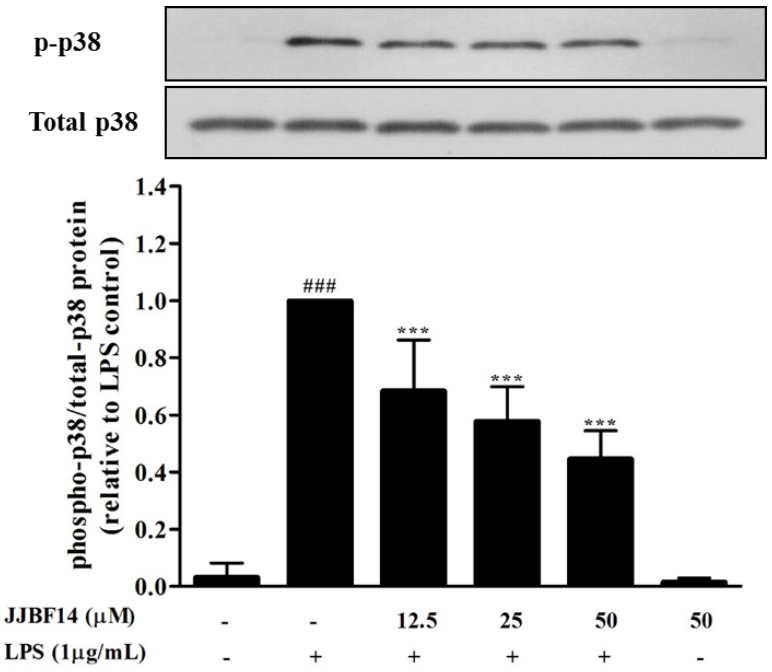

Figure 4-20 Effect of JJBF14 on LPS-induced phosphorylation of MAPKs in RAW264.7 macrophages. Cells were pretreated with JJBF14 (12.5-50μM) for 1 hour and then stimulated with LPS (1μg/mL) for 30 minutes. After incubation, the levels of p-ERK1/2 and t-ERK1/2 (A), p-JNK and t-JNK (B) and p-38 and t-p38 (C) in the whole cell lysates were determined by Western blot analysis. Graph are shown as the mean ± SD (n=3) of densitometric analyses of p-ERK1/2, p-JNK and p-38 which normalized by t-ERK1/2, t-JNK and t-p38 densitometric values. Data are presented as relative to LPS control cells. $^{###}$ P<0.001 compared to control unstimulated cells. $^{***}P$<0.001 compared to the LPS-stimulated cells.

4.14 Effect of JJBF14 on LPS-induced phosphorylation of ATF-2 in RAW264.7 macrophages

Phosphorylation of ATF-2 upon LPS induction enhances its transcriptional activity. Therefore, we determined whether JJBF14 affects LPS induced phosphorylation of ATF-2. As shown in Figure 4-20, LPS stimulation significantly increased the phosphorylation of ATF-2. Treatment with JJBF14 (25 and 50μM) markedly decreased the p-ATF-2. Besides, the induction of p-ATF-2 by LPS was suppressed by SB202190 (a p38 inhibitor).

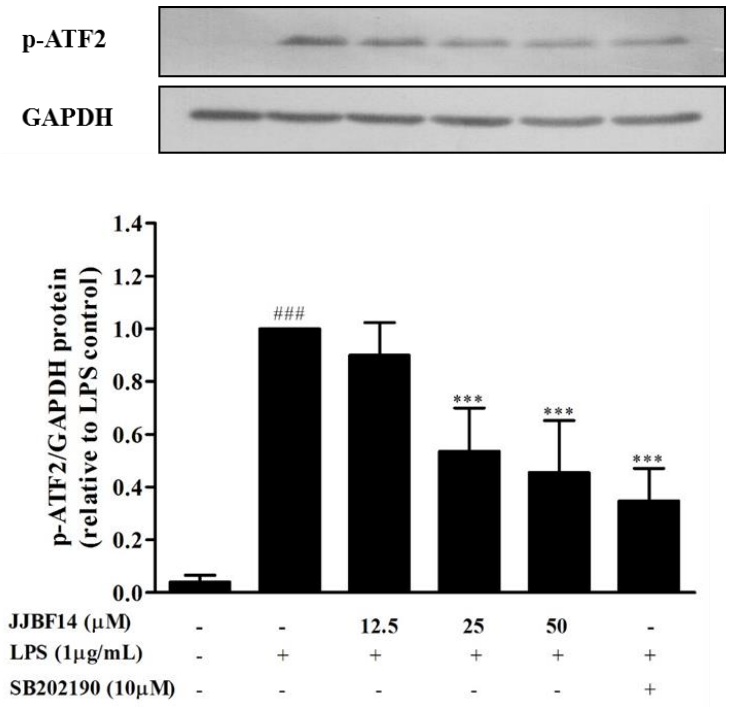

Figure 4-21 Effect of JJBF14 on LPS-induced phosphorylation of ATF-2 in RAW264.7 macrophages. Cells were pretreated with JJBF14 (12.5-50μM) for 1 hour and then stimulated with LPS (1μg/mL) for 30 minutes. After incubation, the whole cell lysates were determined by Western blot analysis. Graph are shown as the mean ± SD (n=3) of densitometric analyses of p-ATF2 which normalized by GAPDH densitometric values. Data are presented as relative to LPS control cells. ### $P<0.001$ compared to control unstimulated cells. *** $P<0.001$ compared to the LPS-stimulated cells.

CHAPTER 5
DISCUSSION AND CONCLUSION

The present study, we evaluated the effect of twenty-six newly synthesized fluorinated triarylmethane derivatives on NO production in LPS-activated RAW264.7 macrophages. To further measure the cell viability of fluorinated triarylmethane derivatives in RAW264.7 macrophages by using the MTT assay and the results are shown in Figure 4-1. Examination of the structure activity relationship (SAR) in fluorinated triarylmethane derivatives have indicated that the tested compounds can be classified into three groups. Firstly, viability of cells treated with fluorinated triarylmethane derivatives having indole group (JJAF1-JJAF7) were less than 30%. JJAF1, JJAF2 and JJAF4 which containing the similarly 6-fluoroindole and benzene moieties, but changing one aryl ring as 2,4,5-trimethoxyphenyl ring, (5-methyl)2-furyl ring and *p*-N,N-dimethylaniline, respectively, decreased the cell viability ranging from 24.33 ± 2.38, 3.25 ± 0.12 and 45.72 ± 4.30%, respectively (Figure5-1). JJAF2 and JJAF3 containing 6-fluoroindole and 5-methyl furan and changing benzene ring to 4-nitrophenyl ring showed the cytotoxicity to 96% (Figure 5-2). On the other hand, bis[(5-methyl)2-furyl](4-nitrophenyl)methane which containing 2 rings of (5-methyl)2-furyl ring and 4-nitrophenyl ring on the same methine carbon showed % cell viability by 96.3 ± 2.9 (Jaratjaroonphong et al., 2014). Moreover, JJAF7 containing 3 rings of 6-fluoroindole showed % cell viability by 3.67 ± 0.18. These results suggest that 6-fluoroindole on the triarylmethane plays an important part for the cytotoxicity. Similarly, changing the aromatic ring from 6-fluoroindole to indole with 4-fluorobenzaldehyde (JJAF5 and JJAF6) still showed the cytotoxicity (Figure 5-3). Therefore, the cytotoxicity might be due to the effect of fluorine atom on the six-position of indole and indole that consist in the structure of triarylmethane.

As these results, the second groups of fluorinated triarylmethanes without 6-fluoroindole and indole ring were then tested. The selected synthesized triarylmethane analogues containing two rings of 2,4,6-trimethoxyphenyl and one ring of variety of fluorine position on benzene ring (JJBF1-JJBF6) showed the viability of cells more than 80% except that of JJBF3 was 60% (Figure 5-4). Unfortunately, the inhibitory

activities on NO production were less than aminoguanidine (51% inhibition). These results might be due to the steric effect of two methoxy groups at C2 and C6 position of two aromatic rings. Gratifyingly in the case of fluorinated triarylmethane that derived from the condensation of 1,2,4-trimethoxybenzene with a variety of fluorinated benzaldehyde (JJBF7-JJBF12) showed the viability of cells more than 80%. Besides, JJBF9-JJBF12 exhibited the inhibitory activities on NO production more than 80%. Furthermore, the viability of cells treated with fluorinated triarylmethane that synthesized by condensation of 1,2,3-trimethoxybenzene with a variety of fluorinated benzaldehyde (JJBF13-JJBF18) was more than 95%. Moreover, JJBF13-JJBF15 exhibited moderate inhibitory activities on NO production more than 70%. These results suggest that decreasing the steric effect of methoxy group on benzene ring increased the inhibitory activities on NO production and was not effect on cytotoxicity. Moreover, 4-fluorophenyl ring with 2,4,5-trimethoxybenzene or 2,3,4-trimethoxybenzene ring also increased the inhibitory activities on NO production. Changing the trimethoxybenzene to bis(N,N-dimethylaniline) with 4-fluorophenyl ring (JJCF1) can enhance the inhibitory effect without significant cytotoxicity. Among these derivatives, six compounds including JJBF9, JJBF10, JJBF11, JJBF12, JJBF14, JJBF15 and JJCF1 were more potent of NO inhibitory activity than other compounds.

The IC_{50} values of NO inhibitory activity of selected fluorinated triarylmethane derivatives were ranging from 6.89 ± 0.47 to 18.76 ± 0.85 µM which less than aminoguanidine (56.91 ± 1.47 µM). Moreover, therapeutic index of JJBF14 and JJCF1 were higher than another compounds. The structure of JJCF1 is similar to malachite green (MG), a triarylmethane dye that contain two rings of bis(N,N-dimethylaniline) and benzene ring which widely used in a numerous industries such as aquaculture, food, medical and textile (Srivastava, Sinha, & Roy, 2004). Nevertheless, the use of this dye has been concerned about its toxicity such as alteration of histopathological of internal organs, mutagenic, carcinogenic and teratogenic effects (Srivastava et al., 2004). Therefore, JJBF14 was chosen to further investigate to get insight into the mechanism of anti-inflammatory effects in LPS-induced macrophages RAW264.7.

NO and PGE_2 are important inflammatory mediators in initiate response in activated macrophages (Bosca, Zeini, Traves, & Hortelano, 2005; Brown, Cosseau, Gardy, & Hancock, 2007). NO is involved in pathogenesis and control of infection diseases contributed to tumors, auto immune, acute and chronic diseases (Bogdan, 2001). Besides, PGE_2 is a lipid-derived bioactive substance that act as vasodilator to recruitment inflammatory cells leading to swelling and edema at the site of inflammation (Hinz & Brune, 2002; Nakanishi & Rosenberg, 2013). Furthermore, PGE_2 production is involved in fever and pain response. Thus, reducing the levels of NO and PGE_2 production from LPS-stimulation may be an effective strategy for suppressing inflammatory response. In the present study, LPS was used as inflammatory stimulant since LPS has been reported to increase the levels of NO, PGE_2, iNOS and COX-2 (Chiu & Lin, 2008; Senthil Kumar & Wang, 2009). The results showed that JJBF14 suppressed the overproduction of NO with an IC_{50} value at 9.32 ± 0.98 µM. Which is better than that of aminoguanidine, an iNOS inhibitor, for 5-6 times. Nevertheless, JJBF14 exhibited weak inhibitory activity on PGE_2 production.

In our ongoing study to develop novel anti-inflammatory agents, our research group reported that the synthetic bis(heteroaryl)alkane derivative namely bis[(5-methyl)2-furyl] (4-nitrophenyl)methane (BFNM) exhibited the inhibition of NO and PGE_2 with and IC_{50} values of 42.4 ± 1.9 µM and 36.1 ± 6.3 µM, respectively (Udompong, Mankhong, Jaratjaroonphong, & Srisook, 2017). In the present study, our findings showed that JJBF14 inhibited NO production with greater potency than BFNM for 4.5 times. However, BFNM show much more potent on LPS-induced PGE_2 production than JJBF14.

To investigate the mechanism underlying the inhibitory activity on NO and PGE_2 generation by JJBF14 in LPS-activated RAW264.7 macrophages, the effect of JJBF14 on iNOS and COX-2 activity and expression was examined. As shown in Figure 4-9, JJBF14 did not inhibit iNOS and COX-2 enzyme activity whereas aminoguanidine and indomethacin did, respectively. However, our data provide evidences that JJBF14 (12.5-50 µM) effectively reduced LPS-induced protein and mRNA expression of iNOS (Figure 4-7 and 4-8). The data suggest that suppression of

NO by JJBF14 was due to reduced iNOS protein and mRNA expression not by inhibition of iNOS activity.

We next examined whether JJBF14 can also modulate the expression of COX-2, a major enzyme that produce PGE_2 in LPS-induced RAW264.7 macrophages (Kang, Wingerd, Arakawa, & Smith, 2006; Ricciotti & FitzGerald, 2011). In the present study, we showed that JJBF14 at 12.5-50 μM decreased LPS-induced COX-2 protein expression whereas it did not significantly change COX-2 gene expression and COX-2 activity (Figure 4-12 and 4-13). Thus, the effect of JJBF14 on PGE_2 inhibition might be mainly from the suppression of COX-2 expression. Dixon, Kaplan, Mcintyre, Zimmerman, and Prescott (2000) have demonstrated that post-transcription and transcription are regulatory point for COX-2 gene expression. Besides, there are evidences that post-translational level can regulate COX-2 enzyme (Alexanian & Sorokin, 2017). Mbonye et al. (2008) demonstrated that COX-2 protein can be degraded via N-glycosylation and substrate-dependent suicide inactivation. Therefore, JJBF14 probably suppressed PGE_2 production through the regulation at the post-translational level. In addition, similar observation was reported by Kang et al. (2012). Lycorine, a natural alkaloid extracted from *Amaryllidaceae*, has been shown to decrease the protein level of both iNOS and COX-2 in RAW264.7 macrophages. Besides, it also suppressed LPS-induced iNOS but not COX-2 gene expression. Although, iNOS and COX-2 expression, was induced by LPS both genes are regulated by different sets of transcription factor. The mouse iNOS promoter requires the consensus sequence for transcription factor such as NF-κB, NF-IL6, CRE, IRE, TNF-RE, Oct, GAS, ISRE and TATA box (Chu, Marks-Konczalik, Wu, Banks, & Moss, 1998; Lowenstein et al., 1993; Xie, 1997; Xie, Whisnant, & Nathan, 1993). However, the transcription factor NF-κB seem to be the most important one for maximal iNOS promoter activity in RAW264.7 cells (Kim, Lee, Yi, & Paik, 1997; Xie, Kashiwabara, & Nathan, 1994). Previous study identified several response elements that regulated LPS-induced mouse COX-2 gene. In the mouse promoter, CRE-2, AP-1, E-box, CRE-1, NF-κB and C/EBP are necessary for COX-2 promoter activity (Kang et al., 2006; Mestre et al., 2001). It has been proposed that NF-κB, C/EBP, CRE-1 and AP-1 site are important for regulating COX-2 transcription in LPS-induced macrophage (Kang et al., 2006). Taken together, our results suggest that

inhibition of iNOS and COX-2 expression by JJBF14 may be by different transcriptional pathway.

NSAIDs are the most commonly drug used for effective in pain and inflammatory disorder (Rao, Kabir, & Mohamed, 2010). The generally mechanism of classical NSAIDs is blocking the production of PGE_2 by the inhibition of constitutive COX-1 and inducible COX-2 enzymes. While the undesired side effect occurs from COX-1 inhibition, causing various side effects including gastrointestinal damage, kidney and renal failure (Conaghan, 2012; Suleyman, Demircan, & Karagoz, 2007). Herein, we also observed the effect of JJBF14 on COX-1 expression. As a result, the treatment with LPS significantly inhibited COX-1 protein and mRNA expression compared to control unstimulated cells (Figure 4-14 to 4-16). It has been reported that LPS or IFNγ/LPS treatment attenuated of the constitutive COX-1 expression in macrophage RAW264.7 (Lee et al., 2011). In a previous study, the expression of COX-2 was up-regulated and COX-1 down regulated in astrocyte cells after LPS activation (Nieves et al., 2012). Furthermore, Liu and Rose (1996) reported that treatment with LPS cause down-regulated of COX-1 in rat lung and heart. The transcriptional activation of COX-1 contains GC-rich, SP1 like elements and lacking of TATA box (Kraemer, Meade, & DeWitt, 1992; Smith, Garavito, & DeWitt, 1996). In response to LPS, SP1 protein is dephosphorylated and degraded resulting in down-regulation of SP1-DNA binding activity *in vivo* (Ye & Liu, 2002). Thus, it indicates that LPS operates COX-1 and COX-2 expression by distinct mechanism. In addition, COX-1 protein expression in JJBF14 treatment was not different from that of control cells. Moreover, JJBF14 also attenuated the reduction of LPS-regulated COX-1 protein expression. It is postulated that JJBF14 exerted the selective inhibitory effect on COX expression.

Cytokines like TNF-α and IL-1β have been reported to be released at the early stages of immune response to infection, wound and stress (Duque & Descoteaux, 2014). During inflammatory processes, IL-1β is a potent mediator that involved in cell proliferation, differentiation and apoptosis (Lopez-Castejon & Brough, 2011; Ren & Torres, 2009). Besides, TNF-α is a strong pro-inflammatory cytokine that produced by macrophages or monocytes and plays a crucial role activation and recruitment of inflammatory cells. Furthermore, TNF-α has been shown to act in the

development of many acute and chronic inflammatory diseases including sepsis and rheumatoid arthritis (Parameswaran & Patial, 2010). Therefore, the suppression of TNF-α and IL-1β is considered as a therapeutic opportunity. Hence, we also observed the inhibitory effect of JJBF14 on TNF-α and IL-1β production. Our results showed that JJBF14 suppressed the LPS-induced TNF-α but not IL-1β production. The cis-acting elements assigned on the promoter region of murine TNF-α including NF-κB binding sites, C/EBPβ, AP-1 and TATA motif (Kuprash et al., 1999; Lee, Sung, Kim, & Kim, 2003). Kuprash et al. (1999) suggested that NF-κB play a major role in transcriptional up-regulation of the TNF-α gene by LPS-induced macrophage cells. Moreover, they proposed that the several NF-κB site in the TNF-α promoter appears to ensure maximal activation of TNF-α gene by LPS. The murine IL-1β promoter contains a number of recognition site for LPS-induced macrophage cells, including NF-IL6, CRE, IFN regulatory factor (IRF), AP-1 and STAT (Baldassare, Bi, & Bellone, 1999; Zhang, Saccani, Shin, & Nikolajczyk, 2008). Godambe, Chaplin, Takova, Read, and Bellone (1995) have identified NF-IL6 regulatory element is necessary for IL-1β expression in response to LPS. Furthermore, they suggested that both C/EBPβ and C/EBPδ are major in IL-1β gene activation. Taken together, JJBF14 may suppress TNF-α and IL-1β production by different transcription requirement for the activation.

NF-κB is an important transcription factor in regulation of many genes that code for mediating the pro-inflammatory responses (Ghosh & Hayden, 2008; Liu, Zhang, Joo, & Sun, 2017). Under basal conditions, NF-κB is bound to IκB-α, a representative inhibitor protein, in the cytoplasm. After exposure to LPS, phosphorylation of IκB-α by IKK leads to its degradation. Consequently, NF-κB dissociates from IκB-α and translocates into nucleus, thereby initiating the transcription of target genes (Lawrence, 2009; Newton & Dixit, 2012). To determine molecular mechanism of JJBF14 on LPS-induced inflammatory-responsive genes, we examined the effect of JJBF14 on the nuclear translocation of p65 NF-κB and phosphorylation of IκB-α. We demonstrated that LPS stimulation for 15 and 30 minutes markedly promoted the translocation of p65 NF-κB and phosphorylation of IκB-α (Figure 4-19). Herein, we showed that pretreatment with JJBF14 for 1 hour led to significant blockade of LPS-induced p65 NF-κB nuclear translocation at 30

minutes of LPS activation. JJBF14 also inhibited IκB-α phosphorylation in LPS activated cells. Therefore, these results indicated that JJBF14 inactivated by suppressing IκB-α phosphorylation and p65 NF-κB translocation.

Apart from NF-κB, recent reports have demonstrated that the MAPKs kinase including JNK, ERK1/2 and p38 are implicated in the induction of pro-inflammatory mediators and cytokines in activated macrophage (Kaminska, 2005; Frazier, Xue, Luce, & Liu, 2012; Udompong et al., 2017). We, therefore, examined the role of MAPKs pathway activation in LPS-induced mediator and cytokine expressions in RAW264.7 macrophages. In the present study, we observed that LPS-induced phosphorylation of ERK, JNK and p38 MAPK. JJBF14 attenuated the LPS-induced phosphorylation of p38, whereas the phosphorylation levels of JNK and ERK1/2 were unchanged (Figure 4-20). These results suggest that JJBF14 prevented the inflammatory activities in LPS-induced macrophages predominantly by blocking phosphorylation of p38. A similar observation was found in anti-inflammatory effect of dysifragilone A, a sesquiterpene aminoquinone which prevented the activation of p38 but not JNK and ERK1/2 in RAW264.7 cells induced by LPS (Li et al., 2018).

Transcription factor ATF-2 is known to be a major target of p38 MAPK kinase (Hirose, Maekawa, Shinagawa, & Ishii, 2009; Yu et al., 2014). It has been reported that ATF-2 associates in the transcriptional stimulation of the iNOS and COX-2 gene expression (Yu et al., 2014; Udompong et al., 2017). Thus, the further experiment determined whether JJBF14 regulate the phosphorylation of ATF-2. The current findings, JJBF14 significantly repressed the levels of ATF-2 phosphorylation (Figure 4-21). Furthermore, SB202190 (an inhibitor of p38 MAPK) significantly prevented the stimulation of LPS-induced transcription by ATF-2 which is in accordance with the reports of Hirose et al. (2009) and Udompong et al. (2017). Collectively, it is implied that JJBF14 inhibited iNOS and COX-2 expression, at least in part, by suppressing the phosphorylation of p38 and ATF-2. This result is similar to the effect of other compounds such as 3-(2-hydroxyphenyl)-1-(5-methyl-furan-2-y-l) propanone (HMP), a chalcone derivative, and BFNM which also suppressed both of p38MAPK and ATF-2 (Liew et al., 2011; Udompong et al., 2017).

In summary, we demonstrated herein, a newly synthesized fluorinated triarylmethane derivative, JJBF14 inhibits LPS-induced inflammatory responses

including, NO and PGE_2 production as well as pro-inflammatory cytokines TNF-α in LPS-stimulated macrophages RAW264.7. These anti-inflammatory effects occur by downregulation of iNOS and COX-2 expression. Furthermore, the possible mechanism of inhibitions exerted by blocking NF-κB activation and p38/ATF-2 signaling pathways as shown in Figure 5-5. Moreover, JJBF14 might be used as a lead compound for upcoming the treatment of inflammation-related diseases.

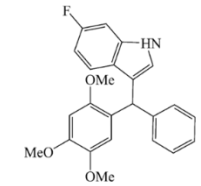

JJAF1 %cell viability = 24.33 ± 2.38

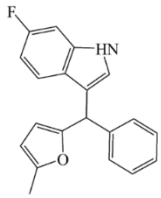

JJAF2 %cell viability = 3.25 ± 0.12

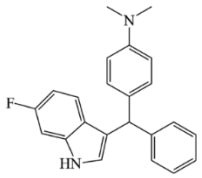

JJAF4 %cell viability = 45.72 ± 4.30

Figure 5-1 Comparing the structure of JJAF1, JJAF2 and JJAF4 all have a 6-fluoroindole and benzene moiety

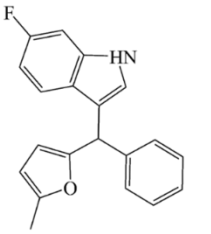

JJAF2 %cell viability = 3.25 ± 0.12

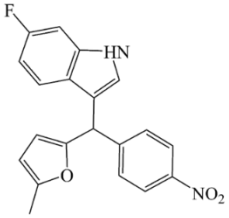

JJAF3 %cell viability = 3.41 ± 0.47

Figure 5-2 Comparing the structure of JJAF2 and JJAF3 all have a 6-fluoroindole and 2-methyl furan

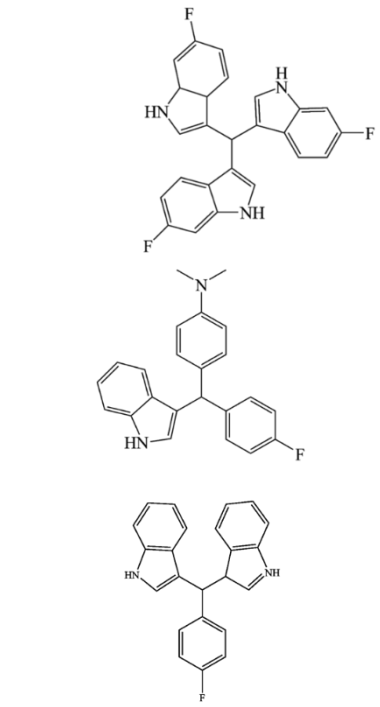

JJAF7 % cell viability = 3.67 ± 0.18

JJAF5 %cell viability = 4.23 ± 0.57

JJAF6 %cell viability = 1.26 ± 0.18

Figure 5-3 Comparing the structure of JJAF7, JJAF5 and JJAF6 all have an indole with 4-fluorobanzaldehyde

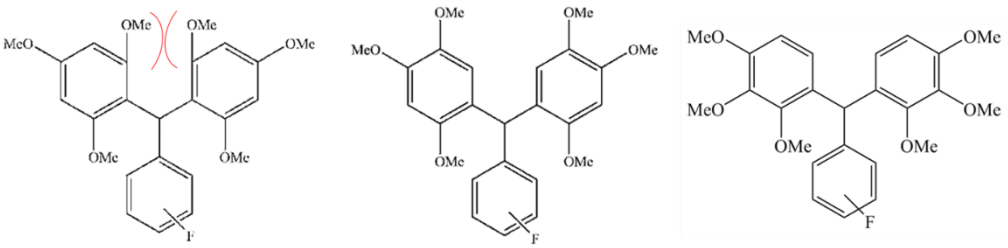

2,4,6-trimethoxybenzene JJBF1-JJBF6

2,4,5-trimethoxybenzene JJBF7-JJBF12

2,3,4-trimethoxybenzene JJBF13-JJBF18

Figure 5-4 Comparing the structure of 2,4,6-trimethoxybenzene, 2,4,5-trimethoxybenzene and 2,3,4-trimethoxybenzene one ring of variety of fluorine position on benzene ring

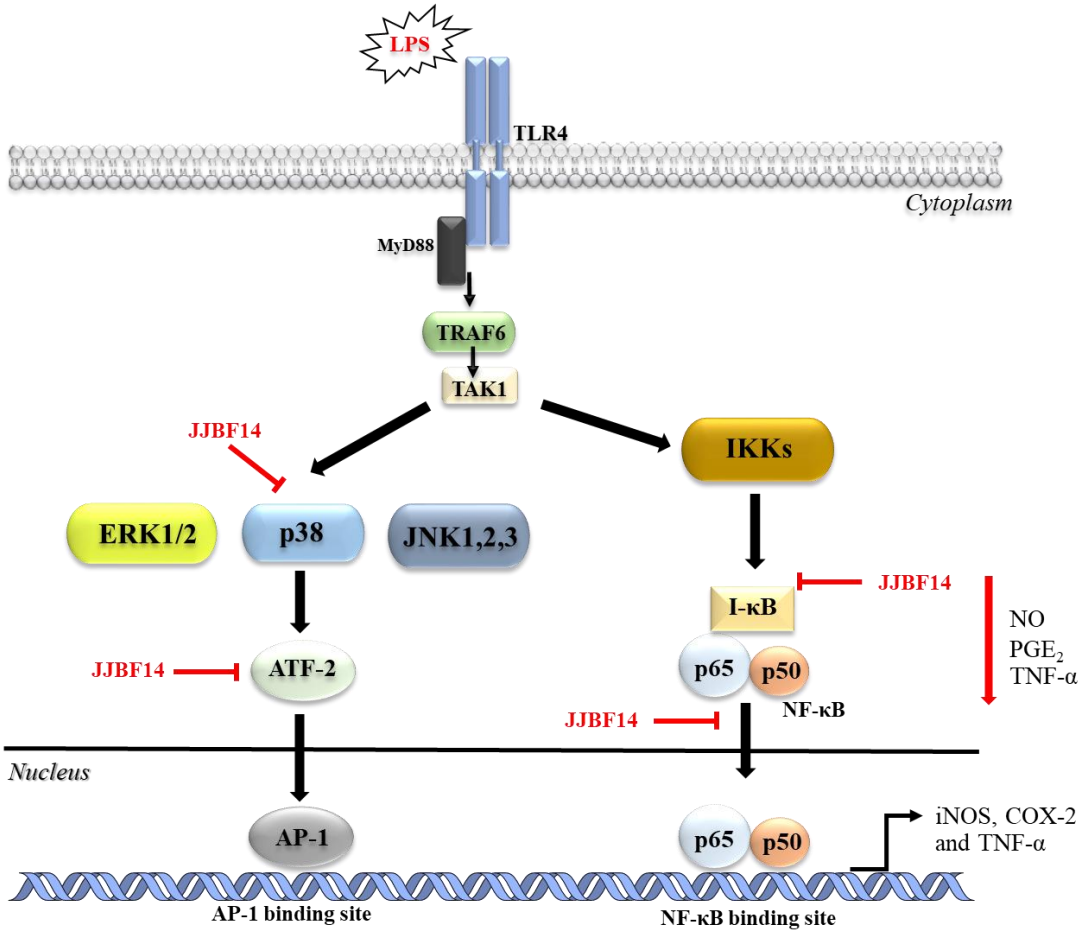

Figure 5-5 The simplified diagram action mechanism responsible for the suppressive effect of JJBF14 on LPS-stimulated inflammatory signaling partway

REFERENCES

Alderton, W. K., Cooper, C. E., & Knowles, R. G. (2001). Nitric oxide synthases: structure, function and inhibition. *Biochemical Journal, 357*(3), 593-615.

Alexanian, A., & Sorokin, A. (2017). Cyclooxygenase 2: protein-protein interactions and posttranslational modifications. *Physiological Genomics, 49*(11), 667-681.

Andrew, P. J., & Mayer, B. (1999). Enzymatic function of nitric oxide synthases. *Cardiovascular Research, 43*(3), 521-531.

Arango Duque, G., & Descoteaux, A. (2014). Macrophage cytokines: involvement in immunity and infectious diseases. *Frontiers in Immunology, 5*, 491.

Ashley, N. T., Weil, Z. M., & Nelson, R. J. (2012). Inflammation: Mechanisms, Costs, and Natural Variation. *Annual Review of Ecology, Evolution, and Systematics, 43*, 385-406.

Atkinson, T. J., Fudin, J., Jahn, H. L., Kubotera, N., Rennick, A. L., & Rhorer, M. (2013). What's new in NSAID pharmacotherapy: oral agents to injectables. P*ain Medicine, 14*(1), 11-17.

Baldassare, J. J., Bi, Y., & Bellone, C. J. (1999). The role of p38 mitogen-activated protein kinase in IL-1 beta transcription. *The Journal of Immunology, 162*(9), 5367-5373.

Barnes, P. J. (2006). How corticosteroids control inflammation: Quintiles Prize Lecture 2005. *British Journal of Pharmacology, 148*(3), 245-254.

Bogdan, C. (2001). Nitric oxide and the immune response. *Nature Immunology, 2*(10), 907-916.

Bosca, L., Zeini, M., Traves, P. G., & Hortelano, S. (2005). Nitric oxide and cell viability in inflammatory cells: a role for NO in macrophage function and fate. *International Journal of Toxicology, 208*(2), 249-258.

Brown, K. L., Cosseau, C., Gardy, J. L., & Hancock, R. E. (2007). Complexities of targeting innate immunity to treat infection. *Trends Immunology, 28*(6), 260-266.

Cargnello, M., & Roux, P. P. (2011). Activation and function of the MAPKs and their substrates, the MAPK-activated protein kinases. *Microbiology and Molecular Biology Reviews, 75*(1), 50-83.

Chiu, F. L., & Lin, J. K. (2008). Tomatidine inhibits iNOS and COX-2 through suppression of NF-kappaB and JNK pathways in LPS-stimulated mouse macrophages. *FEBS Letters, 582*(16), 2407-2412.

Chu, S. C., Marks-Konczalik, J., Wu, H. P., Banks, T. C., & Moss, J. (1998). Analysis of the cytokine-stimulated human inducible nitric oxide synthase (iNOS) gene: characterization of differences between human and mouse iNOS promoters. *Biochemical and Biophysical Research Communications, 248*(3), 871-878.

Conaghan, P. G. (2012). A turbulent decade for NSAIDs: update on current concepts of classification, epidemiology, comparative efficacy, and toxicity. *Rheumatology International, 32*(6), 1491-1502.

Coutinho, A. E., & Chapman, K. E. (2011). The anti-inflammatory and immunosuppressive effects of glucocorticoids, recent developments and mechanistic insights. *Molecular and Cellular Endocrinology*, *335*(1), 2-13.

Craig, R., Larkin, A., Mingo, A. M., Thuerauf, D. J., Andrews, C., McDonough, P. M., & Glembotski, C. C. (2000). p38 MAPK and NF-kappa B collaborate to induce interleukin-6 gene expression and release. Evidence for a cytoprotective autocrine signaling pathway in a cardiac myocyte model system. *Journal of Biological Chemistry, 275*(31), 23814-23824.

De Bosscher, K., Vanden Berghe, W., & Haegeman, G. (2000). Mechanisms of anti-inflammatory action and of immunosuppression by glucocorticoids: negative interference of activated glucocorticoid receptor with transcription factors. *Journal of Neuroimmunology, 109*(1), 16-22.

Dhar, R., Kimseng, R., Chokchaisiri, R., Hiransai, P., Utaipan, T., Suksamrarn, A., & Chunglok, W. (2018). 2',4-Dihydroxy-3',4',6'-trimethoxychalcone from Chromolaena odorata possesses anti-inflammatory effects via inhibition of NF-kappaB and p38 MAPK in lipopolysaccharide-activated RAW 264.7 macrophages. *Immunopharmacology and Immunotoxicology, 40*(1), 43-51.

Dixon, D. A., Kaplan, C. D., McIntyre, T. M., Zimmerman, G. A., & Prescott, S. M. (2000). Post-transcriptional control of cyclooxygenase-2 gene expression. The role of the 3'-untranslated region. *Journal of Biological Chemistry, 275*(16), 11750-11757.

Dunster, J. L. (2016). The macrophage and its role in inflammation and tissue repair: mathematical and systems biology approaches. *Wiley Interdisciplinary Reviews: Systems Biology and Medicine, 8*(1), 87-99.

El-Feky, S. A., Thabet, H. K., & Ubeid, M. T. (2014). Synthesis, molecular modeling and anti-inflammatory screening of novel fluorinated quinoline incorporated benzimidazole derivatives using the Pfitzinger reaction. *Journal of Fluorine Chemistry, 161,* 87-94.

Ericson-Neilsen, W., & Kaye, A. D. (2014). Steroids: pharmacology, complications, and practice delivery issues. *Ochsner Journal, 14*(2), 203-207.

Erridge, C., Bennett-Guerrero, E., & Poxton, I. R. (2002). Structure and function of lipopolysaccharides. *Microbes and Infection, 4*(8), 837-851.

Falasca, M., Hamilton, J. R., Selvadurai, M., Sundaram, K., Adamska, A., & Thompson, P. E. (2017). Class II Phosphoinositide 3-Kinases as Novel Drug Targets. *Journal of Medicinal Chemistry, 60*(1), 47-65.

Font-Nieves, M., Sans-Fons, M. G., Gorina, R., Bonfill-Teixidor, E., Salas-Perdomo, A., Marquez-Kisinousky, L., & Planas, A. M. (2012). Induction of COX-2 enzyme and down-regulation of COX-1 expression by lipopolysaccharide (LPS) control prostaglandin E2 production in astrocytes. *Journal of Biological Chemistry, 287*(9), 6454-6468.

Forstermann, U., & Sessa, W. C. (2012). Nitric oxide synthases: regulation and function. *European Heart Journal, 33*(7), 829-837.

Frazier, W. J., Xue, J., Luce, W. A., & Liu, Y. (2012). MAPK signaling drives inflammation in LPS-stimulated cardiomyocytes: the route of crosstalk to G-protein-coupled receptors. *PLOS ONE, 7*(11), e50071.

Gao, J., Morrison, D. C., Parmely, T. J., Russell, S. W., & Murphy, W. J. (1997). An interferon-gamma-activated site (GAS) is necessary for full expression of the mouse iNOS gene in response to interferon-gamma and lipopolysaccharide. *Journal of Biological Chemistry, 272*(2), 1226-1230.

Ghigo, A., Damilano, F., Braccini, L., & Hirsch, E. (2010). PI3K inhibition in inflammation: Toward tailored therapies for specific diseases. *BioEssays, 32*(3), 185-196.

Ghosh, S., & Hayden, M. S. (2008). New regulators of NF-kappaB in inflammation. *Nature Reviews Immunology, 8*(11), 837-848.

Godambe, S. A., Chaplin, D. D., Takova, T., Read, L. M., & Bellone, C. J. (1995). A novel cis-acting element required for lipopolysaccharide-induced transcription of the murine interleukin-1 beta gene. *Molecular and Cellular Biology, 15*(1), 112-119.

Hawkins, P. T., & Stephens, L. R. (2015). PI3K signalling in inflammation. *Biochimica et Biophysica Acta, 1*851(6), 882-897.

Hinz, B., & Brune, K. (2002). Cyclooxygenase-2--10 years later. *Journal of Pharmacology and Experimental Therapeutics, 300*(2), 367-375.

Hirose, N., Maekawa, T., Shinagawa, T., & Ishii, S. (2009). ATF-2 regulates lipopolysaccharide-induced transcription in macrophage cells. *Biochemical and Biophysical Research Communications, 385*(1), 72-77.

Hoesel, B., & Schmid, J. A. (2013). The complexity of NF-kappaB signaling in inflammation and cancer. *Molecular Cancer Research, 12*, 86.

Hommes, D. W., Peppelenbosch, M. P., & van Deventer, S. J. (2003). Mitogen activated protein (MAP) kinase signal transduction pathways and novel anti-inflammatory targets. *Gut, 52*(1), 144-151.

Hunter, D., Chai, C., & Barr, G. A. (2015). Effects of COX inhibition and LPS on formalin induced pain in the infant rat. *Dev Neurobiol, 75*(10), 1068-1079.

Hunter, T. S., Robison, C., & Gerbino, P. P. (2015). Emerging evidence in NSAID pharmacology: important considerations for product selection. *The American Journal of Managed Care, 21*(7), 139-147.

Hwang, J. M., Yu, J. Y., Jang, Y. O., Kim, B. T., Hwang, K. J., Jeon, Y. M., & Lee, J. C. (2010). A phenolic acid phenethyl urea compound inhibits lipopolysaccharide-induced production of nitric oxide and pro-inflammatory cytokines in cell culture. *International Immunopharmacology, 10(*4), 526-532.

Isanbor, C., & O'Hagan, D. (2006). Fluorine in medicinal chemistry: A review of anti-cancer agents. *Journal of Fluorine Chemistry, 127*(3), 303-319.

Ismail, F. M. D. (2002). Important fluorinated drugs in experimental and clinical use. *Journal of Fluorine Chemistry, 118*(1-2), 27-33.

Jaratjaroonphong, J., Tuengpanya, S., Saeeng, R., Udompong, S., & Srisook, K. (2014). Green synthesis and anti-inflammatory studies of a series of 1,1-bis(heteroaryl)alkane derivatives. *European Journal of Medicinal Chemistry, 83*, 561-568.

Je, J. H., Lee, J. Y., Jung, K. J., Sung, B., Go, E. K., Yu, B. P., & Chung, H. Y. (2004). NF-kappaB activation mechanism of 4-hydroxyhexenal via NIK/IKK and p38 MAPK pathway. *FEBS Lett, 566*(1-3), 183-189.

Jerala, R. (2007). Structural biology of the LPS recognition. *International Journal of Medical Microbiology, 297*(5), 353-363.

Kalkhambkar, R. G., Kulkarni, G. M., Kamanavalli, C. M., Premkumar, N., Asdaq, S. M. B., & Sun, C. M. (2008). Synthesis and biological activities of some new fluorinated coumarins and 1-aza coumarins. *European Journal of Medicinal Chemistry, 43*(10), 2178-2188.

Kaminska, B. (2005). MAPK signalling pathways as molecular targets for anti-inflammatory therapy--from molecular mechanisms to therapeutic benefits. *Biochimica et Biophysica Acta, 1754*(1-2), 253-262.

Kang, J., Zhang, Y., Cao, X., Fan, J., Li, G., Wang, Q., & Yin, Z. (2012). Lycorine inhibits lipopolysaccharide-induced iNOS and COX-2 up-regulation in RAW264.7 cells through suppressing P38 and STATs activation and increases the survival rate of mice after LPS challenge. *International Immunopharmacology, 12*(1), 249-256.

Kang, Y. J., Wingerd, B. A., Arakawa, T., & Smith, W. L. (2006). Cyclooxygenase-2 gene transcription in a macrophage model of inflammation. *Journal of Immunology, 177*(11), 8111-8122.

Kaplan, M. H. (2013). STAT signaling in inflammation. *JAKSTAT, 2*(1), e24198.

Kim, A. R., Lee, M. S., Shin, T. S., Hua, H., Jang, B. C., Choi, J. S., & Kim, H. R. (2011). Phlorofucofuroeckol A inhibits the LPS-stimulated iNOS and COX-

2 expressions in macrophages via inhibition of NF-kappaB, Akt, and p38 MAPK. *Toxicology in Vitro, 25*(8), 1789-1795.

Kim, E. K., & Choi, E. J. (2010). Pathological roles of MAPK signaling pathways in human diseases. *Biochimica et Biophysica Acta, 1802*(4), 396-405.

Kim, H. G., Shrestha, B., Lim, S. Y., Yoon, D. H., Chang, W. C., Shin, D. J., & Kim, T. W. (2006). Cordycepin inhibits lipopolysaccharide-induced inflammation by the suppression of NF-kappaB through Akt and p38 inhibition in RAW 264.7 macrophage cells. *European Journal of Pharmacology, 545*(2-3), 192-199.

Kim, H. J., Lee, H. S., Chong, Y. H., & Kang, J. L. (2006). p38 Mitogen-activated protein kinase up-regulates LPS-induced NF-kappaB activation in the development of lung injury and RAW 264.7 macrophages. *Toxicology, 225*(1), 36-47.

Kim, Y. M., Lee, B. S., Yi, K. Y., & Paik, S. G. (1997). Upstream NF-kappaB site is required for the maximal expression of mouse inducible nitric oxide synthase gene in interferon-gamma plus lipopolysaccharide-induced RAW 264.7 macrophages. *Biochemical and Biophysical Research Communications, 236*(3), 655-660.

Kleinert, H., Pautz, A., Linker, K., & Schwarz, P. M. (2004). Regulation of the expression of inducible nitric oxide synthase. *European Journal of Pharmacology, 500*(1-3), 255-266.

Koh, T. J., & DiPietro, L. A. (2011). Inflammation and wound healing: the role of the macrophage. *Expert Reviews in Molecular Medicine, 13,* e23.

Kraemer, S. A., Meade, E. A., & DeWitt, D. L. (1992). Prostaglandin endoperoxide synthase gene structure: identification of the transcriptional start site and 5'-flanking regulatory sequences. *Archives of Biochemistry and Biophysics, 293*(2), 391-400.

Kuprash, D. V., Udalova, I. A., Turetskaya, R. L., Kwiatkowski, D., Rice, N. R., & Nedospasov, S. A. (1999). Similarities and differences between human and murine TNF promoters in their response to lipopolysaccharide. *Journal of Immunology, 162*(7), 4045-4052.

Lawrence, T. (2009). The nuclear factor NF-kappaB pathway in inflammation. *Cold Spring Harbor Perspectives in Biology*, *1*(6), a001651.

Lee, A. K., Sung, S. H., Kim, Y. C., & Kim, S. G. (2003). Inhibition of lipopolysaccharide-inducible nitric oxide synthase, TNF-alpha and COX-2 expression by sauchinone effects on I-kappaBalpha phosphorylation, C/EBP and AP-1 activation. *British Journal of Pharmacology*, *139*(1), 11-20.

Lee, K. H., Abas, F., Alitheen, N. B., Shaari, K., Lajis, N. H., & Ahmad, S. (2011). A curcumin derivative, 2,6-bis(2,5-dimethoxybenzylidene)-cyclohexanone (BDMC33) attenuates prostaglandin E2 synthesis via selective suppression of cyclooxygenase-2 in IFN-gamma/LPS-stimulated macrophages. *Molecules*, *16*(11), 9728-9738.

Lee, K. H., Chow, Y. L., Sharmili, V., Abas, F., Alitheen, N. B., Shaari, K., & Syahida, A. (2012). BDMC33, A curcumin derivative suppresses inflammatory responses in macrophage-like cellular system: role of inhibition in NF-kappaB and MAPK signaling pathways. *International Journal of Molecular Sciences*, *13*(3), 2985-3008.

Legler, D. F., Bruckner, M., Uetz-von Allmen, E., & Krause, P. (2010). Prostaglandin E2 at new glance: novel insights in functional diversity offer therapeutic chances. *The International Journal of Biochemistry & Cell Biology*, *42*(2), 198-201.

Li, H., Zhang, Q., Jin, X., Zou, X., Wang, Y., Hao, D., & Zhao, F. (2018). Dysifragilone A inhibits LPSinduced RAW264.7 macrophage activation by blocking the p38 MAPK signaling pathway. *Molecular Medicine Reports*, *17*(1), 674-682.

Liew, C. Y., Lam, K. W., Kim, M. K., Harith, H. H., Tham, C. L., Cheah, Y. K., & Israf, D. A. (2011). Effects of 3-(2-Hydroxyphenyl)-1-(5-methyl-furan-2-y-l) propenone (HMP) upon signalling pathways of lipopolysaccharide-induced iNOS synthesis in RAW 264.7 cells. *International Immunopharmacology*, *11*(1), 85-95.

Liu, T., Zhang, L., Joo, D., & Sun, S. C. (2017). NF-kappaB signaling in inflammation. *Signal Transduction and Targeted Therapy*, *2*, 17023.

Liu, X. H., & Rose, D. P. (1996). Differential expression and regulation of cyclooxygenase-1 and -2 in two human breast cancer cell lines. *Cancer Research, 56(*22), 5125-5127.

Lopez-Castejon, G., & Brough, D. (2011). Understanding the mechanism of IL-1beta secretion. *Cytokine & Growth Factor Reviews, 22*(4), 189-195.

Lorsbach, R. B., Murphy, W. J., Lowenstein, C. J., Snyder, S. H., & Russell, S. W. (1993). Expression of the nitric oxide synthase gene in mouse macrophages activated for tumor cell killing. Molecular basis for the synergy between interferon-gamma and lipopolysaccharide. *Journal of Biological Chemistry, 268*(3), 1908-1913.

Lowenstein, C. J., Alley, E. W., Raval, P., Snowman, A. M., Snyder, S. H., Russell, S. W., & Murphy, W. J. (1993). Macrophage nitric oxide synthase gene: two upstream regions mediate induction by interferon gamma and lipopolysaccharide. *Proceedings of the National Academy of Sciences of the United States of America, 90*(20), 9730-9734.

Maeshima, N., & Fernandez, R. C. (2013). Recognition of lipid A variants by the TLR4-MD-2 receptor complex. *Frontiers in Cellular and Infection Microbiology, 3*, 3.

Mbonye, U. R., Yuan, C., Harris, C. E., Sidhu, R. S., Song, I., Arakawa, T., & Smith, W. L. (2008). Two distinct pathways for cyclooxygenase-2 protein degradation. *Journal of Biological Chemistry, 283*(13), 8611-8623.

Medzhitov, R. (2008). Origin and physiological roles of inflammation. *Nature, 454*(7203), 428-435.

Mestre, J. R., Mackrell, P. J., Rivadeneira, D. E., Stapleton, P. P., Tanabe, T., & Daly, J. M. (2001). Redundancy in the signaling pathways and promoter elements regulating cyclooxygenase-2 gene expression in endotoxin-treated macrophage/monocytic cells. *Journal of Biological Chemistry, 276*(6), 3977-3982.

Moodley, I. (2008). Review of the cardiovascular safety of COXIBs compared to NSAIDS. *Cardiovascular Journal of Africa, 19*(2), 102-107.

Nair, V., Thomas, S., Mathew, S. C., & Abhilash, K. G. (2006). Recent advances in the chemistry of triaryl- and triheteroarylmethanes. *Tetrahedron, 62*(29), 6731-6747.

Nakanishi, M., & Rosenberg, D. W. (2013). Multifaceted roles of PGE_2 in inflammation and cancer. *Seminars in Immunopathology, 35*(2), 123-137.

Nathan, C. (2002). Points of control in inflammation. *Nature, 420*(6917), 846-852.

Newton, K., & Dixit, V. M. (2012). Signaling in innate immunity and inflammation. *Cold Spring Harbor Perspectives in Biology, 4*(3), a006049.

Pacher, P., Beckman, J. S., & Liaudet, L. (2007). Nitric oxide and peroxynitrite in health and disease. *Physiological Reviews, 87*(1), 315-424.

Parameswaran, N., & Patial, S. (2010). Tumor necrosis factor-alpha signaling in macrophages. *Critical Reviews in Eukaryotic Gene Expression, 20*(2), 87-103.

Ramamoorthy, S., & Cidlowski, J. A. (2016). Corticosteroids: Mechanisms of Action in Health and Disease. *Rheumatic Diseases Clinics of North America, 42*(1), 15-31, vii.

Rao, P. P., Kabir, S. N., & Mohamed, T. (2010). Nonsteroidal Anti-Inflammatory Drugs (NSAIDs): Progress in Small Molecule Drug Development. *Pharmaceuticals (Basel), 3*(5), 1530-1549.

Ren, K., & Torres, R. (2009). Role of interleukin-1beta during pain and inflammation. *Brain Research Reviews, 60*(1), 57-64.

Ricciotti, E., & FitzGerald, G. A. (2011). Prostaglandins and inflammation. *Arteriosclerosis, Thrombosis, and Vascular Biology, 31*(5), 986-1000.

Rouzer, C. A., & Marnett, L. J. (2009). Cyclooxygenases: structural and functional insights. *Journal of Lipid Research, 50*, 29-34.

Saccani, S., Pantano, S., & Natoli, G. (2002). p38-Dependent marking of inflammatory genes for increased NF-kappa B recruitment. *Nature Immunology, 3*(1), 69-75.

Senthil Kumar, K. J., & Wang, S. Y. (2009). Lucidone inhibits iNOS and COX-2 expression in LPS-induced RAW 264.7 murine macrophage cells via NF-kappaB and MAPKs signaling pathways. *Planta Medica, 75*(5), 494-500.

Simmons, D. L., Botting, R. M., & Hla, T. (2004). Cyclooxygenase isozymes: the biology of prostaglandin synthesis and inhibition. *Pharmacological Reviews, 56*(3), 387-437.

Smith, B. C., Fernhoff, N. B., & Marletta, M. A. (2012). Mechanism and kinetics of inducible nitric oxide synthase auto-S-nitrosation and inactivation. *Biochemistry, 51*(5), 1028-1040.

Smith, W. L., Garavito, R. M., & DeWitt, D. L. (1996). Prostaglandin endoperoxide H synthases (cyclooxygenases)-1 and -2. *Journal of Biological Chemistry, 271*(52), 33157-33160.

Srivastava, S., Sinha, R., & Roy, D. (2004). Toxicological effects of malachite green. *Aquatic Toxicology, 66*(3), 319-329.

Stark, A. K., Sriskantharajah, S., Hessel, E. M., & Okkenhaug, K. (2015). PI3K inhibitors in inflammation, autoimmunity and cancer. *Current Opinion in Pharmacology, 23*, 82-91.

Suleyman, H., Demircan, B., & Karagoz, Y. (2007). Anti-inflammatory and side effects of cyclooxygenase inhibitors. *Pharmacological Reports, 59*(3), 247-258.

Tsao, L. T., Lee, C. Y., Huang, L. J., Kuo, S. C., & Wang, H. P. (2002). Inhibition of lipopolysaccharide-stimulated nitric oxide production in RAW 264.7 macrophages by a synthetic carbazole, LCY-2-CHO. *Biochemical Pharmacology, 63*(11), 1961-1968.

Turner, M. D., Nedjai, B., Hurst, T., & Pennington, D. J. (2014). Cytokines and chemokines: At the crossroads of cell signalling and inflammatory disease. *Biochimica et Biophysica Acta, 1843*(11), 2563-2582.

Udompong, S., Mankhong, S., Jaratjaroonphong, J., & Srisook, K. (2017). Involvement of p38 MAPK and ATF-2 signaling pathway in anti-inflammatory effect of a novel compound bis[(5-methyl)2-furyl](4-nitrophenyl)methane on lipopolysaccharide-stimulated macrophages. *International Immunopharmacology, 50,* 6-13.

Vanhaesebroeck, B., Guillermet-Guibert, J., Graupera, M., & Bilanges, B. (2010). The emerging mechanisms of isoform-specific PI3K signalling. *Nature Reviews Molecular Cell Biology, 11*(5), 329-341.

Villarino, A. V., Kanno, Y., Ferdinand, J. R., & O'Shea, J. J. (2015). Mechanisms of Jak/STAT signaling in immunity and disease. *Journal of Immunology, 194*(1), 21-27.

Vitecek, J., Lojek, A., Valacchi, G., & Kubala, L. (2012). Arginine-based inhibitors of nitric oxide synthase: therapeutic potential and challenges. *Mediators of Inflammation, 2012*, 318087.

Wakabayashi, I., & Yasui, K. (2000). Wogonin inhibits inducible prostaglandin E-2 production in macrophages. *European Journal of Pharmacology, 406*(3), 477-481.

Wegener, G., & Volke, V. (2010). Nitric Oxide Synthase Inhibitors as Antidepressants. *Pharmaceuticals (Basel), 3*(1), 273-299.

Weichhart, T., & Saemann, M. D. (2008). The PI3K/Akt/mTOR pathway in innate immune cells: emerging therapeutic applications. *Annals of the Rheumatic Diseases, 67*(3), 70-74.

Xie, Q. (1997). A novel lipopolysaccharide-response element contributes to induction of nitric oxide synthase. *Journal of Biological Chemistry, 272*(23), 14867-14872.

Xie, Q. W., Kashiwabara, Y., & Nathan, C. (1994). Role of transcription factor NF-kappa B/Rel in induction of nitric oxide synthase. *Journal of Biological Chemistry, 269*(7), 4705-4708.

Xie, Q. W., & Nathan, C. (1993). Promoter of the mouse gene encoding calcium-independent nitric oxide synthase confers inducibility by interferon-gamma and bacterial lipopolysaccharide. *Transactions of the Association of American Physicians, 106*, 1-12.

Xie, Q. W., Whisnant, R., & Nathan, C. (1993). Promoter of the mouse gene encoding calcium-independent nitric oxide synthase confers inducibility by interferon gamma and bacterial lipopolysaccharide. *Journal of Experimental Medicine, 177*(6), 1779-1784.

Yang, Y., Yang, W. S., Yu, T., Sung, G. H., Park, K. W., Yoon, K., & Cho, J. Y. (2014). ATF-2/CREB/IRF-3-targeted anti-inflammatory activity of Korean red ginseng water extract. *Journal of Ethnopharmacology, 154*(1), 218-228.

Ye, X., & Liu, S. F. (2002). Lipopolysaccharide down-regulates Sp1 binding activity by promoting Sp1 protein dephosphorylation and degradation. *Journal of Biological Chemistry, 277*(35), 31863-31870.

Yoo, M. S., Shin, J. S., Choi, H. E., Cho, Y. W., Bang, M. H., Baek, N. I., & Lee, K. T. (2012). Fucosterol isolated from Undaria pinnatifida inhibits lipopolysaccharide-induced production of nitric oxide and pro-inflammatory cytokines via the inactivation of nuclear factor-kappaB and p38 mitogen-activated protein kinase in RAW264.7 macrophages. *Food Chemistry, 135*(3), 967-975.

Yu, T., Li, Y. J., Bian, A. H., Zuo, H. B., Zhu, T. W., Ji, S. X., & Cho, J. Y. (2014). The regulatory role of activating transcription factor 2 in inflammation. *Mediators of Inflammation, 2014*, 950472.

Zhang, J. M., & An, J. (2007). Cytokines, inflammation, and pain. *International Anesthesiology Clinics, 45*(2), 27-37.

Zhang, Y., Saccani, S., Shin, H., & Nikolajczyk, B. S. (2008). Dynamic protein associations define two phases of IL-1beta transcriptional activation. *Journal of Immunology, 181*(1), 503-512.

APPENDIX

APPENDIX A
CULTURE MEDIA AND SOLUTION

1. Fluorinated triarylmethane derivatives preparation

Dissolved Fluorinated triarylmethane derivatives as a stock solution at 50 mM with DMSO

Table A-1 Molecular weight and volume of DMSO for dissolved Fluorinated triarylmethane derivatives

Compound	Molecular weight (g/mol)	Weight (mg)	DMSO (μL)
JJAF1	391.15	2.4	122.7
JJAF2	305.12	2.7	177.0
JJAF3	350.11	2.5	142.8
JJAF4	344.17	2.4	139.5
JJAF5	344.17	2.3	133.7
JJAF6	340.14	2	117.6
JJAF7	415.13	2	96.4
JJBF1	442.18	1.7	76.9
JJBF2	442.18	1.7	76.9
JJBF3	442.18	2.3	104.0
JJBF4	460.17	3.2	139.1
JJBF5	492.18	3.3	134.1
JJBF6	492.18	2.7	109.7
JJBF7	442.18	2.7	122.1
JJBF8	442.18	3.2	144.7
JJBF9	442.18	2.8	126.6
JJBF10	460.17	3.3	143.4
JJBF11	492.18	2.6	105.7
JJBF12	492.18	2.1	85.3

Table A-1 (continued)

Compound	Molecular weight (g/mol)	Weight (mg)	DMSO (µL)
JJBF13	442.18	4.5	203.5
JJBF14	442.18	4.4	199.0
JJBF15	442.18	1.2	54.3
JJBF16	460.17	4.4	191.2
JJBF17	492.18	4.6	186.9
JJBF18	492.18	4.1	166.6
JJCF1	348.2	2.4	137.9

2. Dulbecco's Modified Eagle Medium (DMEM) with phenol red

DMEM powder (Gibco, USA.) 13.5 g

$NaHCO_3$ 3.7 g

Dissolve by sterile water for injection 900 mL and adjust pH to 7.1-7.2. After that, add antibiotic Penicillin/Streptomycin 10 mL and sterilize by filter sterilization. Lastly, add heat-inactivated fetal bovine serum 100 mL.

3. Dulbecco's Modified Eagle Medium (DMEM) without phenol red

DMEM powder (Sigma, USA.) 10 g

$NaHCO_3$ 3.7 g

D-glucose 3.5 g

Dissolve by sterile water for injection 900 mL and adjust pH to 7.1-7.2. After that, add antibiotic Penicillin/Streptomycin 10 mL and make volume to 1000 mL by sterile water for injection. Lastly, sterilize solution by filter sterilization.

4. 1X Hank's Balanced Salt Solution (HBSS)

NaCl 8 g

$NAHCO_3$ 0.35 g

KCl 0.4 g

KH_2PO_4 0.06

D-Glucose	1	g
NA_2HPO_4	0.048	g

Add distilled water 900 mL. Adjust pH to 7.1-7.2 and make volume to 1000 mL with distilled water. Sterilize solution by filter sterilization.

5. 5 mg/mL Thiazolyl Blue Tetrazolium Bromide (MTT)

Dissolve MTT 0.125 g in 1X PBS 25 mL and sterilize by filter sterilization and keep in -20 °C

6. Griess regent (100 mL)

Sulfanilamide	1	g
N-(1-napthyl)-ethylene diamine	0.1	g
Distilled water	95	mL
Phosphoric acid	5	mL

APPENDIX B

ELECTROPHORESIS AND WESTERN BL

1. 1X Phosphate buffered saline (PBS)

NaCl	8	g
KCl	0.2	g
KH_2PO_4	0.24	g
Na_2HPO_4	1.44	g

Add distilled water 950 mL. Adjust pH to 7.4 and make volume to 1000 mL with distilled water. Sterilize solution by autoclave.

2. Protein lysis buffer

1 M Tris-HCl, pH 7.4	12	mL
4 M NaCl	3.75	mL
0.5 M EGTA	1	mL
20% SDS	0.5	mL
20% sodium deoxycholate	5	mL
10% Nonidet P-40	10	mL

Adjust volume to 100 mL by distilled water and autoclave. Keep in 4 °C

3. Protein lysis buffer for iNOS, COX-1 and COX-2 (1.5 mL)

Protein lysis buffer	1,470	mL
0.1 M DTT	15	µL
100 X Protease inhibitor cocktail (PI)	15	µL

4. Protein lysis buffer for MAPKs (1.5 mL)

Protein lysis buffer	1,455	µL
0.1 M DTT	15	µL
100 X PI	15	µL
100 X Phosphatase inhibitor cocktail (PhosStop)	15	µL

5. 30% (w/v) Monomer solution

Acrylamide	29.2	g

Bis-acrylamide	0.8	g

Adjust volume to 100 mL by distilled water and sterilize solution by filter sterilization. Keep in 4 °C

6. 4X Separating gel buffer

Tris	45.5	g

Add distilled water 200 mL. Adjust pH to 8.8 and make volume to 250 mL with distilled water. Keep in 4 °C

7. 4X Stacking gel buffer

Tris	6	g

Add distilled water 80 mL. Adjust pH to 6.8 and make volume to 100 mL with distilled water. Keep in 4 °C.

8. 10% (w/v) Sodium dodecyl sulfate (SDS)

SDS	10	g

Add distilled water 100 mL. Keep at room temperature.

9. 10% (w/v) Ammonium persulfate (APS)

APS	0.1	g

Add distilled water 1 mL. Aliquots the solution into Eppendorf and keep in -20°C.

10. 6X Protein loading buffer

SDS	1.2	g
Distilled water	1.285	mL
2M Tris-HCl , pH 6.8	1.875	mL
Bromophenol blue	0.06	g
Glycerol	6	mL
β-mercaptoethanol	0.84	mL

Dissolve the solution and aliquots into Eppendorf and keep in -20°

11. 10X Tris-glycine running buffer, pH 8.3

Tris	30	g
Glycine	144.2	g
SDS	10	g

Add distilled water 1000 mL. Keep at room temperature.

12. Transfer buffer

Tris	3.03	g
Glycine	14.42	g

Add distilled water 900 mL and methanol 100 mL. Keep at room temperature.

13. Tris buffered saline (TBS)

2 M Tris-HCl, pH 7.5	5	mL
4 M NaCl	37.5	mL

Make volume to 1000 mL by distilled water. Keep at room temperature**.**

14. Tris buffered saline with Tween 20 (TBS-T)

2 M Tris-HCl, pH 7.5	5	mL
4 M NaCl	37.5	mL
Tween 20	1	mL

Make volume to 1000 mL by distilled water. Keep at room temperature**.**

15. Blocking solution

Skim milk power	5	g
TBS-T	100	mL

16. 10% Separating gel for 2 gels

30% monomer solution	3.3	mL
4X running buffer	2.5	mL
10% SDS	0.1	mL
Distilled water	4	m

10% APS	50	µL
TEMED	5	µL

17. 4% Stacking gel for 2 gels

30% monomer solution	0.44	mL
4X stacking gel buffer	0.83	mL
10% SDS	33	µL
Distilled water	2.03	mL
10% APS	20	µL
TEMED	2	µL

18. Stripping solution

10% SDS	2	mL
2 M Tris-HCl, pH 7.4	0.32	mL
B-mercaptoethanol	70	µL

Make volume to 10 mL by distilled water.

APPENDIX C

AMPLIFICATION CURVE AND MELTING CURVE OF iNOS, COX-1, COX-2 AND EF-2

(A)

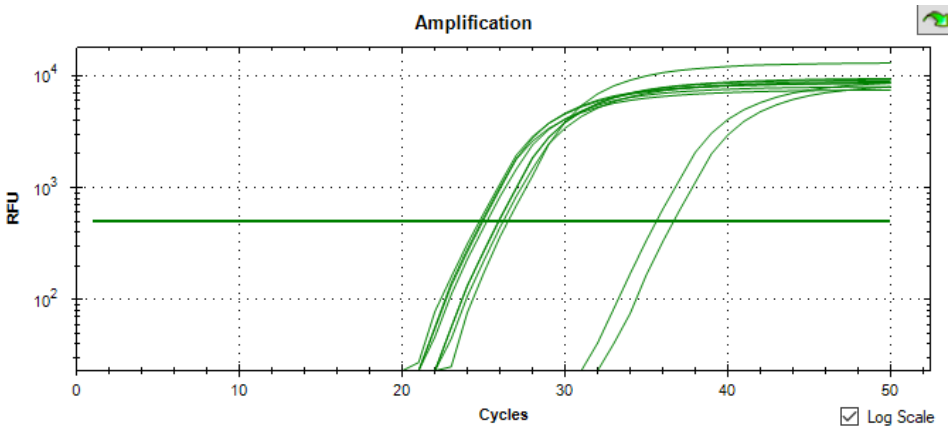

(B)

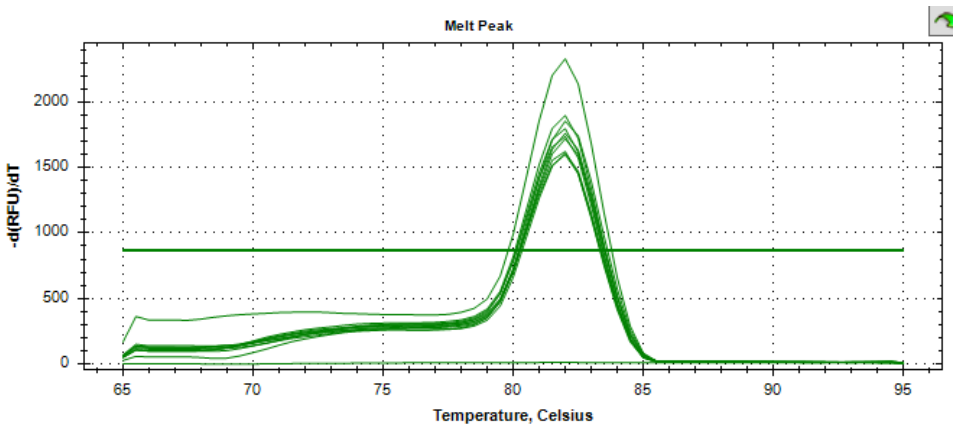

Figure C-1 Amplification curve (A) and melting curve (B) of iNOS

(A)

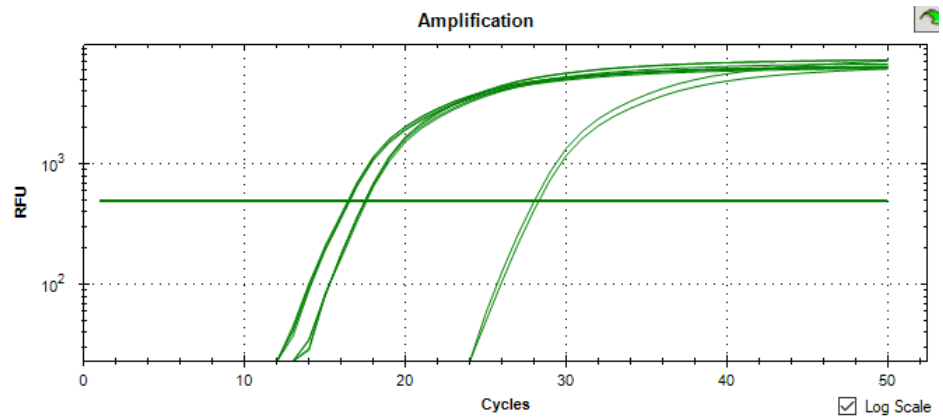

(B)

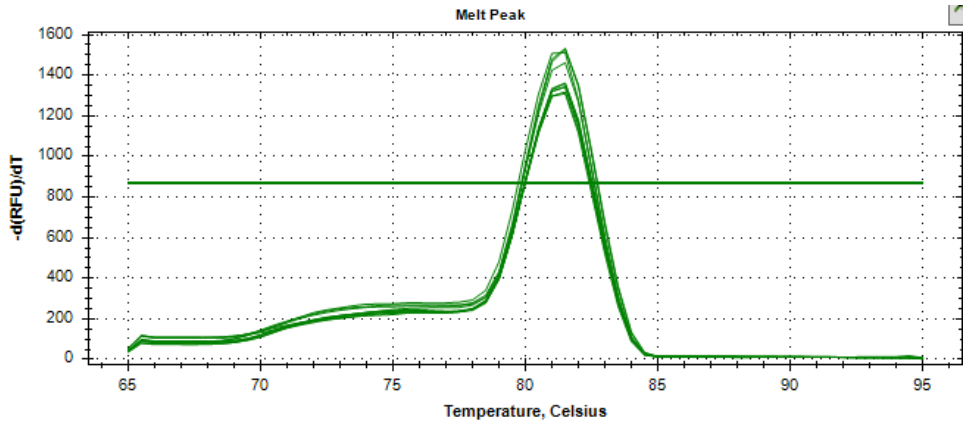

Figure C-2 Amplification curve (A) and melting curve (B) of COX-2

(A)

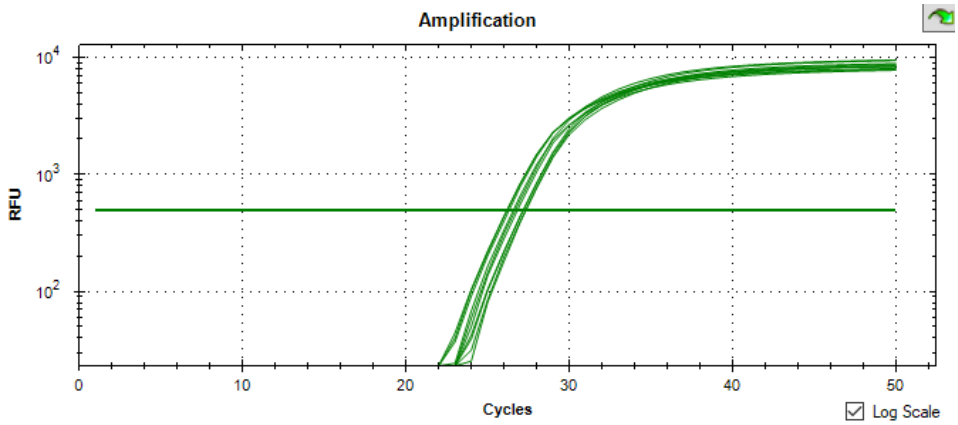

(B)

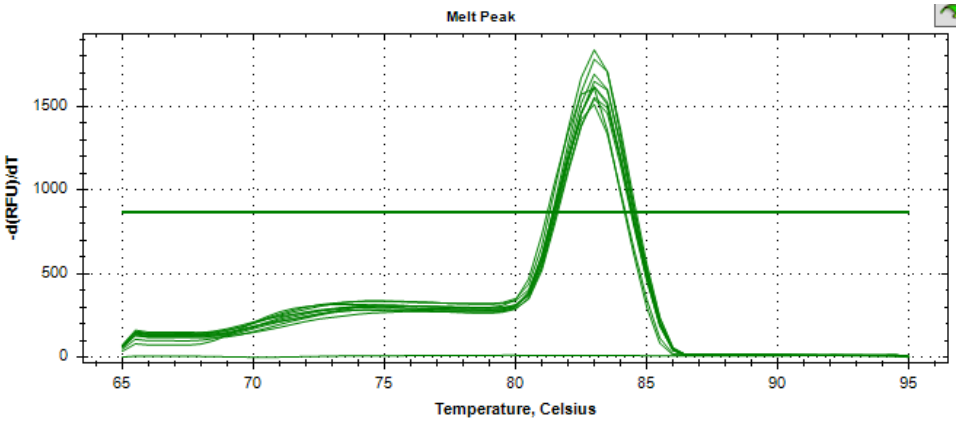

Figure C-3 Amplification curve (A) and melting curve (B) of COX-1

(A)

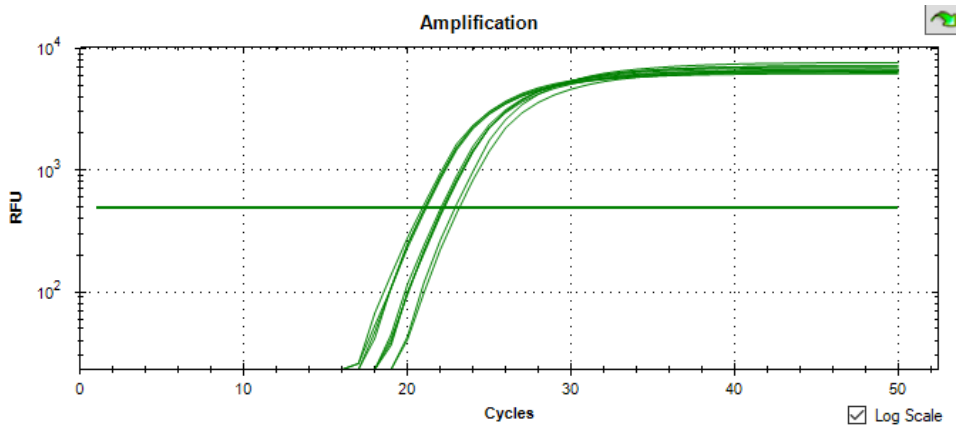

(B)

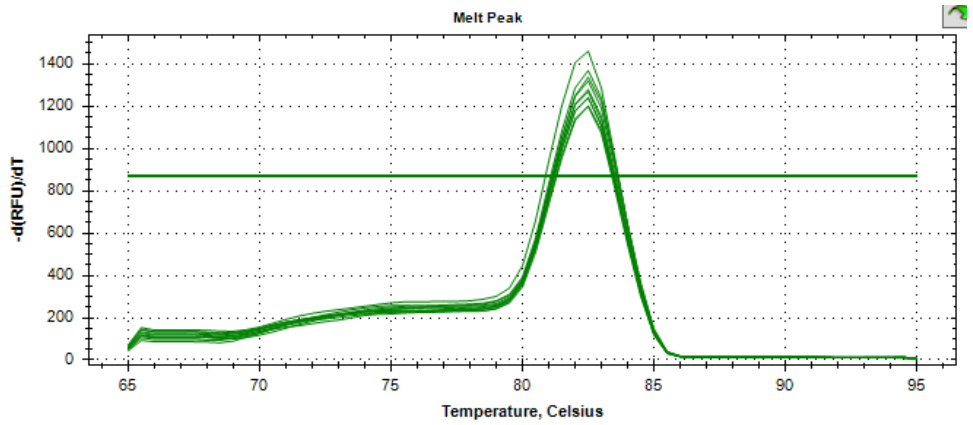

Figure C-4 Amplification curve (A) and melting curve (B) of EF-2